Aus dem Institut für Pathologie
der Universität zu Lübeck
Direktor: Prof. Dr. med. Sven Perner

Die immunologische Tumormikroumgebung in plattenepithelialen Tumoren des Kopf-Hals-Bereichs – ein bedeutender Einflussfaktor auf Therapie und Prognose

Inauguraldissertation
zur
Erlangung der Doktorwürde
der Universität zu Lübeck
- Aus der Sektion Medizin -
vorgelegt von
Christian Watermann
aus Ahlen
Lübeck 2021

1. Berichterstatter: Prof. Dr. med. Sven Perner

2. Berichterstatter: Priv.-Doz. Dr. med. Dr. med. dent. Hans-Christian Jacobsen

Tag der mündlichen Prüfung: 02.11.2022

Zum Druck genehmigt. Lübeck, den 02.11.2022

-Promotionskommission der Sektion Medizin-

Der Dissertationsschrift liegen im Sinne einer kumulativen Promotion folgende Originalarbeiten zu Grunde:

1. Immunologic "cold" squamous cell carcinomas of the head and neck are associated with an unfavorable prognosis.
Ribbat-Idel J, Perner S, Kuppler P, Klapper L, Krupar R, **Watermann C**, Paulsen FO, Offermann A, Bruchhage KL, Wollenberg B, Idel C.
Front Med (Lausanne). 2021 Jan 27;8:622330.

2. Performance of different diagnostic PD-L1 clones in head and neck squamous cell carcinoma.
Ribbat-Idel J, Dressler FF, Krupar R, **Watermann C**, Paulsen FO, Kuppler P, Klapper L, Offermann A, Wollenberg B, Rades D, Laban S, Reischl M, Bruchhage K-L, Idel C, Perner S.
Front Med (Lausanne). 2021 Apr 27;8:640515.

3. Recurrent HNSCC harbor an immunosuppressive tumor immune microenvironment suggesting successful tumor immune evasion.
Watermann C, Pasternack H, Idel C, Ribbat-Idel J, Brägelmann J, Kuppler P, Offermann A, Jonigk D, Kühnel MP, Schröck A, Dreyer E, Rosero C, Nathansen J, Dubrovska A, Tharun L, Kirfel J, Wollenberg B, Perner S*, Krupar R*.
Clin Cancer Res. 2021 Jan 15;27(2):632-644. *These authors contributed equally.

4. In silico analysis reveals EP300 as a panCancer inhibitor of anti-tumor immune response via metabolic modulation.
Krupar R*, **Watermann C***, Idel C, Ribbat-Idel J, Offermann A, Pasternack H, Kirfel J, Sikora AG, Perner S.
Sci Rep. 2020 Jun 10;10(1):9389. *These authors contributed equally.

Inhaltsverzeichnis

1. Deutsche Zusammenfassung

1.1 Einleitung

1.1.1 Epidemiologie von plattenepithelialen Tumoren des Kopf-Hals-Bereichs (HNSCC)

Plattenepitheliale Karzinome des Kopf-Hals-Bereichs (HNSCC, engl. head and neck squamous cell carcinoma) stellen eine heterogene Tumorentität dar, zu der sowohl Tumore der Lippe und der Mundhöhle als auch des Pharynx (Nasopharynx, Oropharynx, Hypopharynx) und des Larynx gehören. Insgesamt machen HNSCC derzeit die achthäufigste Tumorentität weltweit mit mehr als 800.000 jährlichen Fällen aus (54). Hierbei sind die Hauptrisikofaktoren zur Tumorentstehung Tabak- und Alkoholkonsum sowie, insbesondere beim Oropharynxkarzinom, die chronische Infektion mit einem Hochrisikotyp des Humanen Papillomavirus (HPV) (22, 30, 42). Ein Großteil der erkrankten Patienten ist männlich, das mittlere Erkrankungsalter liegt bei etwa 65 Jahren (29, 54).
Die Prognose bei Diagnosestellung ist derzeit weiterhin schlecht. Zwar liegt die 5-Jahres-Überlebensrate im lokal begrenzten Tumorstadium bei 68-84%, im regional fortgeschrittenen Tumorstadium jedoch nur noch bei 33-65% und beim Vorliegen von Fernmetastasen bei 8-35% (18, 52, 56). Aufgrund einer zumeist späten Diagnosestellung, bei der über 60% der HNSCC Patienten bereits im fortgeschrittene Tumorstadium III oder IV sind, sowie des häufigen Auftretens von Tumor-Rezidiven in bis zu 60% der Fälle liegt die 5-Jahres-Überlebensrate insgesamt zwischen 40-65% (1, 49, 52).

1.1.2 Aktuelle Therapieoptionen des HNSCC

Zurzeit besteht die Standardtherapie im frühen Tumorstadium I oder II aus einer operativen Resektion des Tumors oder einer Strahlentherapie, je nach operativer Zugänglichkeit des Befundes und Komorbiditäten des Patienten (29). Im fortgeschrittenen Tumorstadium III oder IV wird zumeist eine operative Entfernung des Tumors mit Resektion der drainierenden Lymphknoten (Neck Dissection) in Kombination mit einer adjuvanten Strahlentherapie und gegebenenfalls einer platinbasierten Chemotherapie durchgeführt (17, 29, 40). Bei inoperablem Befund, dem Vorliegen von Fernmetastasen oder anderweitigen Kontraindikationen für eine Operation kann alternativ eine definitive simultane Chemoradiotherapie (CRT) erfolgen (17, 29).
Mit Hilfe der genannten Therapiemöglichkeiten können zwar gute Erfolge bei der Behandlung der Ersterkrankung erzielt werden, das häufige Auftreten von Tumor-Rezidiven wird jedoch nicht verhindert (17). Im Rezidivstadium ist aufgrund von Voroperationen, Komorbiditäten oder Radioresistenz der Tumorzellen eine chirurgische oder strahlentherapeutische Behandlung des Tumors oft nicht mehr möglich (49). Zur Therapie von HNSCC Rezidiven stand daher lange nur eine Platin-basierte Chemotherapie in Kombination mit Cetuximab, einem gegen den epidermal-

growth-factor-receptor (EGFR) gerichteten Antikörper, zur Verfügung. Die Ansprechraten auf diese Therapie liegen bei 20-30% und die mediane Überlebenszeit beträgt 10,1 Monate (49, 62). Seit 2016 in den USA und 2017 in Europa sind die beiden gegen das programmed cell death protein 1 (PD1) gerichteten monoklonalen Antikörper Pembrolizumab und Nivolumab zur Therapie des rezidivierten oder metastasierten HNSCC zugelassen (9, 15). PD1 ist ein Immun-Checkpoint Molekül, welches an der Zelloberfläche von T- und B-Lymphozyten exprimiert wird und die entzündliche Aktivität der Immunzellen inhibiert. Tumorzellen exprimieren häufig den PD1 Liganden PDL1 (progammed death ligand 1) und können durch die Bindung an PD1 eine gegen sie gerichtete Immunantwort unterdrücken (16, 43). Die genannten Substanzen gehören zur Gruppe der Immun-Checkpoint-Inhibitoren und können durch die Blockade der immunsuppressiven PD1-PDL1 Interaktion eine aktive, gegen den Tumor gerichtete Immunzellantwort generieren oder reaktivieren. In anderen Tumorentitäten, wie dem malignen Melanom oder dem Nicht-Kleinzelligen Lungenkarzinom (NSCLC), wurden durch diese neuartigen Therapiekonzepte bereits deutliche Behandlungserfolge erzielt (13, 41). Beim HNSCC ist die Therapieansprechrate mit etwa 15% derzeit vergleichsweise gering und auch die Überlebenszeit der Patienten konnte im Vergleich zur bisherigen Standardtherapie mit einem Platinderivat und Cetuximab nur geringfügig verbessert werden (9, 15).

Als wichtige Kriterien für das Therapieansprechen auf Immun-Checkpoint-Inhibitoren werden zum einen die PDL1-Expressionsstärke des Tumorgewebes, die mittels immunhistochemischer Analyse bestimmt werden kann, und zum anderen die Zusammensetzung der Tumorimmunumgebung angesehen (8, 25, 37). Zudem stellt die Tumormutationslast (TMB, engl. tumor mutational burden) einen unabhängigen prädiktiven Faktor des Therapieansprechens dar (20). Hierbei wird die Anzahl nicht-synonymer Mutationen des Tumors mittels Sequenzierung der nächsten Generation (NGS, engl. next generation sequencing) bestimmt. Bei hoher TMB entstehen vermehrt modifizierte Peptidsequenzen, die als Neoantigene über eine Präsentation mittels Haupthistokompatibilitätskomplex I (MHC I) eine antitumorale T-Zell-Immunantwort generieren können. Diese wiederum bildet eine entscheidende Grundlage des Wirkmechanismus von Immun-Checkpoint-Inhibitoren.

In den verschiedenen Tumorentitäten ist zumeist eine Bestimmung der PDL1-Expression des Tumorgewebes in der pathologischen Diagnostik erforderlich, um die entsprechende Substanz gemäß den Leitlinien anwenden zu dürfen (8, 9). Hierzu wird üblicherweise der Anteil der Tumorzellen mit einer spezifischen membranären immunhistochemischen Färbung gegen PDL1 an allen Tumorzellen als „tumor positivity score“ (TPS), der Anteil der Fläche der positiv gefärbten Immunzellen an allen Tumor-Immunzellen als „immune cell score“ (IC) sowie der Anteil der Fläche aller positiv gefärbten Zellen an der Gesamttumorfläche als „combined positivity score“ (CPS)

bestimmt (8). Derzeit stehen hierfür verschiedene anti-PDL1-Antikörper-Klone zur Verfügung. In den USA ist die Anwendung des in der Diagnostik zu verwendenden Antikörper-Klons durch die Federal Drug Administration (FDA) entsprechend der Zulassungsstudien zum Teil vorgeschrieben. Beim fortgeschrittenen Nicht-Kleinzelligen-Lungenkarzinom (NSCLC) ist beispielsweise die Anwendung von Pembrolizumab auf eine vorherige diagnostische Testung mit dem Antikörper-Klon 22C3 beschränkt (45). Die European Medicines Agency (EMA) schreibt jedoch keine Nutzung eines spezifischen Antikörper-Klons vor (51). In Studien zum NSCLC und anderen Tumorentitäten konnten vergleichbare Färberesultate bei Verwendung verschiedener Antikörper bestätigt werden, beim HNSCC ist eine solche Studie noch ausstehend (51). Zur therapeutischen Anwendung von Pembrolizumab ist beim HNSCC Rezidiv ein TPS ≥ 50% in der Zweitlinientherapie nach Cisplatin-Versagen beziehungsweise ein CPS ≥ 1 in der palliativen Erstlinientherapie erforderlich (8).

1.1.3 Die immunologische Tumormikroumgebung und ihre Beeinflussung durch den Tumormetabolismus

Die immunologische Tumormikroumgebung (TIME, engl. tumor immune microenvironment) gilt als essenzieller Einflussfaktor sowohl auf die Prognose als auch auf das Therapieansprechen bei den meisten soliden Tumoren. Grundlegend lässt sich das Immunzellinfiltrat von Tumoren entsprechend der prognostischen Relevanz in drei verschiedene Kategorien wie folgt einteilen (3, 37, 46, 48, 60):

1. „Heiße“ (hot) Tumore mit einer dichten Infiltration durch antitumorale Immunzellen. Hierzu zählen insbesondere CD8+ zytotoxische T-Zellen, CD4+ T-Helfer-Zellen und Natürliche Killerzellen (NK-Zellen) sowie eine hohe Expression zytotoxischer Proteine wie Perforin und Granzym.
2. „Kalte“ (cold) Tumore mit Infiltration durch wenige der oben genannten antitumoralen Immunzellen und vermehrt protumoralen Immunzellen wie regulatorischen T-Zellen und myeloiden Suppressorzellen (MDSC engl. Myeloid-derived suppressor cells).
3. Vom Immunzellinfiltrat „ausgesparte“ Tumore (excluded), bei denen sich lediglich in der Peripherie des Tumors aktive Immunzellen finden.

Die beste Ansprechrate auf die neuartigen Immun-Checkpoint-Inhibitoren wird im Allgemeinen und auch bei Kopf-Hals-Karzinomen bei „heißen“ Tumoren erzielt (25). Zudem zeichnet sich diese Gruppe von Tumoren durch eine bessere Prognose als immunologisch „kalte“ Tumore aus (48).

Beeinflusst wird das Tumorimmunzellinfiltrat unter anderem durch den Tumormetabolismus. Hier ist seit langem der „Warburg-Effekt“ bekannt, unter dem man die Energiegewinnung von Tumorzellen mittels anaerober Glykolyse statt aerober oxidativer Phosphorylierung trotz ausreichend vorhandenen Sauerstoffs versteht (23). Durch die anaerobe Glykolyse kommt es in der extra-

zellulären Matrix von Tumoren vermehrt zur Akkumulation von Laktat. Dieses wiederum hat einen immunsuppressiven Effekt auf zytotoxische T-Zellen und NK-Zellen und schützt so den Tumor vor einer effektiven antitumoralen Immunantwort (31, 32, 38). Dementsprechend konnte für viele Tumorentitäten einschließlich HNSCC gezeigt werden, dass ein anaerober Tumormetabolismus mit einer „kalten" TIME assoziiert und durch eine schlechte Prognose gekennzeichnet ist (31).

1.1.4 Fragestellung und Zielsetzung

Das Ziel der im Folgenden vorgestellten Studien war es, die TIME von Patienten mit Kopf-Hals-Karzinomen besser zu charakterisieren und wichtige Einflussfaktoren zu bestimmen, um mögliche neue immuntherapeutische Angriffspunkte zu erarbeiten und bestehende Therapiekonzepte zu verbessern.

Zunächst stellten wir hierzu eine umfassende retrospektive Kohorte von Patienten zusammen, von denen Tumormaterial zur weiteren Analyse und klinisch-pathologische Daten vorlagen. Diese Kohorte wurde zur Erarbeitung der Forschungsfragen der ersten drei aufgeführten Originalarbeiten verwendet. Für die Originalarbeit 3 konnte zudem auf eine umfangreiche HNSCC Validierungskohorte des Instituts für Pathologie der Universitätsklinik Bonn zurückgegriffen werden.

In der Originalarbeit 1 arbeiteten wir heraus, ob es möglich ist, anhand der Verteilung und der Zusammensetzung des Immunzellinfiltrats im routinemäßigen Hämatoxylin-Eosin (HE) gefärbtem histologischen Schnitt eine Aussage über die Prognose zu treffen. Originalarbeit 2 widmete sich der Frage, ob die Nutzung verschiedener anti-PDL1-Antikörper in der immunhistochemischen Bestimmung der PDL1-Expression gleichwertige Ergebnisse erbringt. Auf der Evaluation der PDL1-Expression ist in den meisten Fällen die weitere Therapieentscheidung zur Anwendung von Immun-Checkpoint-Inhibitoren begründet. Originalarbeit 3 beschäftigte sich mit Unterschieden in der Zusammensetzung des Tumorimmuninfiltrats von Primärtumoren und Rezidiven und deren Einfluss auf die Rezidiventstehung sowie dem Zusammenhang mit einer vorangegangenen Chemoradiotherapie (CRT). Das Ziel der in dieser Studie erstmals durchgeführten Differenzierung des Immuninfiltrats des Tumorrezidivs vom Primärtumor war es, eine immunonkologische Grundlage zur Verbesserung der weiterhin stark eingeschränkten Therapiemöglichkeiten in der Rezidivsituation zu schaffen. In Originalarbeit 4 führten wir eine bioinformatische *in silico* Analyse von HNSCC anhand frei verfügbarer Expressions- und Mutationsdaten der The-Cancer-Genome-Atlas (TCGA) Datenbank durch, um mögliche neue therapeutische Angriffspunkte zu finden, die einen Einfluss auf eine effektive antitumorale Immunantwort haben. Hierbei konnten wir die Histon-Acetyltransferase E1A Binding Protein P300 (EP300) als wichtigen Modulator der TIME in HNSCC sowie in einer Vielzahl anderer solider Tumorentitäten identifizieren und die zugrundeliegenden Mechanismen mittels funktioneller Analysen weiter ausarbeiten.

1.2 Material und Methoden

1.2.1 Zusammenstellung von HNSCC Patienten Kohorten

Ein wesentlicher Bestandteil der Analysen der Originalarbeiten 1, 2 und 3 basiert auf zwei großen retrospektiven HNSCC Patienten Kohorten. Von den Patienten lagen jeweils archivierte Gewebeproben und ausführliche klinisch-pathologische Daten vor. Die Hauptkohorte (Lübeck) bestand aus 419 Patienten, die in den Jahren 2001-2016 gemäß den aktuellen deutschen Leitlinien am Institut für Hals-Nasen-Ohrenheilkunde der Universitätsklinik Schleswig-Holstein, Campus Lübeck, behandelt wurden und deren Gewebeproben am Institut für Pathologie der Universität zu Lübeck archiviert wurden. Von 63 Patienten lagen sowohl Gewebeproben vom Primärtumor als auch vom korrespondierenden Tumorrezidiv und von 13 dieser Patienten ebenfalls vom Zweitrezidiv vor. Die Validierungskohorte (Bonn) wurde zur unabhängigen Validierung der Daten der Originalarbeit 3 genutzt und bestand aus 237 Primärtumoren und 45 Rezidiven, die in Kooperation mit dem Institut für Pathologie der Universität Bonn zur Verfügung gestellt wurden.

Aus den vorliegenden Gewebeproben wurden zur weiteren Analyse Gewebemikroarrays (TMA, engl. tissue microarray) erstellt. Hierzu wurde das jeweilige Tumorareal von einem erfahrenen Pathologen am HE-Schnittpräparat markiert und mit dem zugrundeliegenden Paraffin-Blockpräparat korreliert. Aus diesem wurden unter Verwendung eines semi-automatischen Tissuearrayers (Estigen AlphaMetrix Biotech, Rödemark, Deutschland) drei repräsentative Tumorareale von 0,6 mm Durchmesser ausgestanzt und in einen TMA-Paraffinblock überführt. Auf diese Weise ließen sich bis zu 180 Einzelproben von bis zu 60 Patienten auf einem histologischen Schnitt darstellen.

Die jeweiligen Studien wurden von den Ethikkommissionen der Universität zu Lübeck und der Universität Bonn entsprechend der Deklaration von Helsinki geprüft und zugelassen. Von den eingeschlossenen Patienten lag die generelle Einwilligung zur Teilnahme an wissenschaftlichen Studien vor. Die Patientendaten wurden vor der weiteren Analyse anonymisiert.

1.2.2 Immunhistochemische Analysen

Zur spezifischen Identifizierung einzelner Immunzelltypen des Tumorimmuninfiltrats anhand der Expression von Marker-Proteinen (Originalarbeit 3) sowie zur Evaluation der Färbeintensität bei Verwendung verschiedener anti-PDL1-Antikörper-Klone (Originalarbeit 2) wurden immunhistochemische Färbungen erstellt. Hierzu wurden 4 µm dicke Paraffinschnitte der zuvor erstellten TMAs mit dem OptiView DAB IHC Detection Kit auf einem Ventana BenchMark Ultra (beide Roche, Basel, Schweiz) gegen die folgenden Antikörper gemäß den Herstellerangaben gefärbt: CD4 (SP35, Ventana), CD8 (SP57, Ventana), CD20 (L26, Ventana), CD1A (EP3622, Cell Marque), CD68 (KP-1,

Ventana), CD56 (MRQ-42, Cell Marque), FOXP3 (236A/E7, Invitrogen), PD1 (NAT105, Cell Marque), Tryptase (G3, Cell Marque), CD15 (MMA, Ventana), DC-LAMP (101E1.01, Novus Biologicals), PDL1 (verschiedene Klone: E1L3N (Cell Signaling Technology), SP263 (Ventana), SP142 (Ventana), 28-8 (Abcam), 22C3 (Agilent Dako Omnis)). Zur Identifizierung von tertiären lymphoiden Strukturen (TLS) in Originalarbeit 3 wurden zudem immunhistochemische Doppelfärbungen gegen CD20 (rot, L26, Ventana) und ERG (braun, EPR3864, Abcam) am ganzen histologischen Schnittpräparat durchgeführt. Die Spezifität der angewendeten immunhistochemischen Färbung wurde jeweils durch einen erfahrenen Pathologen bestätigt. Bei Auswertung der TMA-basierten immunhistochemischen Färbungen wurde jeweils der Mittelwert aus drei TMA-Stanzen pro Patient berechnet.

In Originalarbeit 2 wurden der TPS, IC und CPS der verschiedenen PDL1 Färbungen von zwei unabhängigen Pathologen unter Verblindung gegenüber den Patientendaten bestimmt, um hierdurch die Situation in der Routine-Diagnostik bestmöglich abzubilden.

Die quantitative Auswertung der Zusammensetzung des Immunzellinfiltrats in Primärtumoren und Rezidiven in Originalarbeit 3 erfolgte unter Verwendung des semiautomatischen Bildanalyseprogramms Definiens Developer XD 2.0. Hierbei wurde die Anzahl des jeweiligen Immunzellsubtyps in Relation zur Tumorfläche in mm^2 anhand der Expression des jeweils spezifischen Markerproteins bestimmt. Sowohl intratumorale Immunzellen als auch Immunzellen im angrenzenden Tumorstroma wurden hierbei berücksichtigt. Die *in vitro* Spheroid-Experimente der Originalarbeit 3 wurden auf dieselbe Weise unter Verwendung von QuPath 0.1.2 ausgewertet. Zur Analyse der TLS wurde mithilfe von QuPath 0.1.2 am ganzen histologischen Schnitt die Anzahl der TLS, definiert als Aggregate von CD20+ B-Lymphozyten in Assoziation zu ERG+ Venulen, pro Fläche des peritumoralen Stromas in mm^2 nach Annotation durch einen gegenüber den Daten verblindeten erfahrenen Pathologen berechnet.

1.2.3 RNA Extraktion und Genexpressions-Analyse

In Originalarbeit 3 wurde die Expressionsstärke von 730 immunassoziierten Genen *in vivo* und *in vitro* bestimmt. Hierzu wurde von 18 Patienten RNA aus den Paraffin-Blockpräparaten des jeweiligen Primärtumors und des korrespondierenden Rezidivs isoliert, indem sechs bis acht 8 µm dicke Schnitte des Paraffinblocks auf einem Glasobjektträger aufgebracht wurden und das jeweilige Tumorareal in Korrespondenz zum zugrundeliegenden HE-Schnitt mit einem Skalpell entnommen wurde. Nach Deparaffinierung mit Xylen wurde die RNA des Gewebes unter Verwendung des Maxwell RSC Instruments und des Maxwell RSC RNA FFPE Kits (beide Promega, Madison, WI, USA) entsprechend den Herstellerangaben isoliert. Zudem wurde RNA aus *in vitro*

Spheroiden isoliert (vgl. 1.2.4). Hierzu wurde das RNeasy Mini Kit (Qiagen, Hilden, Deutschland) entsprechend den Herstellerangaben verwendet.

Das nCounter PanCancer Immune Profiling Panel (NanoString Technologies, Seattle, WA, USA) wurde zur Analyse der RNA-Expression der beschriebenen Proben entsprechend den Herstellerangaben verwendet. Das genutzte Verfahren basiert auf einer direkten spezifischen Hybridisierung des jeweiligen RNA-Transkripts mit einem farbcodierten Marker-Molekül, sodass kein vorheriges Umschreiben des RNA-Transkripts in cDNA wie bei anderen konventionell genutzten Methoden notwendig ist. Nach erfolgter Hybridisierung wurden die farbcodierten Proben mittels nCounter Digital Analyzer ausgelesen und die gewonnen Daten mittels nSolver 4.0 Analysis Software (beide Nanostring Technologies, Seattle, WA, USA) und R 3.5.0 ausgewertet.

1.2.4 Zellkulturexperimente

Zur weiteren funktionellen Aufarbeitung der *in vivo* Analysen der Originalarbeit 3 wurde ein dreidimensionales Modell einer Kokultur von Tumorspheroiden und Immunzellen entwickelt, um Auswirkungen einer häufig beim HNSCC Rezidiv vorkommenden Therapieresistenz *in vitro* darstellen zu können. Hierzu wurde aus der von einem Hypopharynx-Karzinom stammenden FaDu Zelllinie die Cisplatin-resistente Zelllinie FaDu/CR entwickelt, indem die parentale Zelllinie FaDu/WT über 6 Monate mit von 0,1 µg/mL auf 0,7 µg/ml steigenden Konzentrationen von Cisplatin NeoCorp (Hexal, Holzkirchen, Deutschland) behandelt wurde. Anschließend wurde ein Methyl-thiazolyl-tetrazolium bromide (MTT) assay zur Resistenztestung durchgeführt. Eine strahlentherapieresistente Zelllinie FaDu/RR wurde in Kooperation mit der Arbeitsgruppe von Prof. Anna Dubrovska des Zentrums für Medizinische Strahlenforschung in der Onkologie Dresden zur Verfügung gestellt und bereits umfangreich charakterisiert. Alle Zelllinien wurden bei 5% CO_2, 37 °C und 85% Luftfeuchtigkeit in Dulbecco's Modified Eagle's Medium (Thermo Fisher Scientific, Waltham, MA, USA) mit 10% fetalem Kälberserum (Biochrom, Berlin, Deutschland), 1% Penicillin-Streptomycin und 1% L-Glutamin (beide Thermo Fisher Scientific, Waltham, MA, USA) inkubiert.

Aus den Zelllinien FaDu/WT, FaDu/CR und FaDu/RR wurden dreidimensionale Tumorspheroide geschaffen, indem je 20.000 Zellen in 20 µl Zellkulturmedium als herabhängende Tropfen auf dem Deckel einer 24-Well-Platte aufgebracht und für 5 Tage inkubiert wurden. Die an den Spitzen des Tropfens entstandenen Spheroide wurden daraufhin in die vorher mit Agarose-Gel beschichteten Vertiefungen der 24-Well-Platte zusammen mit 1 ml Zellkulturmedium überführt. Anschließend wurden 50.000 aktivierte mononukleäre Zellen des peripheren Blutes (PBMCs, engl. Peripheral Blood Mononuclear Cells) hinzugefügt und die so erstellte Spheroid-Immunzell-Kokultur für 72 Stunden inkubiert. PBMCs wurden zuvor aus dem Vollblut von gesunden Spendern mittels dichteabhängiger Zentrifugation mit dem Ficoll-Paque Plus (GE Healthcare, Chicago, IL, USA)

isoliert und über 72 Stunden in RPMI-1640 Medium mit 1 µg/ml anti-CD3-Antikörper, 5 µg/ml anti-CD28-Antikörper und FaDu-Zell-Lysaten aktiviert. Zur weiteren Analyse wurden die koinkubierten Spheroide entnommen, mit 4 % Formaldehyd fixiert und in Paraffin eingebettet. Die Auswertung des Immunzellinfiltrats der Spheroide erfolgte mittels immunhistochemischer Färbung wie unter 1.2.2 beschrieben.

1.2.5 Bioinformatische *in silico* Analyse

Die TCGA Datenbank sowie die L1000 Connectivity Map wurden zur *in silico* Analyse in Originalarbeit 4 genutzt. Die TCGA Datenbank ist ein seit 2006 bestehendes amerikanisches Projekt des National Cancer Institute und des National Human Genome Research Institute, das derzeit molekulare Daten auf DNA-, RNA- und Proteinebene sowie histologische Schnittbilder und klinische Daten von über 20.000 Primärtumoren und assoziiertem Normalgewebe von 33 verschiedenen Krebsarten frei zur Verfügung stellt. Im Zuge von Originalarbeit 4 werteten wir Mutations- und Genexpressionsdaten von 7564 Patienten und 18 Krebsentitäten aus, unter denen 530 Plattenepithelkarzinome des Kopf-Hals-Bereichs enthalten waren. Der Zugriff auf die Daten erfolgte über die Plattform CBioPortal (https://www.cbioportal.org) und das Digital Slide Archive (DSA, https://cancer.digitalslidearchive.org). Zur weiteren funktionellen Aufarbeitung wurde auf Daten der L1000 Connectivity Map zurückgegriffen. Diese stellt Informationen von 1,5 Millionen Genexpressions-Profile verschiedener Zelllinien vor und 96 Stunden nach Inkubation mit etwa 5000 niedermolekularen Inhibitoren und etwa 3000 Reagenzien frei zur Verfügung und erlaubt so Veränderungen der Genexpression zu untersuchen. Die Daten wurden mithilfe der Analyseplattform Genevestigator (Nebion AG, Zürich, Schweiz) ausgewertet.

1.2.6 Statistische Auswertung

Folgende Programme wurden zur statistischen Auswertung in den jeweiligen Originalarbeiten verwendet: IBM SPSS Statistics Version 25.0 für Windows (IBM Corp., Armonk, NY, USA; Originalarbeit 1, 3, 4), GraphPad Prism Version 8.3.0 (GraphPad Software, San Diego, CA, USA; Originalarbeit 3, 4) und Python 2.7 (Canopy distribution 1.1.0.1371, Enthought, Austin, TX, USA; Originalarbeit 2). P-Werte kleiner als 0,05 wurden als statistisch signifikant gewertet. Die im Einzelnen verwendeten statistischen Tests werden jeweils im folgenden Ergebnisteil aufgeführt.

1.3. Ergebnisse

1.3.1 Klinisch-pathologische Charakterisierung zweier unabhängiger HNSCC Patienten Kohorten (Originalarbeiten 1-3)

Die Grundlage der *in vivo* untersuchten Forschungsfragen der Originalarbeiten 1 bis 3 bildet die retrospektive HNSCC Hauptkohorte (Lübeck), welche in ihrer Zusammensetzung die Epidemiologie von Kopf-Hals-Karzinom Patienten in Europa und den USA widerspiegelt. 22,5% der 419 eingeschlossenen Patienten waren weiblich, 77,5% männlich. 27,7% zeigten in der immunhistochemischen Analyse eine Expression von p16 als Surrogat-Parameter für eine Infektion mit dem Humanen Papillomavirus (HPV). 25,1% der Patienten entwickelten im Untersuchungszeitraum ein Lokalrezidiv. Von 63 Patienten lag sowohl Tumormaterial vom Primärtumor als auch vom Lokalrezidiv und von 13 dieser Patienten ebenfalls vom Zweitrezidiv vor. 20,8% der Primärtumore waren in der Mundhöhle, 12,2% im Hypopharynx, 33,7% im Oropharynx und 27,2% im Larynx lokalisiert. Bei 6,2% lag eine andere Lokalisation des Primärtumors oder eine Krebserkrankung mit unbekanntem Primärtumor (CUP, engl. cancer of unknown primary) vor. Die Fälle teilten sich etwa zur Hälfte in die niedrigen UICC Tumorstadien I oder II und die hohen Tumorstadien III oder IV auf. Die Fünf-Jahres-Überlebensrate betrug 61,9%.

Eine zweite unabhängige HNSCC Patientenkohorte (Bonn) wurde in Originalarbeit 3 als Validierungskohorte verwendet. Die Validierungskohorte enthielt 237 Primärtumore und 45 Rezidive. Die klinisch-pathologischen Charakteristika glichen in ihrer Zusammensetzung der Hauptkohorte. 71% der Patienten waren männlich, die 5-Jahres-Überlebensrate betrug 64%, 29,4% der Tumore waren in der Mundhöhle lokalisiert, 8,7% im Hypopharynx, 35,9% im Oropharynx und 26% im Larynx. Auch die Verteilung der Tumorstadien war vergleichbar zur Hauptkohorte.

1.3.2 Routinediagnostische Charakterisierung des HNSCC Tumorimmuninfiltrats zur Prognosebestimmung (Originalarbeit 1)

Die prognostische Relevanz der Zusammensetzung des Tumorimmuninfiltrats in Kopf-Hals-Karzinomen ist bereits durch mehrere Arbeitsgruppen beschrieben worden. Eine Übertragung auf die allgemeine Routinediagnostik ist bisher jedoch vor allem auch wegen häufig methodisch aufwendiger Ansätze noch nicht erfolgt. In Originalarbeit 1 teilten wir daher das Tumorimmuninfiltrat von 289 Primärtumoren und 42 Rezidiven der Hauptkohorte am Routinediagnostischen HE-Schnittpräparat in die bereits beschriebenen anerkannten Kategorien „heiß“, „kalt“ und „ausgespart“ ein und korrelierten diese mit den klinisch-pathologischen Daten.

Bei den Primärtumoren konnte der Immun-Phänotyp mehrheitlich als „ausgespart“ (52,6%) charakterisiert werden, während die übrigen Tumore fast gleichermaßen in die Kategorien "kalt"

(24,2%) und "heiß" (23,2%) fielen. Bei den Rezidiven ließ sich die überwiegende Mehrheit entweder als "kalt" (47,6%) oder "ausgespart" (42,9%) und nur ein kleiner Teil als "heiß" (9,5%) definieren. Die Analyse der Überlebensdaten nach der Kaplan-Meier-Methode ergab im Log-rank-Test eine signifikant schlechtere Überlebensrate der „kalten“ Primärtumore im Vergleich zu den „heißen“ oder „ausgesparten“ Primärtumoren ($p<0.017$, nach Bonferroni-Korrektur). Um zu untersuchen, ob die HE-morphologische Kategorisierung des Immunfiltrats als unabhängiger Prognosefaktor dienen kann, führten wir eine multivariate Cox-Regressionsanalyse in Bezug auf das Tumorimmuninfiltrat, Patientenalter, UICC Stadium, T Stadium, Geschlecht, Grading und den p16 Status durch. Sowohl das Immunzell-Verteilungsprofil (Hazard Ratio (HR)=0,527; p=0,003) als auch der p16 Status (HR=0.353; p=0.001) stellten unabhängige Prognosefaktoren in den untersuchten Primärtumoren dar. Bei den HNSCC Rezidiven zeigte sich ein Trend hin zu einer schlechteren Überlebensrate der „kalten“ Rezidive ohne statistisch signifikante Unterschiede.

1.3.3 Bewertung des HNSCC PDL1-Status in Abhängigkeit des verwendeten anti-PDL1-Antikörper-Klons in der Routinediagnostik (Originalarbeit 2)

Zur Bestimmung der PDL1-Expression stehen derzeit verschiedene diagnostisch genutzte anti-PDL1-Antikörper zur Verfügung, die an unterschiedlichen Positionen des PDL1 Moleküls binden. Gründe für die Verwendung verschiedener Antikörper-Klone können je nach Institution in preislichen Unterschieden sowie dem jeweils verfügbaren Färbeautomaten liegen. Bisher lagen noch keine Studienergebnisse zur Variabilität der Färbung und der darauffolgenden Therapieentscheidung in Abhängigkeit des verwendeten Antikörper-Klons im HNSCC vor.

Wir färbten daher die Primärtumore und Rezidive unserer Hauptkohorte mit den für die Routine-Diagnostik verfügbaren anti-PDL1-Antikörper-Klonen SP263, SP142, E1L3N, 28-8 und 22C3 immunhistochemisch an und bestimmten den jeweiligen TPS, IC und CPS durch einen erfahrenen Pathologen. Hierbei zeigte sich eine deutliche Variabilität der Färbungen. Gemessen an der klinischen Konsequenz einer Erstlinientherapie mit Pembrolizumab konnte an der getesteten Kohorte bei Verwendung von SP142 in 14%, bei 22C3 in 18%, bei E1L3N in 48%, bei SP263 in 68% und bei 28-8 in 78% eine Therapieempfehlung ausgesprochen werden. In der statistischen Auswertung möglicher ähnlicher Färbungsmuster durch eine Hauptkomponentenanalyse (PCA, engl. principal component analyis) zeigten sich Ähnlichkeiten des TPS der Antikörper SP142, 22C3 und EL13N sowie 28-8 und SP263, die sich jedoch bei den entsprechenden ICs nicht wiederfanden. Eine nicht-negative Matrix-Faktorisierung (NMF) zeigte eine Clusterbildung von SP263 und 28-8 für k=2 Cluster, die jedoch eine niedrige kophenetische Korrelation besaß. Die maximale kophenetische Korrelation wurde für k=10 Cluster erreicht und entsprach damit der

Anzahl der eingesetzten Klone für den TPS und IC. Eine statistisch stabile Ähnlichkeit der verschiedenen Färbungen bestand somit nicht.

1.3.4 Tumorimmunevasion im HNSCC Rezidiv im Zusammenhang mit aktuellen Therapiekonzepten (Originalarbeit 3)

Bisher beschränkt sich der Einsatz von therapeutisch genutzten anti-PD1-Antikörpern im HNSCC auf rezidivierte oder metastasierte Tumore. Neben der PDL1-Expression des Tumorgewebes ist ein entscheidender Faktor für das Therapieansprechen die Zusammensetzung der TIME. Wir arbeiteten daher in Originalarbeit 3 Unterschiede der TIME in Primärtumoren und Rezidiven der Haupt- und Validierungskohorte heraus und schlossen zur weiteren Aufarbeitung funktionelle *in vitro* Untersuchungen an Tumorspheroiden an.

Zunächst analyisierten wir das Immunzellinfiltrat der Primärtumore und der korrespondierenden Rezidive der Hauptkohorte. Unterschiede in der Verteilung folgender Immunzelltypen wurden hierbei betrachtet: CD8+ zytotoxische T-Zellen, CD20+ B-Lymphozyten, CD4+ T-Helfer Zellen (Th Zellen), FOXP3+ regulatorische T-Zellen (Tregs), PD1+ Zellen, CD56+ Natürliche Killerzellen (NK-Zellen), CD1A+ dendritische Zellen, DC-LAMP+ reife dendritische Zellen, CD68+ Makrophagen, CD15+ neutrophile Granulozyten, Tryptase+ Mastzellen. Zusätzlich wurden Unterschiede in der PDL1-Expression untersucht. Insgesamt konnten wir einen Trend hin zu einer Abnahme der verschiedenen Lymphozyten-Subtypen vom Primärtumor zum Rezidiv und insbesondere zum teils vorhandenen Zweitrezidiv beobachten. Am deutlichsten zeigte sich dies als subtotale Depletion der CD20+ B-Lymphozyten in den Zweitrezidiven ($p=0,036$). Auch die Dichte der CD8+ zytotoxischen T-Zellen als Hauptbestandteil einer aktiven antiumoralen Immunantwort nahm in den Zweitrezidiven signifikant ab ($p=0,045$). CD56+ NK-Zellen und FOXP3+ Tregs nahmen ebenfalls in den Zweitrezidiven signifikant ab ($p=0,036$ und $p=0,047$). Die Dichte der CD68+ Makrophagen, CD15+ neutrophile Granulozyten und Tryptase+ Mastzellen, die allesamt eine myeloische Abstammung aufweisen, zeigten in den Primärtumoren und Rezidiven keine signifikanten Unterschiede. CD1A+ dendritische Zellen stellten den einzigen Zelltyp mit signifikanter Zunahme in den Erst- und Zweitrezidiven dar ($p=0,013$ und $p=0,036$). DC-LAMP+ reife dendritische Zellen wiesen hingegen eine signifikante Abnahme in den Erst- und Zweitrezidiven auf ($p=0,0023$ und $p=0,0719$).

Zur Validierung der Unterschiede im Immuninfiltrat von Primärtumoren und Rezidiven unserer Hauptkohorte führten wir ähnliche Analysen in der Validierungskohorte (Bonn) durch. Hier konnten wir die subtotale Depletion von B-Lymphozyten sowie eine deutliche Abnahme der CD8+ zytotoxischen T-Zellen in den Rezidiven bestätigen (beide $p<0.0001$). Der signifikante Anstieg

CD1A+ dendritischer Zellen in den Rezidiven der Hauptkohorte bestätigte sich in der Validierungskohorte nicht.

Da bereits bekannt ist, dass eine adjuvante Chemoradiotherapie (CRT) die TIME beeinflussen kann, untersuchten wir im Folgenden, ob eine adjuvante CRT im Zusammenhang mit der beobachteten Abnahme verschiedener Immunzellsubtypen in HNSCC Rezidiven steht. Hierzu unterteilten wir unsere Hauptkohorte in eine Subgruppe, die eine CRT vor der Entstehung des ersten oder zweiten Rezidivs erhalten hatte (n=35), und eine zweite Subgruppe, bei der die chirurgische Tumorresektion die einzige Therapie vor der Entstehung des Rezidivs gewesen war (n=28). In der Subgruppenanalyse zeigte sich eine deutliche CRT-Abhängigkeit der Abnahme der B-Lymphozyten in den Rezidiven. Bei vorausgegangener CRT nahmen die B-Lymphozyten von durchschnittlich 471,3 Zellen/mm² in den Primärtumoren zu 23,5 Zellen/mm² in den Rezidiven stark ab (p=0,0006) wohingegen eine konstante Zahl an B-Lymphozyten von etwa 500 Zellen/mm² in der Subgruppe der Rezidive nach alleiniger Resektion zu finden war (p=0,59).

Zur weiteren Aufarbeitung der TIME von Primärtumoren und korrespondierenden Rezidiven nach vorangegangener CRT schlossen wir bei 18 Patienten dieser Subgruppe eine Analyse des mRNA Expressionsprofils von 730 immunassoziierten Genen mittels nCounter PanCancer Immune Profiling Panel (NanoString) an. In einer nicht-überwachten hierarchischen Clusteranalyse nach euklidischer Distanz ergab sich hier für k=2 eine signifikante Aufteilung der Primärtumore und der Rezidive nach CRT basierend auf einer insgesamt höheren normalisierten Expression der immunassoziierten Gene in der Gruppe der Rezidive nach CRT (p=0,018). Dieses Resultat zeigte, dass sich in der RNA-Analyse die TIME der Primärtumore und Rezidive nach CRT jeweils untereinander stärker ähnelten als die TIME des Primärtumors und Rezidivs desselben Patienten. In der weiteren Analyse der RNA-Expressionsdaten bestimmten wir unter Verwendung der NSolver 4.0 Analyse Software die Infiltration durch verschiedene Immunzellsubtypen anhand der RNA-Expression immunassoziierter Markerproteine. Diese Analyse bestätigte die Abnahme der Gesamtzahl der tumor-infiltrierenden Leukozyten (TILs) (p=0,0004), den Verlust von B-Lymphozyten/ TILs (p<0,0001) und den Anstieg von dendritischen Zellen/ TILs (p=0,0002) in den Rezidiven nach CRT, wie bereits in der proteinbasierten immunhistochemischen Aufarbeitung beobachtet. Zudem zeigte die RNA-basierte Analyse einen relativen Anstieg der folgenden myeloischen Zelltypen im Vergleich zur Gesamtzahl der TILs: Neutrophile Granulozyten (p=0,018), Mastzellen (p=0,0057) und Makrophagen (p<0,0001). Bei der Auswertung einzelner stark unterschiedlich exprimierter Gene der beiden Gruppen ergab sich die stärkste Herunterregulation in den Rezidiven nach CRT für CD20, CD19, CD79A und CD22, die alle Teil des B-Lymphozyten-Rezeptorkomplexes sind. Zudem waren die Gene der Chemokininteraktion CCL19, CCR7, CXCL13, CXCR5, CCL14 und LTB, die allesamt im Zusammenhang mit der Entstehung tertiärer lymphoider

Strukturen (TLS) in der Tumorumgebung beschrieben sind, sowie ICAM-2 und ICAM-3, die zur Leukozytenextravasion aus hochendothelialen Venulen in TLS beitragen, in den Rezidiven nach CRT stark herunterreguliert.

Aufgrund der spezifischen Herunterregulation von Genen, die mit TLS und B-Lymphozyten assoziiert sind, verglichen wir das Vorkommen von TLS an den Gewebeschnitten von je 12 gepaarten Primärtumoren und Rezidiven mit und ohne vorherige CRT mittels immunhistochemischer Doppelfärbung gegen CD20 als B-Lymphozyten Marker und ERG als Marker für hochendotheliale Venulen. Hierbei konnten wir eine signifikante Abnahme der Anzahl der TLS an der Tumorfläche in den Rezidiven nach CRT verglichen zu den korrespondierenden Primärtumoren feststellen ($p=0,0113$). In den Rezidiven ohne vorherige CRT zeigte sich relativ zu den korrespondierenden Primärtumoren kein signifikanter Unterschied der Anzahl der TLS ($p=0,5548$).

Zur weiteren funktionellen Aufarbeitung einer möglichen CRT-induzierten Veränderung der TIME verglichen wir im Rahmen von *in vitro* Versuchen die parentale Zelllinie eines Hypopharynxkarzinoms FaDu/WT mit der Cisplatin-resistenten Zelllinie FaDu/CR und der strahlenresistenten Zelllinie FaDu/RR in einem Tumor-Immunzell-Kokultur-Modell. Als Modell zur Analyse des Einflusses der Therapieresistenz gegenüber zytotoxischen Therapien wurden Spheroide der jeweiligen Zelllinie etabliert und mit aktivierten PBMCs von gesunden Spendern koinkubiert. Anders als bei den vorausgegangen *in vivo* Untersuchungen fand sich hier insgesamt eine höhere Immunzellinfiltration sowohl in den FaDu/RR als auch in den FaDu/CR Spheroiden verglichen zu den FaDu/WT Spheroiden gemessen an einer Zunahme der CD45+ Leukozyten, CD8+ zytotoxischen T-Zellen und CD4+ Th Zellen. Für die FaDu/CR Spheroide war diese Zunahme jeweils statistisch signifikant ($p<0.0001$), bei den FaDu/RR Spheroiden zeigte sich ein deutlicher Trend ohne statistische Signifikanz für die untersuchten Immunzellsubtypen. In den Spheroiden beider therapieresistenter Zelllinien zeigte sich zudem eine signifikant höhere PDL1-Expression ($p<0,0001$ für FaDu/CR, $p=0,0263$ für FaDu/RR).

1.3.5 Die Histon-Acetyltransferase EP300 als Inhibitor einer effektiven antitumoralen Immunantwort (Originalarbeit 4)

In Originalarbeit 4 führten wir auf Basis der TCGA Datenbank eine *in silico* Analyse durch, bei der wir mögliche Korrelationen zwischen der Zusammensetzung der TIME und dem Vorkommen spezifischer Genmutationen untersuchten. Hierzu unterteilten wir 530 Patienten der TCGA HNSCC Kohorte in drei Gruppen entsprechend der folgenden Profile der TIME:

1. Eine immunaktivierte antitumorale TIME mit hoher Expression von Genen einer vor allem durch T-Zellen vermittelten zytotoxischen Immunantwort.

2. Eine immununterdrückte TIME mit niedriger Expression von Genen einer zytotoxischen Immunantwort und hoher Expression von Markergenen myeloider Suppressorzellen und Makrophagen.
3. Eine fehlende antitumorale TIME mit niedriger Expression aller immunassoziierten Gene der anderen beiden Gruppen.

Die immunaktivierte Gruppe zeigte nach Kaplan-Meyer Methode und Wilcoxon-Vorzeichen-Rang-Test im Vergleich zu den beiden anderen Gruppen das beste Gesamtüberleben (p=0,0619) und krankheitsfreie Überleben (p=0,0245) und repräsentierte somit die klinisch bekannte prognostische Relevanz der Zusammensetzung der TIME, wie in Originalarbeit 1 beschrieben.

Zur Identifizierung spezifischer nicht-synonymer Genmutationen, die mit einer bestimmten Gruppe der TIME assoziiert sind, überprüften wir die 1519 am häufigsten mutierten Gene der HNSCC Kohorte auf unterschiedliche Verteilungsmuster in den verschiedenen Gruppen. Insgesamt zeigten 9 mutierte Gene eine signifikante Assoziation zu einem bestimmten Typ der TIME. Bei Berücksichtigung des HPV-Status als wichtigen Einflussfaktor auf die Prognose und das molekulare Tumorprofil waren sowohl in allen HNSCC als auch in der Gruppe der HPV-positiven und HPV-negativen HNSCC lediglich der Mutationsstatus von *TP53* und *EP300* mit einer bestimmten TIME assoziiert. *TP53* Mutationen zeigten hierbei eine starke Korrelation zu einer fehlenden antitumoralen TIME und bestätigten somit die methodische Validität unseres Ansatzes, da aus vorausgegangen Studien bereits eine Inhibition der antitumoralen Immunantwort durch *TP53* Mutationen bekannt ist (21). Mutationen von *EP300* korrelierten mit einer immunaktivierten TIME. EP300 ist eine Lysin-Acetyltransferase, die via Chromatin-Remodeling an der Regulation der Transkription einer Vielzahl von Genen beteiligt ist und in der molekularen Struktur sowie der Funktion in enger Verwandtschaft zum CREB binding protein (CBP) steht. Insgesamt ist EP300 hierdurch an vielfältigen zellulären Prozessen beteiligt, zu denen insbesondere Proliferationsprozesse, die Kontrolle des Zellzyklus und der Zelldifferenzierung sowie die Reaktion auf DNA Schäden zählen (2).

Basierend auf der Korrelation von *EP300* Mutationen mit einer immunaktivierten antitumoralen TIME im HNSCC überprüften wir im Folgenden, ob diese Assoziation sich auf weitere solide Tumorentitäten übertragen lässt. Hierzu untersuchten wir 18 der häufigsten soliden Tumorentitäten der TCGA Datenbank mit insgesamt 7564 Patienten auf das Vorhandensein von *EP300* Mutationen. Bei 3,1% (277) der Patienten lag eine *EP300* Mutation vor. Die höchste Mutationsfrequenz fand sich bei HPV-assoziierten Karzinomen des Kopf-Hals-Bereichs (15,4%) und der Zervix (11,8%). Zur Bestimmung der Aktivität der antitumoralen Immunantwort unterteilten wir die Tumore entsprechend Rooney *et al*. anhand der zytolytischen Aktivität in eine Gruppe mit erhöhter antitumoraler Aktivität und eine Gruppe mit erniedrigter antitumoraler

Aktivität (46). Als Maßstab diente hierbei die simultane Hoch- oder Herunterregulation von Perforin (*PFN1*) und Granzym (*GZMB*) als Effektormechanismen von aktivierten CD8+ zytotoxischen T-Zellen. Neben der bereits beobachteten Korrelation in HNSCC zeigten sich auch in plattenepithelialen Karzinomen des Ösophagus, Magenkarzinomen und Prostatakarzinomen eine Korrelation der zytolytischen Aktivität mit dem *EP300* Mutationsstatus.

Aufbauend auf die Hypothese, dass der erhöhten zytolytischen Aktivität bei *EP300* Mutation ein Funktionsverlust des Gens zu Grunde liegt, teilten wir in einem weiteren Schritt die Patienten der 18 soliden Tumorentitäten anhand des RNA-Expressionsstatus von *EP300* zum z-Score=1 in je eine Gruppe mit hoher und mit niedriger *EP300* Expression ein. Hier zeigte sich eine starke Assoziation der Herunterregulation von *EP300* mit einer erhöhten zytolytischen Aktivität bei 17 der 18 Entitäten. Lediglich für Mammakarzinome bestätigte sich diese Assoziation nicht.

Da bereits gezeigt wurde, dass EP300 die Transkription von Genen des Glucose-Metabolismus induziert, und zudem bekannt ist, dass ein glykolytischer Tumormetabolismus durch die Ansammlung von Lactat zu einer Inhibition der antitumoralen TIME führt, untersuchten wir in weiteren Analysen die Auswirkungen der *EP300* Expression auf den Tumormetabolismus (27, 31). Hierzu stellten wir verschiedene Stoffwechselgene zusammen, die entweder einen Glykolyse-dominanten oder einen durch oxidative Phosphorylierung (OXPHOS) dominierten Tumorstoffwechsel charakterisieren. Anhand dieser führten wir eine Entitäten-übergreifende metabolische Charakterisierung aller 18 soliden Tumoren der vorherigen Untersuchungen durch und korrelierten die Ergebnisse mit der *EP300* Expression. Im Vergleich zeigte sich hierbei ein signifikanter Unterschied in der Frequenz der Hochregulation von Glykolyse- und OXPHOS-assoziierten Genen bei Tumoren mit niedriger oder hoher *EP300* Expression. Bei niedriger *EP300* Expression überwog signifikant ein OXPHOS-dominanter Tumormetabolismus, bei hoher *EP300* Expression ein Glykolyse-dominanter Tumormetabolismus.

Zur weiteren Ausarbeitung dieser Ergebnisse führten wir funktionelle *in silico* Analysen durch, indem wir die frei verfügbaren Genexpressionsdaten der L1000 Connectivity Map des Broad Instituts der folgenden 8 Zelllinien vor und nach Behandlung mit dem EP300 Inhibitor C646 verglichen: A375 (malignes Melanom), MCF7 (Adenokarzinom der Brust), A549 und HCC515 (Adenokarzinom der Lunge), PC3 (Prostatakarzinom), HEPG2 (Hepatozelluläres Karzinom), HT29 (Kolorektales Karzinom) und HA1E (immortalisierte Nierenzelllinie). Hier zeigte sich bei 3 der 8 Zelllinien (A375, MCF7 und PC3) ein signifikant herunterregulierter Glykolyse-assoziierter Metabolismus nach Behandlung mit dem EP300 Inhibitor C646 im Vergleich zu DMSO Inkubation. Bei den beiden Zelllinien HT29 und HEPG2 zeigte sich derselbe Trend ohne Signifikanz. Zudem fand sich ein signifikant hochregulierter OXPHOS-assoziierter Metabolismus bei HA1E und HEP2G nach C646 Behandlung, wohingegen dieser bei HT29 und HEP2G signifikant herunterreguliert war.

1.4 Diskussion

Durch die in dieser Dissertationsschrift zusammengefassten Originalarbeiten konnte wir die TIME von HNSCC aus verschiedenen Perspektiven genauer charakterisieren und neue Grundlagen zur Verbesserung von Therapiemöglichkeiten sowie zur prognostischen Einschätzung schaffen.

In den Originalarbeiten 1 bis 3 stellten wir zur Beantwortung der Forschungsfragen die HNSCC Hauptkohorte (Lübeck) zusammen und konnten zudem auf eine Validierungskohorte aus Bonn zurückgreifen. Beide Kohorten spiegelten die Tumorepidemiologie in Deutschland und Europa gut wider. Es lag jeweils eine typische 3:1 Verteilung von männlichen zu weiblichen Patienten vor und auch der Altersdurchschnitt mit etwa 63 Jahren, eine 5-Jahres Überlebensrate von etwa 60% und eine typische Lokalisationsverteilung mit etwa 80% der Karzinome im Bereich der Mundhöhle und des Pharynx und etwa 20% im Bereich des Larynx entsprach der Zusammensetzung anderer großer HNSCC-Kohorten (65, 67). Der Anteil an HPV positiven Karzinomen war mit 27,7% in der Hauptkohorte ebenfalls vergleichbar (55). Da sowohl bei kleinen T1 Karzinomen als auch bei palliativ behandelten UICC Stadium IV Patienten oft nicht genügend Tumormaterial zur Erstellung von TMAs vorlag, waren diese Tumore in unseren Kohorten im Vergleich zu epidemiologischen Datenbanken methodisch bedingt etwas weniger repräsentiert (65, 67).

Durch unsere Analysen in Originalarbeit 1 konnten wir erstmalig einen möglichen Ansatz aufzeigen, wie die Prognoserelevanz der TIME mit niedrigem Ressourcenaufwand in der Routinediagnostik bestimmt werden kann. Im HNSCC und vielen anderen soliden Tumorentitäten ist bereits bekannt, dass ein „heißes“ und auch ein „ausgespartes“ Immunzellinfiltrat mit einer besseren Prognose assoziiert ist als ein „kaltes“ (3, 37, 48, 60). Zumeist wurde in den zugrundeliegenden Studien das Immunzellinfiltrat durch Verwendung immunhistochemischer Färbungen charakterisiert oder die RNA-Expression spezifischer Immunzell-Marker wurde bestimmt, um die einzelnen Immunzellsubtypen darzustellen. Hierdurch ließen sich detaillierte Aussagen über die Zusammensetzung der TIME und die prognostische Auswirkung treffen.

Da zur Etablierung der routinediagnostischen Charakterisierung der TIME zur Prognoseabschätzung aber vor allem ein zeiteffizientes und kostengünstiges Verfahren notwendig ist, nahmen wir in Originalarbeit 1 die Einordnung des Immunzellinfiltrats am in der Diagnostik bereits verfügbarem HE-Schnitt in „heiß“, „kalt“ und „ausgespart“ vor. Die Gruppe der „kalten“ Tumore zeigte hierbei ein signifikant schlechteres Überleben als die beiden anderen Gruppen. Diese Korrelation hatte zudem in der multivariaten Analyse als unabhängiger Prognosefaktor neben dem p16 Status Bestand. Die dargestellte Methode zur Einordnung des Immunzellinfiltrats kann nach weiterer Validierung somit als effektive Ergänzung vor allem bei unklarem TNM-Status

oder schwieriger Bestimmung des Tumor Gradings in der Routinediagnostik zur weiteren Prognoseabschätzung durchgeführt werden.

In den beiden Originalarbeiten 2 und 3 fokussierten wir uns vor allem auf mögliche Ansatzpunkte zur Verbesserung bestehender Therapiekonzepte beim HNSCC Rezidiv, da das Auftreten eines HNSCC Rezidivs derzeit weiterhin maßgeblich die Überlebenszeit limitiert und die Prognose der Patienten auch nach Einführung der Immun-Checkpoint-Inhibitoren Pembrolizumab und Nivolumab nicht grundlegend verbessert werden konnte (8, 9, 15).

Hierbei analysierten wir in Originalarbeit 2 die Varianz bei der immunhistochemischen Bestimmung der PDL1-Expression in Abhängigkeit vom verwendeten anti-PDL1-Anikörper-Klon in der Routinediagnostik. Die Stärke der PDL1-Expression dient als wichtiger Prädiktor für das Therapieansprechen auf die beiden genannten Immun-Checkpoint-Inhibitoren und bildet ein notwendiges diagnostisches Kriterium für oder gegen die Entscheidung einer Therapie mit Pembrolizumab beim HNSCC Rezidiv (9). In unserer Studie zeigten wir, dass es deutliche Unterschiede der Färberesultate je nach verwendetem PDL1-Antikörper-Klon beim HNSCC Rezidiv gibt. Lediglich zwischen den Antikörper-Klonen SP263 und 28-8 fand sich eine geringe Vergleichbarkeit der Resultate. In der Konsequenz ergab sich aus der Varianz der Färberesultate eine starke Abhängigkeit der späteren Therapieentscheidung für oder gegen die Anwendung von Pembrolizumab vom verwendeten Antikörper-Klon in der Routinediagnostik.

Vergleichbare Ergebnisse bei HNSCC konnte auch die Studie von de Ruiter *et al*. zeigen, in der allerdings nur drei verschiedene Antikörperklone verglichen wurden (47). In vorausgegangen Untersuchungen zu den verschiedenen diagnostisch genutzten anti-PDL1-Antikörper-Klonen in anderen soliden Tumorentitäten, wie dem NSCLC, zeigten sich homogenere Färberesultate als beim HNSCC (26, 58). Vergleichbar zu unseren Untersuchungen lag beispielsweise auch beim NSCLC die geringste Sensitivität bei Verwendung des Antikörper-Klons SP142 vor. Neben Unterschieden in Färbeprotokollen oder präanalytischen Maßnahmen kann möglicherweise vor allem auch die ausgeprägte Tumorheterogenität von Kopf-Hals-Karzinomen im Vergleich zu anderen soliden Tumoren als Grund für die Diskrepanz der Färberesultate diskutiert werden (29, 35). Zudem kann der Glykosylierungs-Status des PDL1 Moleküls Einfluss auf die Bindung des jeweiligen anti-PDL1-Antikörpers an sein Epitop nehmen (34).

Unabhängig von diesen möglichen Zusammenhängen ließ sich aus den Untersuchungen der Originalarbeit 2 ableiten, dass die Bestimmung der PDL1-Expression zur therapeutischen Entscheidungsfindung im HNSCC mit Vorsicht betrachtet werden sollte und gegebenenfalls verschiedene Antikörper verwendet werden sollten, um die Sensitivität der Diagnostik zu erhöhen. Eine erste multizentrische Studie zur Etablierung einheitlicher diagnostischer Standards

für die Bestimmung der PDL1-Expression im HNSCC wurde parallel zu unserer Studie veröffentlicht (11). Da derzeit alle von uns untersuchten Antikörper in der Routinediagnostik in Abhängigkeit vom jeweiligen Institut verwendet werden, ist eine Übereinkunft über reproduzierbare und vergleichbare Färbeprotokolle unbedingt notwendig.

Als weiterer essenzieller Faktor sowohl für das Ansprechen auf eine klassische Kombinationstherapie aus Strahlen- und Chemotherapie als auch für das Ansprechen auf Immun-Checkpoint-Inhibitoren gilt die TIME (37, 39). Daher untersuchten wir in Originalarbeit 3 die TIME in HNSCC Rezidiven im Vergleich zu den korrespondierenden Primärtumoren und setzten sie in Kontext zu den bestehenden Therapiekonzepten. Hierzu evaluierten wir zunächst das Immunzellinfiltrat der Haupt- und Validierungskohorte mithilfe einer immunhistochemischen Analyse der Expression immunzellspezifischer Markerproteine. HNSCC Primärtumore und Rezidive zeichneten sich dabei durch deutliche Unterschiede im Immunzellinfiltrat aus. Insgesamt kam es in den Rezidiven zu einem Abfall fast aller Immunzellsubtypen. Insbesondere lag ein signifikanter Abfall von CD8+ zytotoxischen T-Zellen und CD20+ B-Lymphozyten in beiden Kohorten vor. Diese beiden Immunzellsubtypen stellen in HNSCC und anderen soliden Tumorentitäten einen wichtigen Bestandteil einer aktiven antitumoralen Immunzellantwort dar und führen auf diese Weise zudem zu einer Verbesserung des Gesamtüberlebens (3, 37, 46, 60). Insgesamt ist somit von einer Immunevasion mit einer immunsupprimierten TIME im HNSCC Rezidiv im Vergleich zum Primärtumor auszugehen. Ein weiterer Beleg für eine Immunsuppression im HNSCC Rezidiv zeigte sich in einem relativen Anstieg von FOXP3+ Tregs und PD1+ Zellen im Verhältnis zu CD8+ zytotoxischen T-Zellen, die beide zu einer Hemmung einer antitumoralen Immunantwort führen können (16, 28). Lediglich CD1A+ dendritische Zellen waren in der Gruppe der HNSCC Rezidive der Hauptkohorte signifikant häufiger zu finden. DC-LAMP+ dendritische Zellen, die zu einer aktiven T- und B-Zell-vermittelten Immunantwort beitragen können, nahmen in den Rezidiven hingegen ab (57). Da dendritische Zellen insgesamt eine heterogene Gruppe darstellen, sind zur Einordnung des Anstiegs CD1A+ dendritischer Zellen weitergehende Analysen notwendig (64).
Um einen möglichen Einfluss des vorausgegangenen Therapiekonzepts zu evaluieren, schlossen wir eine Subgruppenanalyse an, in der wir Veränderungen des Immunzellinfiltrats von Primärtumoren und Rezidiven mit alleiniger Resektion des Primärtumors der Gruppe mit zusätzlicher adjuvanter CRT nach Resektion des Primärtumors gegenüberstellten. In diesem Zusammenhang ist bereits bekannt, dass eine CRT sowohl durch die Aktivierung von dendritischen Zellen und einer dadurch bedingten Stimulation antigen-spezifischer zytotoxischer T-Zellen einen immunaktivierenden Effekt haben kann, aber auch durch den zytotoxischen Effekt auf

Immunzellen zur langfristigen Immundysfunktion führen und zudem eine Erhöhung protumoraler myeloischer Immunzellsubtypen bedingen kann (12, 19, 53, 61).

In unserer Subgruppenanalyse zeigte sich die Abnahme antitumoraler Immunzellen lediglich in der Gruppe nach adjuvanter CRT, nicht aber nach alleiniger Resektion. Vor allem CD20+ B-Lymphozyten waren bei den Rezidiven nach CRT nahezu vollständig zurückgegangen, bei den Rezidiven nach alleiniger Resektion zeigte sich hier keine signifikante Änderung. Somit konnten wir eine Assoziation der Immunsuppression in HNSCC Rezidiven zu einer vorausgegangenen CRT herstellen, die sich insbesondere in einer nahezu vollständigen B-Lymphozyten Depletion zeigte. B-Lymphozyten machen bis zu 25% der Immunzellen der TIME aus und können zu einer langfristig aktiven antitumoralen Immunantwort durch die Generierung von Gedächtniszellen beitragen (33, 59).

Zur weiteren Aufarbeitung einer CRT-assoziierten Immunsuppression schlossen wir eine mRNA Expressionsanalyse von 730 immunassoziierten Genen bei je 18 Primärtumoren und Rezidiven in der Gruppe nach adjuvanter CRT an. Diese Untersuchung bestätigte auch auf mRNA Ebene den bereits immunhistochemisch beobachteten Rückgang der verschiedenen antitumoralen Immunzellen, insbesondere der B-Lymphozyten, und zeigte zudem eine relative Zunahme protumoraler myeloider Immunzellen wie neutrophiler Granulozyten, Mastzellen und Makrophagen. Außerdem zeigte sich in der Gesamtanalyse eine signifikant größere Ähnlichkeit der Rezidive und Primärtumore jeweils untereinander als zu ihren korrespondierenden Rezidiven mit einer Herunterregulation der meisten immunassoziierten Genen in den Rezidiven.

Hierbei waren vor allem Gene, die in die Initiation und Formation von tertiären lymphoiden Strukturen (TLS) involviert sind, am stärksten herunterreguliert. TLS ähneln in ihrem Aufbau sekundären lymphatischen Organen und kommen insbesondere bei chronischen Entzündungsreaktionen oder im Randbereich solider Tumore vor (14). In den letzten Jahren sind TLS zunehmend in den Fokus immunonkologischer Forschung gerückt, da sie eine wichtige Rolle bei der Aufrechterhaltung einer langanhaltenden und tumorspezifischen antitumoralen Immunantwort spielen und somit zu einer Verlängerung der Überlebenszeit und der lokalen Tumorkontrolle in verschiedenen Entitäten und auch im HNSCC führen (4, 10, 50).

Mittels immunhistochemischer Doppelfärbung gegen CD20 und ERG untersuchten wir in einem weiteren Schritt die genaue Verteilung der TLS in unserer Hauptkohorte und konnten nachweisen, dass die Reduktion der TLS in HNSCC Rezidiven in Assoziation mit einer vorausgegangenen adjuvanten CRT steht, da diese in der Gruppe der Rezidive nach alleiniger Resektion nicht beobachtet wurde. Diese Analyse legt nahe, dass eine CRT zur Reduktion von TLS beiträgt und so die antitumorale Immunantwort negativ beeinflusst.

Zum weiteren Verständnis wie eine Chemotherapie oder Radiotherapie sich auf das Zusammenspiel von Tumorzellen und Immunzellen auswirkt, führten wir im Folgenden *in vitro* Versuche zur funktionellen Aufarbeitung durch. Hierbei erstellten wir aus naiven FaDu/WT, radioresistenten FaDu/RR und Cisplatin-resistenten FaDu/CR Zellen Spheroide und koinkubierten diese mit PBMCs von gesunden Spendern. Sowohl FaDu/RR als auch FaDu/CR Spheroide zeigten nach Koinkubation eine signifikant höhere Infiltration mit CD45+ Lymphozyten und eine höhere PDL1-Expression als die Chemotherapie- und Radiotherapie-naiven FaDu/WT Spheroide. Diese Ergebnisse wiesen auf eine höhere Immunogenität der FaDu Zellen nach zytotoxischer Therapie *in vitro* hin und stehen somit in Kontrast zu unseren *in vivo* Ergebnissen. Wir gehen davon aus, dass die Zunahme an genetischen Alterationen und somit eine erhöhte Neoantigenlast zur erhöhten Immunogenität der Spheroide nach zytotoxischer Therapie führt (63). Da sich *in vivo* ein gegenteiliger Effekt zeigte, ist von einem komplexeren multidimensionalen Prozess der Wirkung zytotoxischer Therapien auf die TIME auszugehen, bei dem möglicherweise vor allem auch die lokale Stromakomponente sowie die Destruktion lokaler und systemischer Immunkomponenten eine übergeordnete Rolle spielen könnte.
Insgesamt konnten wir in Originalarbeit 3 erstmalig aufzeigen, dass es im HNSCC Rezidiv zu einer Immunsuppression kommt, die insbesondere durch eine Abnahme von B-Lymphozyten und TLS in enger Assoziation zur vorherigen Durchführung einer CRT gekennzeichnet ist. Die protumorale TIME im HNSCC Rezidiv kann zum einen zur schlechten Prognose beitragen und zum anderen ein Grund für das schlechte Therapieansprechen auf Immun-Checkpoint-Inhibitoren sein. Erst kürzlich konnte zudem von Helmink *et al.* gezeigt werden, dass das Vorhandensein von TLS das Ansprechen auf Immuntherapien verbessert (24). Unsere Studie gibt somit Anlass, bisherige Therapiekonzepte in Bezug auf ihre immunsuppressive Wirkung zu überdenken und möglicherweise Immuntherapien schon in früheren Erkrankungsstadien bei noch erhaltener aktiver antitumoraler TIME zu implementieren.

Das Ziel der Originalarbeit 4 war es, spezifische genetische Veränderungen im HNSCC zu identifizieren, die in Assoziation zu einem bestimmten Profil der TIME stehen und als mögliche immuntherapeutische Angriffspunkte dienen können. Hierzu griffen wir auf die frei verfügbaren Mutations- und Genexpressionsdaten der TCGA-Datenbank zurück und unterteilten zunächst die HNSCC Kohorte entsprechend der RNA-Expression spezifischer immunassoziierter Gene in 3 Subgruppen, die klinisch relevante Unterschiede in der Zusammensetzung der TIME aufwiesen. Daraufhin identifizierten wir spezifische Mutationen, die signifikant häufiger in einer der 3 Gruppen vorkamen. Neben der bereits bekannten Assoziation von *TP53* Mutationen mit einer fehlenden antitumoralen Immunantwort konnten wir hierbei eine Korrelation zwischen *EP300*

Mutationen und einer aktiven antitumoralen TIME als einzige weitere gruppenspezifische Mutation aufzeigen, die unabhängig vom HPV Status Bestand hatte (21). Diese Korrelation bestätigte sich auch in plattenepithelialen Karzinomen des Ösophagus, Magenkarzinomen und Prostatakarzinomen. Zudem konnten wir entitätsübergreifend in 17 soliden Tumorentitäten einschließlich HNSCC eine Assoziation einer Herunterregulation von *EP300* mit einer Zunahme der zytolytischen Aktivität feststellen.

EP300 ist als Lysin-Acetyltransferase via Chromatin-Remodelling und als Transkriptionscofaktor von beispielsweise E2F an der Regulation einer Vielzahl zellulärer Prozesse beteiligt (44). Auf der einen Seite wird sowohl eine Tumorsuppressorfunktion von EP300 beschrieben, da es zur Promotion anderer Tumorsuppressorgene wie *TP53* oder *RB1* beiträgt (2). Auf der anderen Seite besteht eine Assoziation zu einem aggressiveren Tumorwachstum und einer schlechteren Prognose bei verschiedenen Tumorentitäten einschließlich HNSCC (5, 7).

Die Mechanismen, die zu dieser erhöhten Aggressivität führen, sind bisher nicht bekannt. Dennoch befinden sich EP300 Inhibitoren beispielsweise beim Prostatakarzinom in ersten erfolgsversprechenden Austestungen (66). In Kohärenz zu unseren Ergebnissen konnte in einem Maus-Modell gezeigt werden, dass eine EP300 Inhibition in Wildtypmäusen, nicht aber in immundefizienten Mäusen, zu einer Reduktion des Tumorwachstums führt (36). Diese Beobachtung hebt den in Originalarbeit 4 beschriebenen Effekt einer stärkeren antitumoralen Immunantwort bei niedriger *EP300* Expression oder *EP300* Mutation weiter hervor. Eine kürzlich von Chen et al. veröffentliche Studie konnte die von uns erstmalig beobachtete Assoziation von *EP300* Mutationen mit einer erhöhten zytolytischen Aktivität bestätigen und zudem einen Zusammenhang der Mutationen zu einer erhöhten genomischen Instabilität und einem besseren Ansprechen auf PDL1-Inhibitoren herstellen (6).

In weiteren Analysen der Originalarbeit 4 konnten wir einen möglichen Mechanismus des Einflusses der *EP300* Expression auf die TIME beschreiben, indem wir einen Zusammenhang zwischen kürzlich erschienen Studien zur *EP300* abhängigen Induktion der Transkription von Enzymen des Glucose-Metabolismus und dem Einfluss des Tumormetabolismus auf die TIME herstellen konnten (27). Tumore mit einer hohen *EP300* Expression zeichneten sich in unserer RNA-Expressionsanalyse durch einen überwiegend Glykolyse-abhängigen Tumormetabolismus aus, wohingegen bei niedriger *EP300* Expression ein OXPHOS-abhängiger Metabolismus überwog. Ein Glykolyse-abhängiger Tumormetabolismus ist wiederrum durch die Akkumulation von Laktat und dessen immunsuppressiven Effekt mit einer Abnahme der antitumoralen Immunantwort assoziiert (31, 32). Auch in funktionellen *in silico* Analysen von 8 Zelllinien nach Behandlung mit dem EP300 Inhibitor C646 bestätigte sich dieser Effekt im Sinne einer Abnahme der Expression Glykolyse-assoziierter Gene.

Insgesamt stellt eine Inhibition von EP300 somit einen neuen potentiellen immuntherapeutischen Angriffspunkt zur Therapie von HNSCC und weiteren soliden Tumorentitäten dar.

Zusammenfassend konnten wir in den 4 vorgestellten Originalarbeiten neue Grundlagen zur Verbesserung der Routinediagnostik und Therapie von HNSCC nach immunonkologischen Gesichtspunkten erarbeiten. Eine Einordnung des Tumorimmunzellinfiltrats in die Kategorien „heiß“, „kalt“ und „ausgespart“ am HE-Schnittpräparat könnte nach weiterer Validierung zukünftig zur routinediagnostischen Prognoseabschätzung genutzt werden (Originalarbeit 1). Für die routinediagnostische Analyse der PDL1-Expression sollten bei derzeit starker Inhomogenität der Färbungen nach Möglichkeit mehrere anti-PDL1-Antikörper-Klone genutzt werden oder ein einheitliches Färbeprotokoll durch multizentrische Studien etabliert werden (Originalarbeit 2). Die TIME in HNSCC Rezidiven war durch eine Immunsuppression vor allem nach vorausgegangener CRT gekennzeichnet und könnte so maßgeblich zur schlechten Prognose und dem schlechten Therapieansprechen auf PDL1-Inhibitoren in HNSCC Rezidiven beitragen, sodass unsere Ergebnisse in die Überarbeitung bisheriger Therapiekonzepte miteinbezogen werden sollten (Originalarbeit 3). Als möglichen neuen immuntherapeutischen Angriffspunkt konnten wir die Lysin-Acetyltransferase EP300 ausmachen, dessen Expression via Modulation des Tumormetabolismus mit einer Inhibition der antitumoralen Immunantwort assoziiert war (Originalarbeit 4).

1.5 Kurzzusammenfassung

Plattenepitheliale Karzinome des Kopf-Hals-Bereichs (HNSCC) sind derzeit die achthäufigste Tumorentität weltweit und haben weiterhin eine schlechte Prognose. Insbesondere das häufige Auftreten von Rezidiven führt zu 5-Jahres-Überlebensraten von unter 65%. Auch die Einführung des neuartigen Therapiekonzepts der Immun-Checkpoint-Inhibitoren in der Rezidivsituation konnte die Prognose bisher nicht wesentlich verbessern und bleibt damit bisher hinter den Erfolgen in anderen Tumorentitäten zurück. In den aufgeführten Originalarbeiten untersuchten wir daher immunonkologische Ansatzpunkte, um die Therapie der Patienten und die vorausgehende Diagnostik zu verbessern.

In **Originalarbeit 1** beschrieben wir die von uns erstellte repräsentative HNSCC Kohorte aus 419 Patienten, die auch in den Originalarbeiten 2 und 3 verwendet wurde, umfangreich und setzten sie in Kontext zu epidemiologischen Daten. Zudem konnten wir zeigen, dass eine Einordnung des Tumorimmuninfiltrats in die Kategorien „heiß“, „kalt“ und „ausgespart“ am Hämatoxylin-Eosin gefärbten Schnitt eine unabhängige Abschätzung der Prognose erlaubt.

In **Originalarbeit 2** untersuchten wir die immunhistochemische Färbevariabilität verschiedener routinediagnostisch verwendeter anti-PDL1-Antikörper-Klone. Die Evaluation der PDL1-Expression stellt einen notwendigen diagnostischen Schritt vor der Durchführung einer Therapie mit Immun-Checkpoint-Inhibitoren dar. Unsere Analysen ergaben, dass beim HNSCC eine starke Färbevariabilität vorliegt, die dazu führt, dass die darauf begründete Therapieentscheidung maßgeblich vom diagnostisch verwendeten anti-PDL1-Antikörper-Klon abhängt.

In **Originalarbeit 3** konnten wir deutliche Unterschiede in der immunologischen Tumormikroumgebung (TIME) von HNSCC Primärtumoren und Rezidiven feststellen. Die Rezidive waren durch eine immunsupprimierte und protumorale TIME gekennzeichnet. Der Verlust der antitumoralen Immunantwort trat vor allem in Assoziation zu einer vorausgegangenen Chemoradiotherapie auf und zeigte sich insbesondere im starken Verlust von B-Lymphozyten und tertiären lymphoiden Strukturen. Unsere Ergebnisse legen nahe, Immun-Checkpoint-Inhibitoren, welche idealerweise eine präexistente antitumorale Immunantwort benötigen, zu einem früheren Zeitpunkt in die Therapie von HNSCC einzubinden.

Durch *in silico* Analysen unserer **Originalarbeit 4** konnten wir erstmalig die Lysin-Acetyltransferase EP300 als Inhibitor einer antitumoralen Immunantwort sowohl im HNSCC als auch in einer Vielzahl weiterer solider Tumorentitäten identifizieren. Zudem konnten wir zeigen, dass ein möglicher Mechanismus der Immunsuppression durch eine hohe EP300 Expression in der Induktion eines Glykolyse-dominanten Tumormetabolismus liegt. EP300 stellt somit einen vielversprechenden neuen immuntherapeutischen Angriffspunkt dar.

Zusammenfassend tragen die 4 Originalarbeiten somit nicht nur dazu bei, das komplexe Zusammenspiel von Kopf-Hals-Karzinomen mit ihrer lokalen immunologischen Mikroumgebung besser zu verstehen, sondern helfen auch konkrete Rückschlüsse zu ziehen, wie neue Therapiekonzepte zur optimalen Nutzung der TIME und Verbesserung der Prognose von HNSCC Patienten etabliert werden können.

1.6 Literaturverzeichnis der deutschen Zusammenfassung

1. Argiris A, Karamouzis MV, Raben D, Ferris RL (2008) Head and neck cancer. The Lancet 371:1695–1709. doi: 10.1016/S0140-6736(08)60728-X

2. Attar N, Kurdistani SK (2017) Exploitation of EP300 and CREBBP Lysine Acetyltransferases by Cancer. Cold Spring Harb Perspect Med 7. doi: 10.1101/cshperspect.a026534

3. Bindea G, Mlecnik B, Tosolini M, Kirilovsky A, Waldner M, Obenauf AC, Angell H, Fredriksen T, Lafontaine L, Berger A, Bruneval P, Fridman WH, Becker C, Pagès F, Speicher MR, Trajanoski Z, Galon J (2013) Spatiotemporal dynamics of intratumoral immune cells reveal the immune landscape in human cancer. Immunity 39:782–795. doi: 10.1016/j.immuni.2013.10.003

4. Cabrita R, Lauss M, Sanna A, Donia M, Skaarup Larsen M, Mitra S, Johansson I, Phung B, Harbst K, Vallon-Christersson J, van Schoiack A, Lövgren K, Warren S, Jirström K, Olsson H, Pietras K, Ingvar C, Isaksson K, Schadendorf D, Schmidt H, Bastholt L, Carneiro A, Wargo JA, Svane IM, Jönsson G (2020) Tertiary lymphoid structures improve immunotherapy and survival in melanoma. Nature 577:561–565. doi: 10.1038/s41586-019-1914-8

5. Chen M-K, Cai M-Y, Luo R-Z, Tian X, Liao Q-M, Zhang X-Y, Han J-D (2015) Overexpression of p300 correlates with poor prognosis in patients with cutaneous squamous cell carcinoma. Br J Dermatol 172:111–119. doi: 10.1111/bjd.13226

6. Chen Z, Chen C, Li L, Zhang T, Wang X (2021) Pan-Cancer Analysis Reveals That E1A Binding Protein p300 Mutations Increase Genome Instability and Antitumor Immunity. Frontiers in Cell and Developmental Biology 9:2523. doi: 10.3389/fcell.2021.729927

7. Cho Y-A, Hong J-S, Choe E-J, Yoon H-J, Hong S-D, Lee J-I, Hong S-P (2015) The role of p300 in the tumor progression of oral squamous cell carcinoma. J Oral Pathol Med 44:185–192. doi: 10.1111/jop.12227

8. Cohen EEW, Bell RB, Bifulco CB, Burtness B, Gillison ML, Harrington KJ, Le Q-T, Lee NY, Leidner R, Lewis RL, Licitra L, Mehanna H, Mell LK, Raben A, Sikora AG, Uppaluri R, Whitworth F, Zandberg DP, Ferris RL (2019) The Society for Immunotherapy of Cancer consensus statement on immunotherapy for the treatment of squamous cell carcinoma of the head and neck (HNSCC). J Immunother Cancer 7:184. doi: 10.1186/s40425-019-0662-5

9. Cohen EEW, Soulières D, Le Tourneau C, Dinis J, Licitra L, Ahn M-J, Soria A, Machiels J-P, Mach N, Mehra R, Burtness B, Zhang P, Cheng J, Swaby RF, Harrington KJ, KEYNOTE-040 investigators (2019) Pembrolizumab versus methotrexate, docetaxel, or cetuximab for recurrent or metastatic head-and-neck squamous cell carcinoma (KEYNOTE-040): a randomised, open-label, phase 3 study. Lancet 393:156–167. doi: 10.1016/S0140-6736(18)31999-8

10. Colbeck EJ, Ager A, Gallimore A, Jones GW (2017) Tertiary Lymphoid Structures in Cancer: Drivers of Antitumor Immunity, Immunosuppression, or Bystander Sentinels in Disease? Front Immunol 8:1830. doi: 10.3389/fimmu.2017.01830

11. Crosta S, Boldorini R, Bono F, Brambilla V, Dainese E, Fusco N, Gianatti A, L'Imperio V, Morbini P, Pagni F (2021) PD-L1 Testing and Squamous Cell Carcinoma of the Head and Neck: A Multicenter Study on the Diagnostic Reproducibility of Different Protocols. Cancers (Basel) 13:292. doi: 10.3390/cancers13020292

12. Demaria S, Golden EB, Formenti SC (2015) Role of Local Radiation Therapy in Cancer Immunotherapy. JAMA Oncol 1:1325–1332. doi: 10.1001/jamaoncol.2015.2756

13. Doroshow DB, Sanmamed MF, Hastings K, Politi K, Rimm DL, Chen L, Melero I, Schalper KA, Herbst RS (2019) Immunotherapy in Non-Small Cell Lung Cancer: Facts and Hopes. Clin Cancer Res 25:4592–4602. doi: 10.1158/1078-0432.CCR-18-1538

14. Engelhard VH, Rodriguez AB, Mauldin IS, Woods AN, Peske JD, Slingluff CL (2018) Immune Cell Infiltration and Tertiary Lymphoid Structures as Determinants of Antitumor Immunity. The Journal of Immunology 200:432–442. doi: 10.4049/jimmunol.1701269

15. Ferris RL, Blumenschein G, Fayette J, Guigay J, Colevas AD, Licitra L, Harrington K, Kasper S, Vokes EE, Even C, Worden F, Saba NF, Iglesias Docampo LC, Haddad R, Rordorf T, Kiyota N, Tahara M, Monga M, Lynch M, Geese WJ, Kopit J, Shaw JW, Gillison ML (2016) Nivolumab for Recurrent Squamous-Cell Carcinoma of the Head and Neck. N Engl J Med 375:1856–1867. doi: 10.1056/NEJMoa1602252

16. Forster MD, Devlin M-J (2018) Immune Checkpoint Inhibition in Head and Neck Cancer. Front Oncol 8:310. doi: 10.3389/fonc.2018.00310

17. Foster CC, Melotek JM, Brisson RJ, Seiwert TY, Cohen EEW, Stenson KM, Blair EA, Portugal L, Gooi Z, Agrawal N, Vokes EE, Haraf DJ (2018) Definitive chemoradiation for locally-advanced oral cavity cancer: A 20-year experience. Oral Oncol 80:16–22. doi: 10.1016/j.oraloncology.2018.03.008

18. Gatta G, Botta L, Sánchez MJ, Anderson LA, Pierannunzio D, Licitra L, EUROCARE Working Group: (2015) Prognoses and improvement for head and neck cancers diagnosed in Europe in early 2000s: The EUROCARE-5 population-based study. Eur J Cancer 51:2130–2143. doi: 10.1016/j.ejca.2015.07.043

19. Golden EB, Apetoh L (2015) Radiotherapy and immunogenic cell death. Semin Radiat Oncol 25:11–17. doi: 10.1016/j.semradonc.2014.07.005

20. Goodman AM, Kato S, Bazhenova L, Patel SP, Frampton GM, Miller V, Stephens PJ, Daniels GA, Kurzrock R (2017) Tumor Mutational Burden as an Independent Predictor of Response to Immunotherapy in Diverse Cancers. Mol Cancer Ther 16:2598–2608. doi: 10.1158/1535-7163.MCT-17-0386

21. Guo G, Yu M, Xiao W, Celis E, Cui Y (2017) Local Activation of p53 in the Tumor Microenvironment Overcomes Immune Suppression and Enhances Antitumor Immunity. Cancer Res 77:2292–2305. doi: 10.1158/0008-5472.CAN-16-2832

22. Gupta B, Johnson NW, Kumar N (2016) Global Epidemiology of Head and Neck Cancers: A Continuing Challenge. Oncology 91:13–23. doi: 10.1159/000446117

23. Hanahan D, Weinberg RA (2011) Hallmarks of cancer: the next generation. Cell 144:646–674. doi: 10.1016/j.cell.2011.02.013

24. Helmink BA, Reddy SM, Gao J, Zhang S, Basar R, Thakur R, Yizhak K, Sade-Feldman M, Blando J, Han G, Gopalakrishnan V, Xi Y, Zhao H, Amaria RN, Tawbi HA, Cogdill AP, Liu W, LeBleu VS, Kugeratski FG, Patel S, Davies MA, Hwu P, Lee JE, Gershenwald JE, Lucci A, Arora R, Woodman S, Keung EZ, Gaudreau P-O, Reuben A, Spencer CN, Burton EM, Haydu LE, Lazar AJ, Zapassodi R, Hudgens CW, Ledesma DA, Ong S, Bailey M, Warren S, Rao D, Krijgsman O, Rozeman EA, Peeper D, Blank CU, Schumacher TN, Butterfield LH, Zelazowska MA, McBride

KM, Kalluri R, Allison J, Petitprez F, Fridman WH, Sautès-Fridman C, Hacohen N, Rezvani K, Sharma P, Tetzlaff MT, Wang L, Wargo JA (2020) B cells and tertiary lymphoid structures promote immunotherapy response. Nature 577:549–555. doi: 10.1038/s41586-019-1922-8

25. Herbst RS, Soria J-C, Kowanetz M, Fine GD, Hamid O, Gordon MS, Sosman JA, McDermott DF, Powderly JD, Gettinger SN, Kohrt HEK, Horn L, Lawrence DP, Rost S, Leabman M, Xiao Y, Mokatrin A, Koeppen H, Hegde PS, Mellman I, Chen DS, Hodi FS (2014) Predictive correlates of response to the anti-PD-L1 antibody MPDL3280A in cancer patients. Nature 515:563–567. doi: 10.1038/nature14011

26. Hirsch FR, McElhinny A, Stanforth D, Ranger-Moore J, Jansson M, Kulangara K, Richardson W, Towne P, Hanks D, Vennapusa B, Mistry A, Kalamegham R, Averbuch S, Novotny J, Rubin E, Emancipator K, McCaffery I, Williams JA, Walker J, Longshore J, Tsao MS, Kerr KM (2017) PD-L1 Immunohistochemistry Assays for Lung Cancer: Results from Phase 1 of the Blueprint PD-L1 IHC Assay Comparison Project. J Thorac Oncol 12:208–222. doi: 10.1016/j.jtho.2016.11.2228

27. Huang H, Tang S, Ji M, Tang Z, Shimada M, Liu X, Qi S, Locasale JW, Roeder RG, Zhao Y, Li X (2018) p300-Mediated Lysine 2-Hydroxyisobutyrylation Regulates Glycolysis. Mol Cell 70:663-678.e6. doi: 10.1016/j.molcel.2018.04.011

28. Jie H-B, Gildener-Leapman N, Li J, Srivastava RM, Gibson SP, Whiteside TL, Ferris RL (2013) Intratumoral regulatory T cells upregulate immunosuppressive molecules in head and neck cancer patients. Br J Cancer 109:2629–2635. doi: 10.1038/bjc.2013.645

29. Johnson DE, Burtness B, Leemans CR, Lui VWY, Bauman JE, Grandis JR (2020) Head and neck squamous cell carcinoma. Nat Rev Dis Primers 6:92. doi: 10.1038/s41572-020-00224-3

30. Krupar R, Hartl M, Wirsching K, Dietmaier W, Strutz J, Hofstaedter F (2014) Comparison of HPV prevalence in HNSCC patients with regard to regional and socioeconomic factors. Eur Arch Otorhinolaryngol 271:1737–1745. doi: 10.1007/s00405-013-2693-8

31. Krupar R, Hautmann MG, Pathak RR, Varier I, McLaren C, Gaag D, Hellerbrand C, Evert M, Laban S, Idel C, Sandulache V, Perner S, Bosserhoff AK, Sikora AG (2018) Immunometabolic Determinants of Chemoradiotherapy Response and Survival in Head and Neck Squamous Cell Carcinoma. Am J Pathol 188:72–83. doi: 10.1016/j.ajpath.2017.09.013

32. Krupar R, Robold K, Gaag D, Spanier G, Kreutz M, Renner K, Hellerbrand C, Hofstaedter F, Bosserhoff AK (2014) Immunologic and metabolic characteristics of HPV-negative and HPV-positive head and neck squamous cell carcinomas are strikingly different. Virchows Arch 465:299–312. doi: 10.1007/s00428-014-1630-6

33. Lechner A, Schlößer HA, Thelen M, Wennhold K, Rothschild SI, Gilles R, Quaas A, Siefer OG, Huebbers CU, Cukuroglu E, Göke J, Hillmer A, Gathof B, Meyer MF, Klussmann JP, Shimabukuro-Vornhagen A, Theurich S, Beutner D, von Bergwelt-Baildon M (2019) Tumor-associated B cells and humoral immune response in head and neck squamous cell carcinoma. Oncoimmunology 8:1535293. doi: 10.1080/2162402X.2018.1535293

34. Lee H-H, Wang Y-N, Xia W, Chen C-H, Rau K-M, Ye L, Wei Y, Chou C-K, Wang S-C, Yan M, Tu C-Y, Hsia T-C, Chiang S-F, Chao KSC, Wistuba II, Hsu JL, Hortobagyi GN, Hung M-C (2019) Removal of N-Linked Glycosylation Enhances PD-L1 Detection and Predicts Anti-PD-1/PD-L1 Therapeutic Efficacy. Cancer Cell 36:168-178.e4. doi: 10.1016/j.ccell.2019.06.008

35. Leemans CR, Snijders PJF, Brakenhoff RH (2018) The molecular landscape of head and neck cancer. Nat Rev Cancer 18:269–282. doi: 10.1038/nrc.2018.11

36. Liu Y, Wang L, Predina J, Han R, Beier UH, Wang L-CS, Kapoor V, Bhatti TR, Akimova T, Singhal S, Brindle PK, Cole PA, Albelda SM, Hancock WW (2013) Inhibition of p300 impairs Foxp3^{+} T regulatory cell function and promotes antitumor immunity. Nat Med 19:1173–1177. doi: 10.1038/nm.3286

37. Mandal R, Şenbabaoğlu Y, Desrichard A, Havel JJ, Dalin MG, Riaz N, Lee K-W, Ganly I, Hakimi AA, Chan TA, Morris LGT (2016) The head and neck cancer immune landscape and its immunotherapeutic implications. JCI Insight 1. doi: 10.1172/jci.insight.89829

38. Mendler AN, Hu B, Prinz PU, Kreutz M, Gottfried E, Noessner E (2012) Tumor lactic acidosis suppresses CTL function by inhibition of p38 and JNK/c-Jun activation. Int J Cancer 131:633–640. doi: 10.1002/ijc.26410

39. Miyauchi S, Kim SS, Pang J, Gold KA, Gutkind JS, Califano JA, Mell LK, Cohen EEW, Sharabi AB (2019) Immune Modulation of Head and Neck Squamous Cell Carcinoma and the Tumor Microenvironment by Conventional Therapeutics. Clin Cancer Res 25:4211–4223. doi: 10.1158/1078-0432.CCR-18-0871

40. Oosting SF, Haddad RI (2019) Best Practice in Systemic Therapy for Head and Neck Squamous Cell Carcinoma. Front Oncol 9:815. doi: 10.3389/fonc.2019.00815

41. Ott PA, Hodi FS, Robert C (2013) CTLA-4 and PD-1/PD-L1 blockade: new immunotherapeutic modalities with durable clinical benefit in melanoma patients. Clin Cancer Res 19:5300–5309. doi: 10.1158/1078-0432.CCR-13-0143

42. Polesel J, Talamini R, La Vecchia C, Levi F, Barzan L, Serraino D, Franceschi S, Dal Maso L (2008) Tobacco smoking and the risk of upper aero-digestive tract cancers: A reanalysis of case-control studies using spline models. Int J Cancer 122:2398–2402. doi: 10.1002/ijc.23385

43. Postow MA, Callahan MK, Wolchok JD (2015) Immune Checkpoint Blockade in Cancer Therapy. J Clin Oncol 33:1974–1982. doi: 10.1200/JCO.2014.59.4358

44. Ramos YFM, Hestand MS, Verlaan M, Krabbendam E, Ariyurek Y, van Galen M, van Dam H, van Ommen G-JB, den Dunnen JT, Zantema A, ’t Hoen PAC (2010) Genome-wide assessment of differential roles for p300 and CBP in transcription regulation. Nucleic Acids Res 38:5396–5408. doi: 10.1093/nar/gkq184

45. Reck M, Rodríguez-Abreu D, Robinson AG, Hui R, Csőszi T, Fülöp A, Gottfried M, Peled N, Tafreshi A, Cuffe S, O’Brien M, Rao S, Hotta K, Leiby MA, Lubiniecki GM, Shentu Y, Rangwala R, Brahmer JR, KEYNOTE-024 Investigators (2016) Pembrolizumab versus Chemotherapy for PD-L1-Positive Non-Small-Cell Lung Cancer. N Engl J Med 375:1823–1833. doi: 10.1056/NEJMoa1606774

46. Rooney MS, Shukla SA, Wu CJ, Getz G, Hacohen N (2015) Molecular and genetic properties of tumors associated with local immune cytolytic activity. Cell 160:48–61. doi: 10.1016/j.cell.2014.12.033

47. de Ruiter EJ, Mulder FJ, Koomen BM, Speel E-J, van den Hout MFCM, de Roest RH, Bloemena E, Devriese LA, Willems SM (2021) Comparison of three PD-L1 immunohistochemical assays

in head and neck squamous cell carcinoma (HNSCC). Mod Pathol 34:1125–1132. doi: 10.1038/s41379-020-0644-7

48. Russell S, Angell T, Lechner M, Liebertz D, Correa A, Sinha U, Kokot N, Epstein A (2013) Immune cell infiltration patterns and survival in head and neck squamous cell carcinoma. Head Neck Oncol 5:24

49. Sacco AG, Cohen EE (2015) Current Treatment Options for Recurrent or Metastatic Head and Neck Squamous Cell Carcinoma. J Clin Oncol 33:3305–3313. doi: 10.1200/JCO.2015.62.0963

50. Sautès-Fridman C, Petitprez F, Calderaro J, Fridman WH (2019) Tertiary lymphoid structures in the era of cancer immunotherapy. Nat Rev Cancer. doi: 10.1038/s41568-019-0144-6

51. Savic S, Berezowska S, Eppenberger-Castori S, Cathomas G, Diebold J, Fleischmann A, Jochum W, Komminoth P, McKee T, Letovanec I, Jasarevic Z, Rössle M, Singer G, von Gunten M, Zettl A, Zweifel R, Soltermann A, Bubendorf L (2019) PD-L1 testing of non-small cell lung cancer using different antibodies and platforms: a Swiss cross-validation study. Virchows Arch 475:67–76. doi: 10.1007/s00428-019-02582-0

52. Siegel RL, Miller KD, Jemal A (2019) Cancer statistics, 2019. CA Cancer J Clin 69:7–34. doi: 10.3322/caac.21551

53. Sridharan V, Margalit DN, Lynch SA, Severgnini M, Zhou J, Chau NG, Rabinowits G, Lorch JH, Hammerman PS, Hodi FS, Haddad RI, Tishler RB, Schoenfeld JD (2016) Definitive chemoradiation alters the immunologic landscape and immune checkpoints in head and neck cancer. Br J Cancer 115:252–260. doi: 10.1038/bjc.2016.166

54. Sung H, Ferlay J, Siegel RL, Laversanne M, Soerjomataram I, Jemal A, Bray F (2021) Global Cancer Statistics 2020: GLOBOCAN Estimates of Incidence and Mortality Worldwide for 36 Cancers in 185 Countries. CA Cancer J Clin 71:209–249. doi: 10.3322/caac.21660

55. Tinhofer I, Jöhrens K, Keilholz U, Kaufmann A, Lehmann A, Weichert W, Stenzinger A, Stromberger C, Klinghammer K, Becker E-T, Dommerich S, Stölzel K, Hofmann VM, Hildebrandt B, Moser L, Ervens J, Böttcher A, Albers A, Stabenow R, Reinecke A, Budach V, Hoffmeister B, Raguse JD (2015) Contribution of human papilloma virus to the incidence of squamous cell carcinoma of the head and neck in a European population with high smoking prevalence. Eur J Cancer 51:514–521. doi: 10.1016/j.ejca.2014.12.018

56. Tiwana MS, Wu J, Hay J, Wong F, Cheung W, Olson RA (2014) 25 year survival outcomes for squamous cell carcinomas of the head and neck: population-based outcomes from a Canadian province. Oral Oncol 50:651–656. doi: 10.1016/j.oraloncology.2014.03.009

57. Truxova I, Kasikova L, Hensler M, Skapa P, Laco J, Pecen L, Belicova L, Praznovec I, Halaska MJ, Brtnicky T, Salkova E, Rob L, Kodet R, Goc J, Sautes-Fridman C, Fridman WH, Ryska A, Galluzzi L, Spisek R, Fucikova J (2018) Mature dendritic cells correlate with favorable immune infiltrate and improved prognosis in ovarian carcinoma patients. J Immunother Cancer 6:139. doi: 10.1186/s40425-018-0446-3

58. Tsao MS, Kerr KM, Kockx M, Beasley M-B, Borczuk AC, Botling J, Bubendorf L, Chirieac L, Chen G, Chou T-Y, Chung J-H, Dacic S, Lantuejoul S, Mino-Kenudson M, Moreira AL, Nicholson AG, Noguchi M, Pelosi G, Poleri C, Russell PA, Sauter J, Thunnissen E, Wistuba I, Yu H, Wynes MW, Pintilie M, Yatabe Y, Hirsch FR (2018) PD-L1 Immunohistochemistry

Comparability Study in Real-Life Clinical Samples: Results of Blueprint Phase 2 Project. J Thorac Oncol 13:1302–1311. doi: 10.1016/j.jtho.2018.05.013

59. Tsou P, Katayama H, Ostrin EJ, Hanash SM (2016) The Emerging Role of B Cells in Tumor Immunity. Cancer Res 76:5597–5601. doi: 10.1158/0008-5472.CAN-16-0431

60. Turan T, Kannan D, Patel M, Matthew Barnes J, Tanlimco SG, Lu R, Halliwill K, Kongpachith S, Kline DE, Hendrickx W, Cesano A, Butterfield LH, Kaufman HL, Hudson TJ, Bedognetti D, Marincola F, Samayoa J (2018) Immune oncology, immune responsiveness and the theory of everything. J Immunother Cancer 6:50. doi: 10.1186/s40425-018-0355-5

61. Verastegui EL, Morales RB, Barrera-Franco JL, Poitevin AC, Hadden J (2003) Long-term immune dysfunction after radiotherapy to the head and neck area. Int Immunopharmacol 3:1093–1104. doi: 10.1016/S1567-5769(03)00013-4

62. Vermorken JB, Mesia R, Rivera F, Remenar E, Kawecki A, Rottey S, Erfan J, Zabolotnyy D, Kienzer H-R, Cupissol D, Peyrade F, Benasso M, Vynnychenko I, De Raucourt D, Bokemeyer C, Schueler A, Amellal N, Hitt R (2008) Platinum-based chemotherapy plus cetuximab in head and neck cancer. N Engl J Med 359:1116–1127. doi: 10.1056/NEJMoa0802656

63. Ward JP, Gubin MM, Schreiber RD (2016) The Role of Neoantigens in Naturally Occurring and Therapeutically Induced Immune Responses to Cancer. Adv Immunol 130:25–74. doi: 10.1016/bs.ai.2016.01.001

64. Wculek SK, Cueto FJ, Mujal AM, Melero I, Krummel MF, Sancho D (2019) Dendritic cells in cancer immunology and immunotherapy. Nature Reviews Immunology. doi: 10.1038/s41577-019-0210-z

65. Wienecke A, Kraywinkel K (2019) Epidemiologie von Kopf-Hals-Tumoren in Deutschland. Onkologe 25:190–200. doi: 10.1007/s00761-019-0534-0

66. Zou L-J, Xiang Q-P, Xue X-Q, Zhang C, Li C-C, Wang C, Li Q, Wang R, Wu S, Zhou Y-L, Zhang Y, Xu Y (2019) Y08197 is a novel and selective CBP/EP300 bromodomain inhibitor for the treatment of prostate cancer. Acta Pharmacol Sin 40:1436–1447. doi: 10.1038/s41401-019-0237-5

67. Eurocare Database. http://www.eurocare.it/Database/tabid/77/Default.aspx. Accessed 28 Nov 2021

2. Ethikvotum zu den Originalarbeiten 1-3

UNIVERSITÄT ZU LÜBECK

Universität zu Lübeck · Ratzeburger Allee 160 · 23538 Lübeck

Herrn
Dr. med. Idel
Klinik für Hals-, Nasen- und Ohrenheilkunde

im Hause

per Fax vorab: 500-42014
nachrichtlich:
Frau Prof. Dr. Wollenberg
Direktorin der Klinik für HNO

Ethik-Kommission
Vorsitzender:
Herr Prof. Dr. med. Alexander Katalinic
Universität zu Lübeck
Stellv. Vorsitzender:
Herr Prof. Dr. med. Frank Gieseler
Ratzeburger Allee 160
23538 Lübeck

Sachbearbeitung: Frau Janine Erdmann
Tel.: +49 451 3101 1008
Fax: +49 451 3101 1024

ethikkommission@uni-luebeck.de

Aktenzeichen: 16-277
Datum: 08. November 2016

Sitzung der Ethik-Kommission am 03. November 2016
Antragsteller: Herr Dr. Idel
Titel: Identifizierung und Charakterisierung von tumorspezifischen und tumorassoziierten Mutationen/Regulationsanomalien von Karzinomen der Luft- und Speisewege sowie deren Vorläuferläsionen zur Entwicklung neuer Diagnostik- und Therapieansätze. Retrospektiver Teil

Sehr geehrter Herr Dr. Idel,
der Antrag wurde unter berufsethischen, medizinisch-wissenschaftlichen und berufsrechtlichen Gesichtspunkten geprüft.

Die Kommission hat nach der Berücksichtigung folgender **Hinweise** keine Bedenken: Im Studienprotokoll ist der Zeitraum festzulegen, aus dem die „historischen" Proben stammen und ihre Anzahl ist zu konkretisieren. Der Anonymisierungsprozess ist genauer darzustellen. Eine geschlechterdifferente Auswertung sollte erfolgen.

Bei Änderung des Studiendesigns sollte der Antrag erneut vorgelegt werden.
Über alle schwerwiegenden oder unerwarteten und unerwünschten Ereignisse, die während der Studie auftreten, ist die Kommission umgehend zu benachrichtigen.
Die Deklaration von Helsinki in der aktuellen Fassung fordert in § 35 dazu auf, jedes medizinische Forschungsvorhaben mit Menschen zu registrieren. Daher empfiehlt die Kommission grundsätzlich die Studienregistrierung in einem öffentlichen Register (z.B. unter www.drks.de).
Die ärztliche und juristische Verantwortung des Studienleiters und der an der Studie teilnehmenden Ärzte bleibt entsprechend der Beratungsfunktion der Ethikkommission durch unsere Stellungnahme unberührt.

Mit freundlichem Gruß

i.V.
Prof. Dr. med. Alexander Katalinic
Vorsitzender

☒ Herr Prof. Dr. Katalinic (Soz.med. u. Epidemiologie, Vorsitzender)
Hr. Prof. Dr. Gieseler (Medizinische Klinik I, Stellv. Vorsitzender)
Hr. PD Dr. Bausch (Chirurgie)
Hr. Prof. Dr. Borck (Medizingeschichte u. Wissenschaftsforschung)
☒ Fr. Farries (Amtsgericht Eutin)
☒ Fr. PD Dr. Jauch-Chara (Psychiatrie)
Hr. PD Dr. Lauten (Kinder- u. Jugendmedizin)
Frau Martini (Caritas)
☒ Hr. Prof. Dr. Moser (Neurologie)
☒ Hr. Prof. Dr. Raasch (Pharmakologie)
Hr. Prof. Dr. Rehmann-Sutter (MGWF)
Hr. Schneider (Landgericht Lübeck)
☒ Fr. Prof. em. Dr. Schrader (Plastische Chirurgie)
☒ Hr. Dr. Vonthein (Med. Biometrie u. Statistik)
Fr. Prof. Dr. Zühlke (Humangenetik)

3. Danksagung

Abschließend möchte ich mich bei allen bedanken, die an der Entstehung der Publikationen mitgewirkt haben, die dieser Dissertationsschrift zugrunde liegen, und mich auf dem Weg zur Promotion unterstützt haben.

Mein besonderer Dank gilt hierbei meinem Doktorvater Prof. Dr. Sven Perner für die Betreuung dieser Arbeit und sein großes Engagement, mich sowohl in wissenschaftlichen Fragestellungen als auch in meiner persönlichen Entwicklung zu unterstützen. Diese Zusammenarbeit wird meine medizinische Tätigkeit auch langfristig maßgeblich beeinflussen.

Weiterhin gilt mein Dank der gesamten Arbeitsgruppe „Kopf-Hals-Karzinome“. Insbesondere möchte ich mich hier für die enge Zusammenarbeit mit PD Dr. Rosemarie Krupar bedanken. Ihre gute Intuition für spannende Fragestellungen und die Weitergabe ihrer wissenschaftlichen Erfahrung hat maßgeblich zum Gelingen dieser Arbeit beigetragen. Die zahlreichen Gespräche zum gemeinsamen Forschungsvorhaben sowie das offene Ohr auch für viele persönliche Fragestellungen waren für mich immer wegweisend und sind es noch.

Ein großer Dank gilt den Medizinisch-Technischen Laborassistenten Eva Dreyer und Wenzel Vogel für die Erstellung der Tissue Micro Arrays sowie die Unterstützung bei den zahlreichen immunhistochemischen Färbungen. Beim gesamten Team des Instituts für Pathologie der Universität Lübeck möchte ich mich für die freundliche Aufnahme ins Team und die gute Kooperation und Unterstützung der verschiedenen Arbeitsgruppen untereinander bedanken.

Besonders möchte ich mich auch bei meinen Eltern Andrea und Dr. Norbert Watermann, meinem Bruder Johannes Watermann und meiner Partnerin Mona Pawelzik für die Unterstützung in jeglicher Hinsicht bedanken.

4. Lebenslauf und Veröffentlichungen

Persönliche Daten:

Name:	Christian Watermann
Geburtsdatum:	13.01.1994
Geburtsort:	Ahlen, NRW
Familienstand:	Ledig
E-Mail:	christian.watermann@t-online.de

Ausbildung:

10/2014 – 11/2021	**Medizinstudium** Universität zu Lübeck 1. Abschnitt der ärztlichen Prüfung (09/2016): Note 1,0 2. Abschnitt der ärztlichen Prüfung (10/2020): Note 2,0 3. Abschnitt der ärztlichen Prüfung (11/2021): Note 1,0
Seit 06/2017	**Medizinischer Doktorand** Institut für Pathologie des UKSH, Campus Lübeck, und Forschungszentrum Borstel, Leibniz Lungen Zentrum Titel der Dissertation: Die immunologische Tumormikroumgebung in plattenepithelialen Tumoren des Kopf-Hals-Bereichs – ein bedeutender Einflussfaktor auf Therapie und Prognose Doktorvater: Prof. Dr. med. Sven Roger Perner
06/2013	**Abitur** Albertus-Magnus-Gymnasium, Beckum Abschlussnote: 1,0

Praktisches Jahr des Medizinstudiums:

06/2021 – 10/2021	**Pathologie**, Institut für Pathologie des Universitätsklinikums Schleswig-Holstein, Campus Lübeck
03/2021 – 06/2021	**Chirurgie**, Asklepios Klinikum Bad Oldesloe
11/2020 – 03/2021	**Innere Medizin**, Sana Kliniken Lübeck

Wissenschaftliche Poster und Präsentationen:

06/2019	**Vortrag, 103. Jahrestagung der Deutschen Gesellschaft für Pathologie e.V. Frankfurt** Titel: Primary and recurrent head and neck squamous carcinomas are strikingly different regarding their immune microenvironment
05/2019	**Posterpräsentation und Flash Talk, 9th Mildred Scheel Cancer Conference, Bonn** Titel: Analysis of the immune microenvironment reveals significant differences between primary and recurrent head and neck squamous cell carcinoma
10/2018	**Posterpräsentation, Cancer-Immuno-Oncology Symposium, Lübeck** Titel: Primary and recurrent head and neck squamous carcinomas are strikingly different regarding their immune microenvironment

---

Wissenschaftliche Projektförderung:

08/2018	**Promotionsstipendium „Lübecker Exzellenzmedizin“** Projekttitel: Immunologische Mechanismen der Rezidiventstehung und Therapieresistenz in Plattenepithelkarzinomen des Kopf-Hals-Bereichs

---

Weitere Auszeichnungen:

2012 - 2018	Mitglied des Bundeskaders Rettungsschwimmen (mehrfacher Juniorenweltmeister im Mannschaftswettbewerb, 2015-2018 Teil der Freiwassernationalmannschaft)
06/2013	Bestenurkunde des Landes Nordrhein-Westfalen zum Abitur Karl-von-Frisch Abiturientenpreis im Fach Biologie GDCH Abiturientenpreis im Fach Chemie

---

Wissenschaftliche Veröffentlichungen:

1. Cracking it - successful mRNA extraction for digital gene expression analysis from decalcified, formalin-fixed and paraffin-embedded bone tissue.

Saraji A, Offermann A, Stegmann-Frehse J, Hempel K, Kang D, Krupar R, **Watermann C**, Jonigk D, Kühnel MP, Kirfel J, Perner S, Sailer V.

PLoS One. 2021 Sep 16;16(9):e0257416.

2. Analysis of tripartite motif (TRIM) family gene expression in prostate cancer bone metastases.

Offermann A, Kang D, **Watermann C**, Weingart A, Hupe MC, Saraji A, Stegmann-Frehse J, Kruper R, Schüle R, Pantel K, Taubert H, Duensing S, Culig Z, Aigner A, Klapper W, Jonigk D, Philipp Kühnel M, Merseburger AS, Kirfel J, Sailer V, Perner S.

Carcinogenesis. 2021 Sep 6. Epub ahead of print.

3. Performance of different diagnostic PD-L1 clones in head and neck squamous cell carcinoma.

Ribbat-Idel J, Dressler FF, Krupar R, **Watermann C**, Paulsen FO, Kuppler P, Klapper L, Offermann A, Wollenberg B, Rades D, Laban S, Reischl M, Bruchhage K-L, Idel C, Perner S.

Front Med (Lausanne). 2021 Apr 27;8:640515.

4. Recurrent HNSCC harbor an immunosuppressive tumor immune microenvironment suggesting successful tumor immune evasion.

Watermann C, Pasternack H, Idel C, Ribbat-Idel J, Brägelmann J, Kuppler P, Offermann A, Jonigk D, Kühnel MP, Schröck A, Dreyer E, Rosero C, Nathansen J, Dubrovska A, Tharun L, Kirfel J, Wollenberg B, Perner S*, Krupar R*.

Clin Cancer Res. 2021 Jan 15;27(2):632-644. *These authors contributed equally.

5. Immunologic "cold" squamous cell carcinomas of the head and neck are associated with an unfavorable prognosis.

Ribbat-Idel J, Perner S, Kuppler P, Klapper L, Krupar R, **Watermann C**, Paulsen FO, Offermann A, Bruchhage KL, Wollenberg B, Idel C.

Front Med (Lausanne). 2021 Jan 27;8:622330.

6. In silico analysis reveals EP300 as a panCancer inhibitor of anti-tumor immune response via metabolic modulation.

Krupar R*, **Watermann C***, Idel C, Ribbat-Idel J, Offermann A, Pasternack H, Kirfel J, Sikora AG, Perner S.

Sci Rep. 2020 Jun 10;10(1):9389. *These authors contributed equally.

Lübeck, 28.12.2021

5. Originalarbeiten

Im Folgenden sind die 4 Originalarbeiten, die dieser Dissertationsschrift zugrunde liegen, angehangen.

frontiers in Medicine

ORIGINAL RESEARCH
published: 27 January 2021
doi: 10.3389/fmed.2021.622330

Immunologic "Cold" Squamous Cell Carcinomas of the Head and Neck Are Associated With an Unfavorable Prognosis

Julika Ribbat-Idel[1†], Sven Perner[1,2†], Patrick Kuppler[1], Luise Klapper[1], Rosemarie Krupar[2], Christian Watermann[1], Finn-Ole Paulsen[1], Anne Offermann[1], Karl-Ludwig Bruchhage[3], Barbara Wollenberg[4†] and Christian Idel[3†]*

[1] Institute of Pathology, University of Luebeck and University Hospital Schleswig-Holstein, Luebeck, Germany, [2] Pathology, Research Center Borstel, Leibniz Lung Center, Borstel, Germany, [3] Department of Otorhinolaryngology, University of Luebeck, Luebeck, Germany, [4] Department of Otorhinolaryngology, München rechts der Isar Technical University Munich, Munich, Germany

OPEN ACCESS

Edited by:
Luigi Tornillo,
University of Basel, Switzerland

Reviewed by:
Annette Staebler,
University of Tübingen, Germany
Heiko Golpon,
Hannover Medical School, Germany

***Correspondence:**
Julika Ribbat-Idel
Julika.Ribbat-Idel@uksh.de

[†] These authors have contributed equally to this work

Specialty section:
This article was submitted to Pathology, a section of the journal Frontiers in Medicine

Received: 28 October 2020
Accepted: 05 January 2021
Published: 27 January 2021

Citation:
Ribbat-Idel J, Perner S, Kuppler P, Klapper L, Krupar R, Watermann C, Paulsen F-O, Offermann A, Bruchhage K-L, Wollenberg B and Idel C (2021) Immunologic "Cold" Squamous Cell Carcinomas of the Head and Neck Are Associated With an Unfavorable Prognosis. Front. Med. 8:622330. doi: 10.3389/fmed.2021.622330

Background: Head and neck squamous cell carcinoma (HNSCC) represents a common cancer worldwide. Past therapeutic advances have not significantly improved HNSCC prognosis. Therefore, it is necessary to further stratify HNSCC, especially with recent advances in tumor immunology.

Methods: Tissue microarrays were assembled from tumor tissue samples and were complemented with comprehensive clinicopathological data of $n = 419$ patients. H&E whole slides from resection specimen ($n = 289$) were categorized according to their immune cell infiltrate as "hot," "cold," or "excluded."

Results: Investigating tumor immune cell patterns, we found significant differences in survival rates. Immunologic "hot" and "excluded" HNSCCs are associated with better overall survival than "cold" HNSCC patients ($p < 0.05$). Interestingly, the percentage of all three patterns is nearly identical in p16 positive and negative HNSCCs.

Conclusions: Using a plain histological H&E approach to categorize HNSCC as being immunologic "hot," "cold," or "excluded" can offer a forecast of patients' prognosis and may thus aid as a potential prognostic tool in routine pathology reports. This "hot-cold-excluded" scheme needs to be applied to more HNSCC cohorts and possibly to other cancer types to determine prognostic meaning, e.g., regarding OS or DFS. Furthermore, our cohort reflects epidemiological data in the national, European, and international context. It may, therefore, be of use for future HNSCC characterization.

Keywords: HNSCC, FFPE, tumor microenvironment, hot, cold, excluded, p16, HPV

INTRODUCTION

HNSCCs are the 6th most common cancer in humans (1, 2). Today the common therapies consist of surgery and/or chemoradiotherapy, which can have excruciating side effects. With the surgical approaches, patients may suffer from visible defacements, scars, and functional impairments like dysphagia or permanent voice changes. Chemoradiotherapy itself may lead to severe functional

damages as well. Patients tend to suffer from dysphagia by xerostomia and necrosis, atrophy and fibrosis of the bone and the different parts of soft tissue (3).

Given these therapy-induced impairments, the prognosis is still rather poor. With an increasing tumor stage, there is a decreasing survival. For UICC stage III and IV, the 2-year survival is around 30%. Thirty to fifty percentage develop a recurrent disease (RD) which is mirrored in poor disease-free survival (DFS) (1, 4–6). Changes in therapy regimes have not improved this fate significantly for decades. The use of a neoadjuvant and also of adjuvant chemotherapy is still controversial (4, 7–9).

Especially with growing knowledge about tumor immune microenvironment (TIME), as described later in this introduction, another promising therapy option was the treatment with immune checkpoint inhibitors (ICI), with PD-L1 and PD-1 as the most prominent ICIs. PD-L1 expression on tumor cells is increased by irradiation of the tumor (10). Administering antibodies against PD-L1 and PD-1 has shown to be very successful in the treatment of several solid tumors, e.g., melanoma of the skin (11). The effects of monotherapy with these antibodies in HNSCC are, although a major improvement to current chemotherapeutic treatment standards, rather disillusioning in the overall survival (OS) (12, 13). In other publications, it has been suggested that combinational therapy might be a solution (14). However, the specific drug combination with the most promising effect on patient outcomes has yet to be found.

Clinical trials rely on biomarkers to select the most suitable patients to receive costly therapy and prevent applying potentially harmful drugs to patients that will not benefit. Thus, there is a need for research tools that can be employed for preclinical investigations. These would need to reflect typical patient features and offer a representative cancer cohort in order to test if a newly targeted antigen is actually present on tumor cells or tumor immune cells. Ideally, they could then be used to shape opinion as to whether a new drug should be considered to be passed on into the clinical trial setting.

Intratumoral immune cells have recently advanced into the focus of research groups regarding many solid tumors. Studies have been investigating the TIME in regards to their structure and contents, revealing a labyrinthian interdepending system of cells and cytokines. In several studies, researchers tried to adapt the TIME for better treatment response. Especially irradiation of tumors could induce apoptosis in cancer cells, leading to an antigen download on antigen-presenting cells by an increased MHC expression. This might be important for an increased treatment response by immune checkpoint inhibitors. On the other hand, strong irradiation can lead to lymphodepletion, so a lot of research is still needed (15). Studies of our research team showed that the composition of immune cell infiltrates contributes to improved chemoradiotherapy response in HNSCC (16).

It has been widely accepted that TIME can be categorized as being immunologic "hot" (immune cell infiltrates within the tumor), "cold" (no immune cell infiltration), or "excluded" (immune cells at tumor boundaries) (17, 18). Evaluation of immune cell parameters showed an association with survival rates and allowed prediction of response to treatments (19). In colorectal cancer, for instance, the observation of immune cell density and localization allowed a more reliable prediction of survival than the classical TNM system (20). Mainly the categories "hot" and "cold" were defined by the presence of lymphocytes, e.g., in melanomas (21). In HNSCC, the genomes of two HNSCC cohorts were analyzed for cytokine expression and the authors defined two patterns, namely high and low CD8+ T cell inflamed phenotype (22). However, genomic analyses are very expensive and also error-prone. This is why we divided the cancers as immunologically "hot," "cold," or "excluded" by the distribution of immune cells based on H&E analysis.

However, there are still questions to be answered such as: Do these categories exist in all solid tumor types? And can they assist in predicting patient outcome? Hypothesizing that there is a difference in the OS of HNSCC patients with different TIME patterns in primary tumors (PT), these questions are pursued in the study at hand to provide another piece in the highly complex puzzle of tumor immunology.

TABLE 1 | Localization of primary tumors.

Anatomical site	Frequency (absolute number)
CUP[a]	3.1% ($n = 13$)
Hypopharynx	12.2% ($n = 51$)
Larynx	27.2% ($n = 114$)
Oral cavity	20.8% (n=87)
Oropharynx	33.7% (n=141)
Other	3.1% ($n = 13$)

[a] *Cancer of Unknown Primary.*

RESULTS

Cohort Characteristics

We established a cohort of 419 HNSCC patients (22.5% female, 77.5% male) with 27.7% being p16 positive. Tissue of $n = 4$ patients was not evaluable for p16.

The majority of HNSCC PT were located in the oropharynx, larynx and oral cavity, followed by hypopharynx (**Table 1**). Thirteen cases were cancers of unknown primary (CUP). 48.9% of oropharynx squamous cell carcinoma (OPSCC) were p16 positive and therefore met the criterion of the newly established subtype of "p16 positive oropharynx carcinomas" according to the latest edition of TNM classification (23) and WHO classification (24). Out of these, $n = 43$ were available to TIME evaluation.

The cohort can be subdivided into two arms: patients with a local RD (25.1%) vs. patients that did not experience a cancer relapse (74.9%). Five-year survival rates ranged from 51.8 to 54.8% for oral cavity and hypopharynx cancer, respectively, to 65.0 and 67.2% for oropharynx and larynx cancer, respectively. Five-year survival rate for the whole cohort was 61.9%, for recurrent disease patients it was 55.3%. 87.6% of patients had reported nicotine abuse, whereas 43.1% had acknowledged alcohol abuse.

TNM and UICC Stages

All cases were re-classified according to the 8th edition of TNM classification. 50.2% of patients were classified T1/T2 and 45.4% were classified T3/4. The remaining 4.3% were TX or T0 (as in CUP). This levels with 41.1% UICC stages I/II and 58.8% UICC stages III/IV (**Figure 1**, **Table 2**). No statistically significant differences were found for "hot," "cold," or "excluded" tumors when assessing TIME in early vs. late UICC stages (**Supplementary Figure 1**).

PT therapy included surgery (78.8%), irradiation (59.5%) and chemotherapy (30.9%). 52% of patients suffered from nodal positive HNSCC, which was treated by surgery and irradiation in 87% and by chemotherapy in 45.2%. 13.4% developed distant metastasis (DM). 5.8% of patients reappeared with a second cancer type.

Intratumoral Immune Cell Pattern

Two hundred eighty-nine patients received resection as first-line treatment. Their specimen of PT ($n = 289$) and RD ($n = 42$) were categorized according to their immune cell infiltrate as being "hot," "cold," or "excluded." In PT, the majority showed an "excluded" phenotype (52.6%) whereas the rest was almost evenly divided as "cold" (24.2%) and "hot" (23.2%). In RDs, the vast majority was either "cold" (47.6%) or "excluded" (42.9%) with only a small portion being "hot" (9.5%). Interestingly, immunologic "hot," "cold," and "excluded" tumors were found in equal proportions in p16 negative and p16 positive HNSCCs (**Figure 2**). 75.1% of p16 positive PTs and 76.7% of p16 negative PTs were immune infiltrated (meaning either "hot" or "excluded").

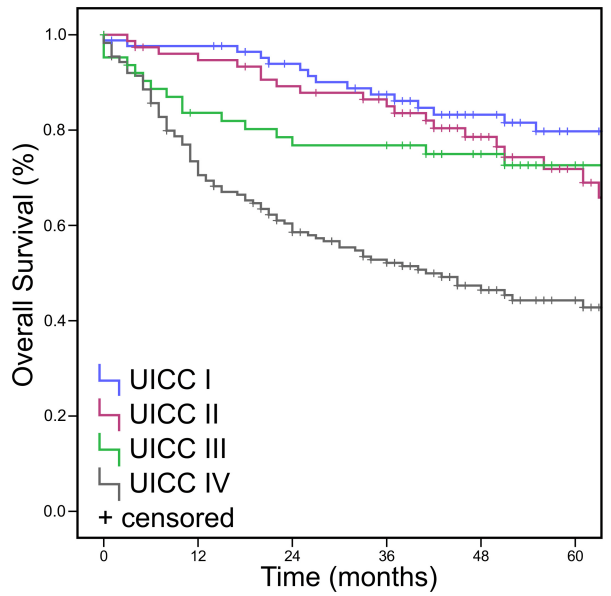

FIGURE 1 | Overall Survival Data (OS, Kaplan Meier) for UICC stage. UICC stage after re-assessment according to the eighth edition of TNM classification. $p < 0.05$.

Survival data by Kaplan-Meier analysis and log-rank test showed significantly lower OS for "cold" PTs when compared to "hot" or "excluded" HNSCC (**Figure 3A**) after Bonferroni adjustment of the *p*-values. Accordingly, 5-year survival rates were worst for immunologic "cold" tumors.

We performed univariate and multivariate Cox regression analyses to state whether the presence or absence of immune cell infiltration of tumors ("hot" or "excluded" vs. "cold" tumors) is a significant prognostic factor for the OS of HNSCC patients and if it is independent of other prognostic factors (**Supplementary Table 1**). We evaluated the three immune cell patterns ("hot," "cold," "excluded") and UICC stages, T stages, p16 status, sex, grading, and patient age for their prognostic value regarding OS of HNSCC patients. In the univariate analysis, it was revealed that the immune cell infiltration (Hazard Ratio (HR) = 0.547; $p = 0.005$), p16 expression ($HR = 0.344$; $p = 0.001$), T stage ($HR = 1.927$; $p = 0.001$), and UICC stage ($HR = 2.212$; $p < 0.001$) were significant prognostic factors for the OS. The multivariate analysis determined the immune cell infiltration pattern ($HR = 0.527$; $p = 0.003$) and the p16 expression ($HR = 0.353$; $p = 0.001$) as independent prognostic factors for the OS of HNSCC patients.

No significant difference was found for OS when assessing TIME in RD ($p > 0.05$) (**Figure 3B**) and in TIME in regards to p16 status ($p > 0.025$ and $p > 0.016$, respectively) (**Figures 3C,D**). Neither were there significant differences in DFS for TIME in PT or RD (**Figure 4**).

Furthermore, no significant difference was found when observing TIME in different PT locations. In the hypopharynx, larynx, and oral cavity, roughly 55% were "excluded," about 20% were "hot" and circa 25% were "cold" (**Supplementary Figure 2**). When analyzing OS in different PT locations, we found a better OS for "excluded" oral cavity HNSCCs in comparison to "hot"

TABLE 2 | TNM and UICC stages.

T status	Frequency (absolute number)	N/M status	Frequency (absolute number)	UICC stage	Frequency (absolute number)
T0/CUP	3.6% ($n = 15$)	N0	42.6% ($n = 176$)	I	22.0% ($n = 91$)
T1	22.6% ($n = 94$)	N1	17.7% ($n = 73$)	II	19.1% ($n = 79$)
T2	27.6% ($n = 115$)	N2	25.2% (n =1 04)	III	15.7% ($n = 65$)
T3	25.0% ($n = 104$)	N3	14.0% ($n = 58$)	IV	43.1% ($n = 178$)
T4	20.4% ($n = 85$)	n/a	($n = 8$)	n/a	($n = 6$)
TX	0.7 ($n = 3$)	M0	86.6% ($n = 362$)		
n/a	(n=3)	M1	13.4% ($n = 56$)		
		n/a	($n = 1$)		

Re-classification according to TNM (8th edition) and UICC stage.

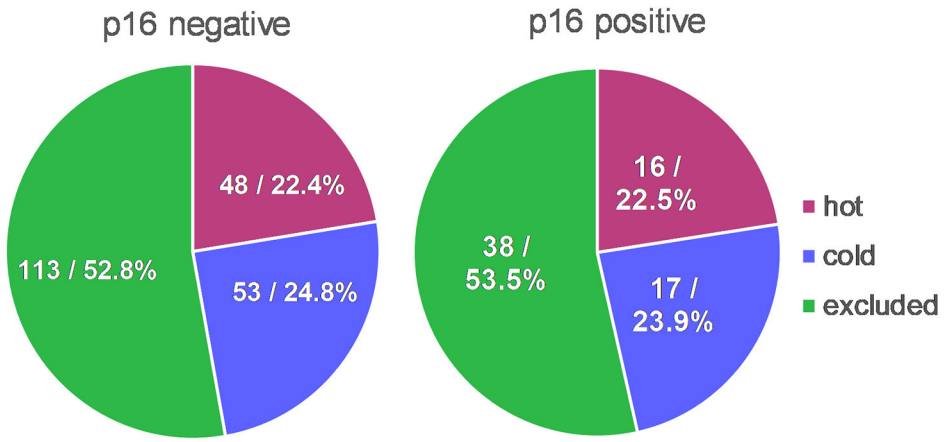

FIGURE 2 | TIME in context with p16 status. Distribution of immunologic "hot," "cold," and "excluded" tumors were almost identical in p16 positive HNSCCs in comparison to p16 negative HNSCCs.

and "excluded" oral cavity HNSCCs ($p = 0.048$, **Figure 3G**). No significant differences were found for TIME in other PT locations (**Figures 3E–H**).

We compared OS for resected PT in combination with different therapy regimes. We found that "cold" tumor show a worse OS than inflamed (i.e., "hot" plus "excluded") HNSCCs if the primary tumor was only treated by surgery (**Supplementary Figure 3A**) or by a combined regimen of surgery with an adjuvant radiochemotherapy (**Supplementary Figure 3C**). There was no difference if the tumors were treated in a combined regimen of surgery and adjuvant irradiation without chemotherapy **Supplementary Figure 3B**).

DISCUSSION

Introducing ICI into cancer treatment dramatically changed the fate of many cancer patients. Especially in melanoma patients, there have been large improvements in DFS and OS (16, 25–27). For patients with advanced HNSCC, the prognosis is still very poor, even after the introduction of ICI therapy in HNSCC (28). As a lot of research effort is underway many clinical trial studies compete for a limited number of participants. For wise guidance of patients into clinical trials, we need preclinical tools to estimate the success of new treatment agents.

Cohort Characteristics

We created a cohort of 419 HNSCC patients which is well-representative of tumor epidemiology and tumor properties. This cohort reflects the typical HNSCC patients' characteristics with a male to female ratio of ∼3:1 (29, 30) and a mean age of 62 years for male and 63 years for female patients. We found a positive p16 status as a surrogate marker for HPV infection in 27.7% of all HNSCC tumors (∼50% of all OPSCC tumors and 17% of non-oropharyngeal HNSCC) resembling other German (23.5%) and multinational (25.9%) data (31–34). Frequencies in cancer sites in German patients show the majority in the oral cavity and pharynx [79%] and a minority in the larynx [21%] which is also reflected by our cohort (29, 30). It also mirrors the epidemiological data of national and European data [EUROCARE-5 Study (35)] regarding the 5-year survival rate of 61.9%. With 22.6% of cases being staged as T1 (vs. 25% up to 44% in Germany), our cohort seems to lack in T1 cancer patients. This is most likely because—in order to set up a tissue-based cohort—one needs a certain amount of tumor mass to construct representative TMA cores. This naturally rules out small cancer (such as many T1 diseases) that would not yield enough tumor tissue. UICC stage IV stretches from 40% in larynx cancer to 75% in pharyngeal cancer and about half the cases of other localizations (30). In our cohort, we found 43.1% of patients in UICC stage IV. This, again, may be attributed to a selection bias as our cohort is mainly based on resectable cancers that have actually been surgically removed. UICC stage IV often reflects a palliative setting where the patient may not benefit from tumor surgery and may, therefore, undergo chemotherapy, irradiation, or best supportive care instead. So less UICC stage IV tumor material might have been available in the first place as we set up the cohort.

TIME by H&E as a Prognostic Factor

TIME in cancers can be categorized as being either "hot," "cold," or "excluded" by observing the distribution of immune cells in the tumor and its close neighborhood. An immunologic "hot" or "inflamed" tumor offers immune cells distributed diffusely throughout the tumor. A "cold" or "immune desert" tumor lacks immune cells whereas an "excluded" tumor shows immune cells in the desmoplastic septa of the tumor borders (18) (**Figure 5**, **Supplementary Figure 4**). It is well-known that in several tumor

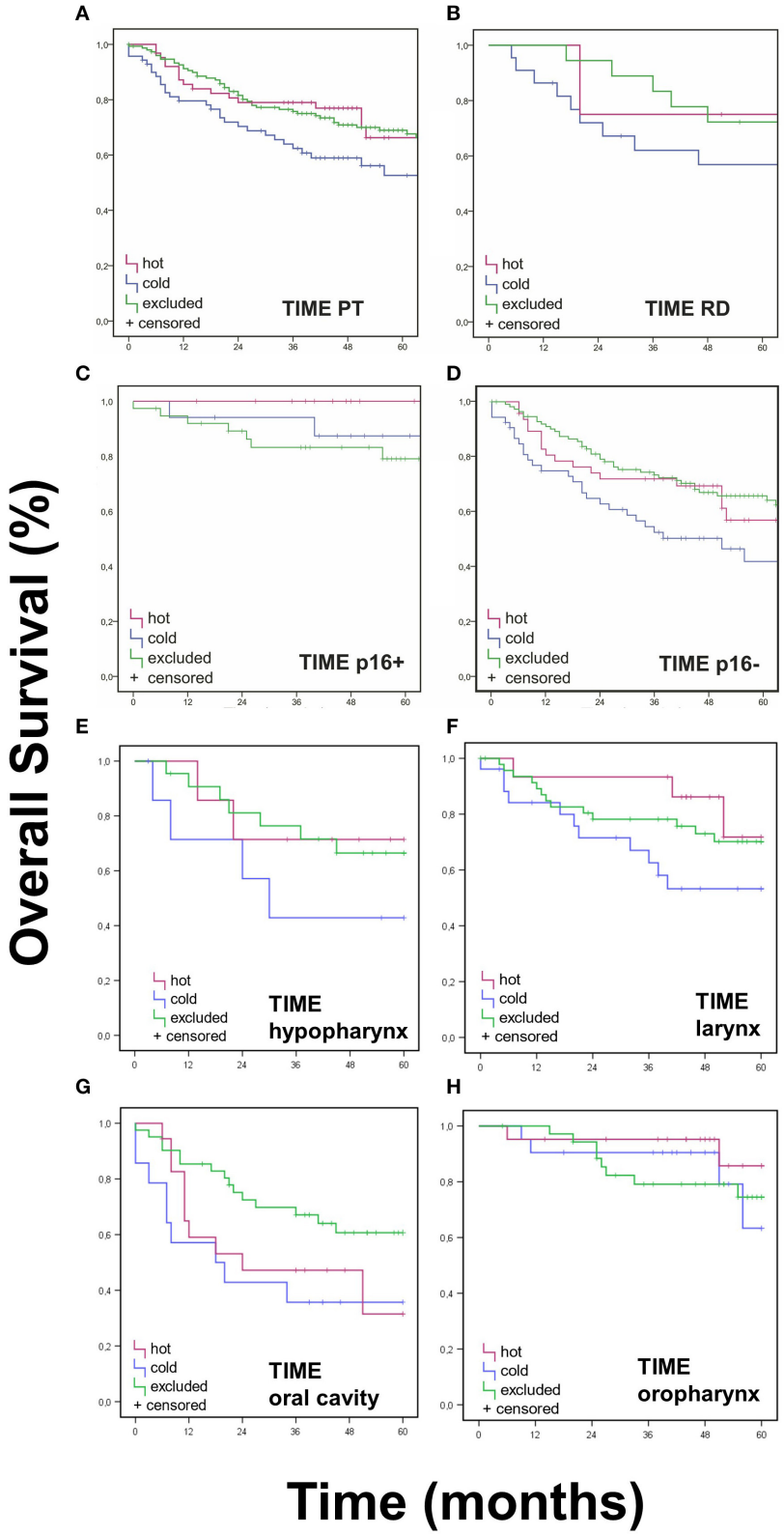

FIGURE 3 | Overall Survival Data for TIME pattern. Immune cell infiltrates were classified as either "hot," "cold," or "excluded" tumors. **(A,B)** OS (Kaplan Meier) was statistically different for TIME assessment in PT ($p < 0.017$), but not in RD ($p > 0.025$). **(C,D)**. Neither was OS significantly different regarding p16 status ($p > 0.017$). **(G)** A better OS for "excluded" oral cavity HNSCCs was observed in comparison to "hot" and "excluded" oral cavity HNSCCs ($p < 0.017$). **(E,F,H)**. No significant differences were found for TIME in other PT locations ($p > 0.017$).

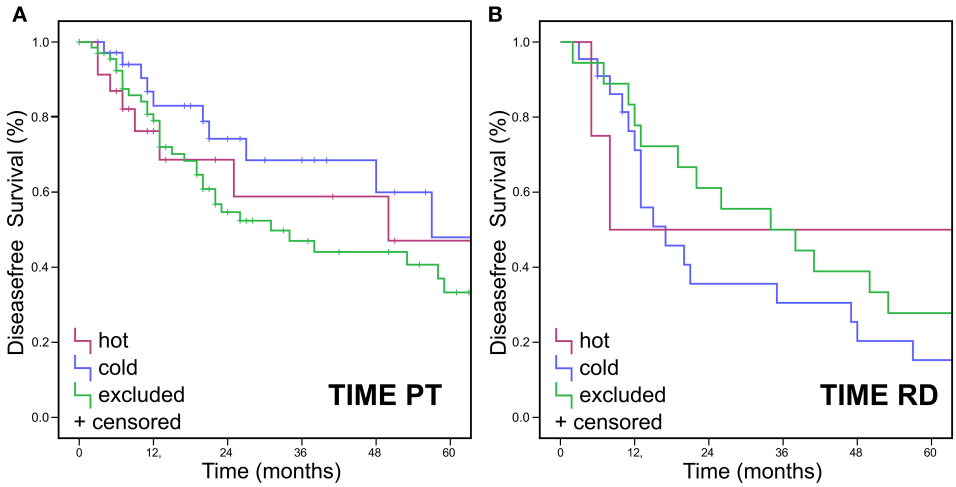

FIGURE 4 | Disease free Survival Data for TIME pattern. Immune cell infiltrates were classified as either "hot," "cold," or "excluded" tumors. DFS (Kaplan Meier) showed no statistically significant differences for DFS in **(A)** PT or **(B)** RD.

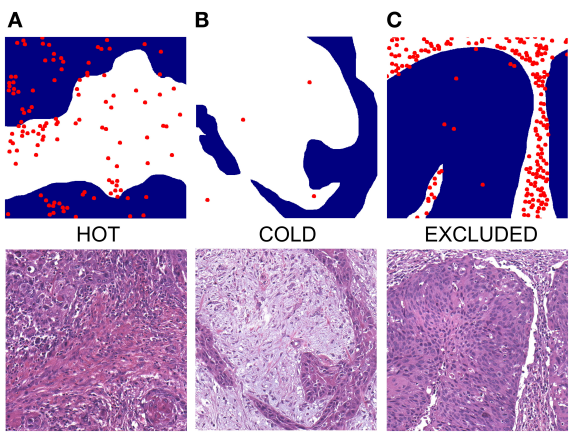

FIGURE 5 | Exemplified depictions of **(A)** "hot", **(B)** "cold," and **(C)** "excluded" HNSCC. The upper row shows graphical TIME patterns with blue reflecting the area of cancer cells, white representing stroma, and red dots flagging the localization of immune cells. The lower row shows photomicrographs of matching typical H&E slides.

types the "hot" tumors are associated with a better OS (36). It has been shown that high counts of immune cells such as CD3- and CD8-positive lymphocytes within the margins of the tumor microenvironment predict a better clinical outcome in HNSCC (37). Moreover, studies suggest a crucial role of tumor-infiltrating lymphocytes (TIL) in the outcome of laryngeal squamous cell cancer concerning DFS and OS and are therefore considered of high interest in the assessment of clinical prognosis (38). We applied the categories "hot," "cold," or "excluded" on HNSCCs by reading routine H&E slides of resection specimens. To our knowledge, this is the first study to investigate the immune cell pattern in HNSCC by a plain histological approach.

Especially for "cold" tumors, our data showed significantly worse survival courses with worse OS and 5-year survival (**Figure 3A**). This is in accordance with a recent Cancer Genome Atlas (TCGA) data analysis of squamous cell carcinoma that also produced "cold" tumors to be associated with the worst prognosis (39).

Characterizing TIME as being either "hot," "cold," or "excluded" can easily be done by any pathologist. It is also more cost-effective and time-saving than immunohistochemical analyses as it only requires standard H&E stained slides. These categories, therefore, propose to be a cheap and intriguing prognostic marker that may be considered to be included in routine pathology reports for HNSCC. In daily routine diagnostics, **Figure 5** may be used as a reference for appreciating typical TIME patterns in H&E slides. More (multi-centered) studies need to be conducted to further distinguish this "hot-cold-excluded" scheme as a potential prognostic tool.

TIME and TNM Staging

The best and universally applied prognostic system so far was and still is grading and tumor staging by TNM/UICC. The H&E categorization in "hot," "cold," and "excluded" could, however, serve as a valuable amendment to it. Especially in an irresectable setting, where no pTNM staging can be established, it might be of use as an addendum to cTNM when assessed on an excisional biopsy specimen. Supposedly, it could also aid in therapeutic decision making when a cancer is right in between two stages. However, before incorporating immune cell phenotypes as predictive markers in clinical practice, further investigation of TIME with special regard to representative classification systems has yet to be conducted. We shall be eager to await validation testing being performed on other cohorts and see the "hot-cold-excluded" scheme being applied to verify prognostic meaning, e.g., regarding OS or DFS. Within early and late UICC stages,

there were no statistically significant differences in OS of TIME categories (**Supplementary Figure 1**).

TIME, ICI Treatment and p16

Knowing distribution patterns of immune cell types in HNSCC could now be used to elucidate if the immune type influences the outcome of an ICI treatment. Our results reveal a minority of RD to be "hot" (9.5%). So far, the only approved ICIs in Germany for the treatment of HNSCC are nivolumab and pembrolizumab. They are, however, solely approved for the treatment of RDs and not for PTs. Before that, approval studies of these drugs were mainly conducted on RD patients (28). These observations might be a part of the explanation for the worse outcome of HNSCC patients receiving ICI treatment when comparing them to other cancer types like melanoma. This hypothesis still needs further investigation. On the one hand, we must increase the patient number when analyzing TIME in RD HNSCCs to get a better estimate of the different immune types. On the other hand, we have to generate new cohorts to analyze the histology of RDs of patients before receiving an ICI treatment and compare it with the outcome of these patients under ICI treatment.

Our data show that "cold" HNSCCs show a worse OS when treated with resection only or with resection plus adjuvant chemoradiotherapy. There was no difference if the treatment was resection plus adjuvant irradiation (**Supplementary Figure 3**). The findings in the resection only therapy group might reflect that patients with a "cold" tumor do have a worse survival than inflamed tumors in general as this treatment is without any selective pressure of the cancer cells for therapy resistance. The different results in the groups with an adjuvant treatment are the more interesting ones because there is selective pressure for treatment resistance. The decision criteria for an adjuvant treatment are quite clear in the guidelines. If patients have lymph node metastasis without extracapsular spread (N+ ECS–) in the neck dissection they receive adjuvant irradiation only. If they have ECS in the lymph node metastasis (N+ ECS+) they receive combined adjuvant irradiation with platin-based chemotherapy. The results presented here might mean that patients suffering from "cold" N+ ECS+ HNSCC might not benefit from adjuvant combined radiochemotherapy like patients with an inflamed tumor. To get a better understanding it would be important to know if N+ ECS+ tumors that were treated with resection plus adjuvant irradiation only because of chemotherapy contraindications (e.g., kidney failure) would show a difference in OS after separating into "cold" and "inflamed" tumors. If these courses would show no difference between these two groups it might show a better response of inflamed tumors after additive chemotherapy in our presented data here. But if the "cold" N+ ECS+ tumors still had a worse OS after treatment with surgery and adjuvant irradiation only it might reflect that "cold" N+ ECS+ tumors have a worse OS in comparison to inflamed N+ ECS+ tumors in general. Our cohort limits the ability to answer these questions. We are curious to see what other (bigger? multi-center?) cohorts might show in retrospective studies when analyzing TIME in regards to treatment outcomes.

In our cohort, we could show that immunologic "hot," "cold," and "excluded" tumors are equally distributed in p16 positive and negative HNSCCs. This might be an explanation of why there was no difference in the subgroup analysis of HPV positive vs. negative tumors in the KEYNOTE study series leading to the FDA approval of pembrolizumab in the treatment of HNSCCs (12, 13). However, the worst OS for p16 positive HNSCC lies within the "excluded" tumors (**Figure 3C**) and not within the "cold" tumors like the rest of the cohort. It seems worthwhile mentioning that this finding is only a trend without statistical significance. All tumors in this cohort were analyzed for p16 expression, independent of the site of origin. p16 itself is a tumor suppressor which can also be expressed independently of HPV status (40). So the p16 expression may not be driven by HPV after all but may be caused by an upregulation of the tumor suppressor p16 due to an overexpression of different other protooncogenes. Creating subgroups within the p16 positive and negative OPSCCs and non-OPSCCs, the subgroups would get too small to yield significant results. It will be interesting to see results on this by analyses on larger cohorts.

In the subgroup analysis of PT site of origin, the tumors of the oral cavity showed a significant difference in OS (**Figure 3G**). Only in this subgroup, the "excluded" tumors had significantly better survival than "hot" or "cold" ones as this difference could not be found in the other sites of origin. This might be another indicator that HNSCCs are indeed a heterogeneous group of cancers rather than one entity. In another study of our group, the oral cavity HNSCCs also showed a significantly lower expression of EVI1 in comparison to HNSCCs of the oropharynx, hypopharynx, and larynx (41). The results presented here might be another hint into this direction, but whether another cytokine profile exists in oral cancers or other factors lead to better survival in "excluded" tumors of the oral cavity need further functional analysis in the future. The detachment of p16 positive OPSCCs is widely accepted and appreciated by TNM and WHO (23, 24). If more unique features of oral cavity HNSCCs are identified in the future they might meet a similar fate like p16 positive OPSCCs and be declared as a distinct entity.

HPV positive HNSCCs have been reported to be more inflamed than HPV negative ones (37). Our data showed no significant connection between p16 status and TIME. When re-grouping "hot" and "excluded" as immune infiltrated and comparing this new category to "cold" tumors we could show that immune infiltrated PTs did not track with p16 positive status (**Figure 2**). Therefore, TIME cannot be used to predict p16 status by observing the tumor immune cell pattern. Our cohort contains a limited number of cases with p16 positive, surgically resected OPSCC that were evaluable for TIME status. Further testing is needed on larger OPSCC cohorts which allows comprehensive analyses of the recently established p16 positive OPSCC regarding the prognostic value of the categorization into hot, cold, or excluded.

The results presented here are merely a stopover, demonstrating the usefulness of tissue cohorts. We want to use our cohort and the knowledge of the different TIME types to investigate factors leading to either a "cold," "excluded," or "hot" tumor to get a better understanding of cancer immunology in HNSCC.

Conclusion

In conclusion, we have constructed a large and well-characterized tumor tissue cohort with comprehensive clinicopathological data. The cohort is well-representative of HNSCC patients and provides us with a subtle device to further investigate ICI-naïve HNSCC. Furthermore, we assessed TIME by reading the tumoral immune infiltrate pattern. We showed that the categorization of HNSCC as being either immunologic "hot," "cold," or "excluded" results in statistically significant differences in OS. This cheap and easy classification may, therefore, be an intriguing prognostic tool that may be considered to be applied in routine pathology reports of HNSCC, possibly even as an amendment to staging and grading. However, further evaluation is warranted and validation testing on other cohorts is needed. This "hot-cold-excluded" scheme needs to be applied to more HNSCC cohorts and possibly to other cancer types to determine prognostic meaning, e.g., regarding OS or DFS.

MATERIALS AND METHODS

Cohort Creation

This retrospective study was conducted following the Declaration of Helsinki. It was approved by the local Ethics Committee (Ethics Committee of the University of Luebeck, AZ 16-277). The REMARK (Reporting Recommendations for Tumor Marker Prognostic Studies) checklist (42) was consulted. Planning for a target power of 80%, an effect size of 30%, and a standard deviation of 60%, we aimed for a sample size of 62 patients per group, summing up to a cohort of (at least) 186 patients.

German state law requires hospital staff to report all first-time diagnosis of cancer to regional Cancer Registries ("Krebsregister"). This is done by using the international code of disease (ICD). For our study, we researched the hospital database for ciphers for squamous cell carcinoma (ICD-O-3) and head and neck regions [ICD-10, C section (43)]. This provided us with a list of 1,266 patients. This list was double-checked for redundancies and non-squamous cell malignancies of the head and neck, e.g. lymphoma, melanoma, SNUC, etc. Those cases were excluded. We then cross-referenced this list with the clinical patient database (Agfa Orbis®) and the pathology tissue database (Nexus®) using pseudonyms. Every case was re-evaluated by a board-certified otorhinolaryngologist and a board-certified pathologist regarding the anatomical site, cancer type, and amount of available tissue. Cases were removed from the cohort if they contained too little an amount of tumor tissue or if tumor tissue had been used up during routine diagnostic procedures. Clinical data were obtained from patients' archives and Agfa Orbis® (list of clinicopathological features in **Supplementary Table 2**).

Then, H&E slides and paraffin blocks were drawn from the archives. After checking paraffin blocks for appropriate tumor amount the cohort was finalized with $n = 419$ patients. Patient data were anonymized. We assembled tumor tissue from PT, lymph node metastasis (LM), RD, and DM. Tissue samples were re-evaluated to classify each case according to the latest TNM classification (8th edition) and UICC stages accordingly. p16 status was determined by immunohistochemical staining of p16 (p16 CINtec ready to use kit, clone E6H4™, mouse monoclonal antibody, Roche Ventana Medical Systems, Tucson, AZ, USA). Regions of interest (ROIs) were annotated on H&E slides and paraffin blocks were matched. Three 0.1 cm cores (triplets) were punched out of every tumor to reflect heterogeneity and were then arranged in acceptor blocks as tissue microarrays (TMAs). Each TMA contained tissue triplets of 55 cancers and 5 normal mucosa samples.

Definitions of "Hot," "Cold", and "Excluded"

For assessment of immune cell distribution status, we analyzed H&E whole slides from those patients from our cohort that underwent resection of PT ($n = 289$) or RD ($n = 42$). We distinguished three categories to determine TIME by reading H&E slides by the following criteria:

"Hot"—More than 2% tumor immune cells, of which more than 50% are distributed diffusely throughout the tumor, i.e. in the tumor stroma and between cancer cells.
"Excluded"—More than 2% tumor immune cells, of which more than 50% are exclusively limited to tumor stroma areas.
"Cold"—Up to 1% tumor immune cells, regardless of location.

If both "hot" and "excluded" patterns were present the one reflecting the majority was assigned. Two board-certified pathologists (JRI, RK) assessed the slides using Olympus BX50 microscope with fluorite objectives with plano-correction (Olympus Europa, Hamburg, Germany). They achieved matching results in 96% ($n = 276$). A third pathologist (SP, head of the department) was consulted to reach a consensus in the discrepant cases. **Figure 5** shows a graphical depiction of these definitions and typical H&E impressions. More examples are to be found in **Supplementary Figure 4**. Divergent interpretations are shown in **Supplementary Figure 5**.

Statistical Analyses and Software

Statistical analysis was performed using IBM SPSS Statistics 25 for Windows (IBM Corp., Armonk, NY, USA). Sixty-months OS and DFS were calculated by the Kaplan-Meier method and log-rank test for statistical significance. Individuals lost to follow-up were censored. Univariate and multivariate Cox regression analyses were performed to evaluate the association among the three immune profiles ("hot," "cold," "excluded") and UICC stages, T stages, p16 status, sex, grading, and patient age. Unless multiple hypothesis testing was applied. $p < 0.05$ were considered statistically significant. For multiple hypothesis testing, we applied the Bonferroni method to adjust the p-value as follows. Three hypotheses were tested for PT, namely postulating a difference in the OS for different TIME patterns, postulating a difference in the OS between p16 positive and negative PTs, and postulating a difference in the DFS of patients with different TIME patterns. The Bonferroni adjusted p-value was $p = 0.05/3 = 0.017$. Two hypotheses were tested to RD, namely assuming a difference in the OS for different TIME patterns, and assuming a difference in the DFS for different TIME patterns. This newly adjusted p-value was $p = 0.05/2 = 0.025$.

We used the following software to create artwork, edit photomicrographs, and compile data visualization. Inkspace (version 0.92.4, The Inkscape Project c/o Software Freedom Conservancy, Brooklyn, NY, USA, https://inkscape.org/). Krita (version 4.2.8, Stichting Krita Foundation, Deventer, The Netherlands, https://krita.org). GIMP (version 2.10.14, The GIMP Project c/o GNOME Foundation, Orinda, CA, USA, https://www.gimp.org). Some data visualization was aided by Daniel's XL Toolbox add-in for Excel (version 7.3.4, by Daniel Kraus, Würzburg, German, www.xltoolbox.net).

DATA AVAILABILITY STATEMENT

The raw data supporting the conclusions of this article will be made available by the authors, without undue reservation.

ETHICS STATEMENT

The studies involving human participants were reviewed and approved by Ethics Committee of the University of Luebeck. Written informed consent for participation was not required for this study in accordance with the national legislation and the institutional requirements.

AUTHOR CONTRIBUTIONS

CI and SP: conceptualization. JR-I, RK, and CI: methodology. AO and PK: validation. LK: formal analysis. CI: investigation. SP and BW: resources. LK and CW: data curation. JR-I: writing—original draft preparation and visualization. RK and JR-I: writing—review and editing. BW and CI: supervision. SP and K-LB: project administration. LK, CI, and F-OP: funding acquisition. All authors contributed to the article and approved the submitted version.

FUNDING

This research was funded by a clinical scientist fellowship of the Medical Faculty of the University of Lübeck (J26-2018) to CI. Fellowships of the Mildred Scheel doctoral program of the German Cancer Aid awarded to LK and F-OP (grant numbers 70113940 and 70112679, respectively).

ACKNOWLEDGMENTS

We thank medical technical staff Wenzel Vogel and Eva Dreyer for excellent technical support. Franz Dressler provided us with highly appreciated statistical advice.

SUPPLEMENTARY MATERIAL

The Supplementary Material for this article can be found online at: https://www.frontiersin.org/articles/10.3389/fmed.2021.622330/full#supplementary-material

Supplementary Figure 1 | Overall survival for "hot," "cold," and "excluded" tumors in UICC stages I/II and UICC stages III/IV.

Supplementary Figure 2 | TIME in different locations of PTs.

Supplementary Figure 3 | Overall survival for "hot", "cold", and "excluded" tumors after different therapy approaches.

Supplementary Figure 4 | Additional examples of TIME categories.

Supplementary Figure 5 | Examples of divergent TIME interpretation. Both were interpreted as both "hot" and "excluded". With help of the third observer, a consensus was reached that **(A)** classifies as "excluded" and **(B)** as "hot".

Supplementary Table 1 | Univariate and multivariate cox regression for the OS. $*$ = $p \leq 0.05$; ** = $p \leq 0.01$; *** = $p \leq 0.001$). Compared were the immune infiltration of the tumors ("hot" and "excluded" vs. "cold"), the T stage, UICC stage, p16 expression, grading, sex, and age of HNSCC patients.

Supplementary Table 2 | List of clinicopathological features.

REFERENCES

1. Parker SL, Tong T, Bolden S, Wingo PA. Cancer statistics, 1996. *CA: Cancer J Clin*. (1996) 46:5–27. doi: 10.3322/canjclin.46.1.5
2. Vokes EE, Weichselbaum RR, Lippman SM, Hong WK. Head and neck cancer. *N Engl J Med*. (1993) 328:184–94. doi: 10.1056/NEJM199301213280306
3. Larson DL, Lindberg RD, Lane E, Goepfert H. Major complications of radiotherapy in cancer of the oral cavity and oropharynx. A 10 year retrospective study. *Am J Surg*. (1983) 146:531–6. doi: 10.1016/0002-9610(83)90247-7
4. Ervin TJ, Clark JR, Weichselbaum RR, Fallon BG, Miller D, Fabian RL, et al. An analysis of induction and adjuvant chemotherapy in the multidisciplinary treatment of squamous-cell carcinoma of the head and neck. *J Clin Oncol*. (1987) 5:10–20. doi: 10.1200/JCO.1987.5.1.10
5. Chin D, Boyle GM, Porceddu S, Theile DR, Parsons PG, Coman WB. Head and neck cancer: past, present and future. *Expert Rev Anticancer Ther*. (2006) 6:1111–8. doi: 10.1586/14737140.6.7.1111
6. Bernier J. A multidisciplinary approach to squamous cell carcinomas of the head and neck: an update. *Curr Opin Oncol*. (2008) 20:249–55. doi: 10.1097/CCO.0b013e3282faa0b1
7. Stell PM, Rawson NS. Adjuvant chemotherapy in head and neck cancer. *Br J Cancer*. (1990) 61:779–87. doi: 10.1038/bjc.1990.175
8. Murdoch D. Standard, and novel cytotoxic and molecular-targeted, therapies for HNSCC: an evidence-based review. *Curr Opin Oncol*. (2007) 19:216–21. doi: 10.1097/01.cco.0000264952.98166.99
9. Sher DJ, Yan J, Day A, Sumer BD, Pham N-L, Khan S, et al. Comparative effectiveness of primary radiotherapy versus surgery in elderly patients with locally advanced oropharyngeal squamous cell carcinoma. *Oral Oncol*. (2019) 88:18–26. doi: 10.1016/j.oraloncology.2018.11.004
10. Seyedin SN, Tang C, Welsh JW. Author's view: radiation and immunotherapy as systemic therapy for solid tumors. *Oncoimmunology*. (2015) 4:e986402. doi: 10.4161/2162402X.2014.986402
11. Topalian SL, Hodi FS, Brahmer JR, Gettinger SN, Smith DC, McDermott DF, et al. Five-year survival and correlates among patients with advanced melanoma, renal cell carcinoma, or non-small cell lung cancer treated with nivolumab. *JAMA Oncol*. (2019) 5:1411–20. doi: 10.1001/jamaoncol.2019.2187
12. Larkins E, Blumenthal GM, Yuan W, He K, Sridhara R, Subramaniam S, et al. FDA approval summary: pembrolizumab for the treatment of recurrent or metastatic head and neck squamous cell carcinoma with disease progression on or after platinum-containing chemotherapy. *Oncologist*. (2017) 22:873–8. doi: 10.1634/theoncologist.2016-0496
13. Ferris RL, Blumenschein G, Fayette J, Guigay J, Colevas AD, Licitra L, et al. Nivolumab for recurrent squamous-cell carcinoma of the head and neck. *N Engl J Med*. (2016) 375:1856–67. doi: 10.1056/NEJMoa1602252

14. Binder DC, Engels B, Arina A, Yu P, Slauch JM, Fu Y-X, et al. Antigen-specific bacterial vaccine combined with anti-PD-L1 rescues dysfunctional endogenous T cells to reject long-established cancer. *Cancer Immunol Res*. (2013) 1:123–33. doi: 10.1158/2326-6066.CIR-13-0058
15. Newton JM, Hanoteau A, Liu H-C, Gaspero A, Parikh F, Gartrell-Corrado RD, et al. Immune microenvironment modulation unmasks therapeutic benefit of radiotherapy and checkpoint inhibition. *J Immunother Cancer*. (2019) 7:216. doi: 10.1186/s40425-019-0698-6
16. Krupar R, Hautmann MG, Pathak RR, Varier I, McLaren C, Gaag D, et al. Immunometabolic determinants of chemoradiotherapy response and survival in head and neck squamous cell carcinoma. *Am J Pathol*. (2018) 188:72–83. doi: 10.1016/j.ajpath.2017.09.013
17. Kather JN, Suarez-Carmona M, Charoentong P, Weis C-A, Hirsch D, Bankhead P, et al. Topography of cancer-associated immune cells in human solid tumors. *eLife*. (2018) 7:e36967. doi: 10.7554/eLife.36967
18. Chen DS, Mellman I. Elements of cancer immunity and the cancer–immune set point. *Nature*. (2017) 541:321–30. doi: 10.1038/nature21349
19. Galon J, Bruni D. Approaches to treat immune hot, altered and cold tumors with combination immunotherapies. *Nat Rev Drug Discov*. (2019) 18:197–218. doi: 10.1038/s41573-018-0007-y
20. Mlecnik B, Tosolini M, Kirilovsky A, Berger A, Bindea G, Meatchi T, et al. Histopathologic-based prognostic factors of colorectal cancers are associated with the state of the local immune reaction. *J Clin Oncol*. (2011) 29:610–8. doi: 10.1200/JCO.2010.30.5425
21. Bonaventura P, Shekarian T, Alcazer V, Valladeau-Guilemond J, Valsesia-Wittmann S, Amigorena S, et al. Cold tumors: a therapeutic challenge for immunotherapy. *Front Immunol*. (2019) 10:168. doi: 10.3389/fimmu.2019.00168
22. Saloura V, Izumchenko E, Zuo Z, Bao R, Korzinkin M, Ozerov I, et al. Immune profiles in primary squamous cell carcinoma of the head and neck. *Oral Oncol*. (2019) 96:77–88. doi: 10.1016/j.oraloncology.2019.06.032
23. Wittekind C. *TNM: Klassifikation Maligner Tumoren*. 8th ed. Weinheim: Wiley VCH Verlag GmbH (2017). p. 336.
24. El-Naggar AK, Chan JKC, Rubin Grandis J, Takata T, Slootweg PJ, International Agency for Research on Cancer. *WHO Classification of Head and Neck Tumours [Internet]*. 4th ed. Lyon: International Agency for Research on Cancer (2017). p. 347.
25. McArthur GA, Ribas A. Targeting oncogenic drivers and the immune system in melanoma. *J Clin Oncol*. (2012) 31:499–506; doi: 10.1200/JCO.2012.45.5568
26. An Q, Liu Z. Comparative efficacy and safety of combination therapies for advanced melanoma: a network meta-analysis. *BMC Cancer*. (2019) 19:43. doi: 10.1186/s12885-018-5259-8
27. Ichiki Y, Taira A, Chikaishi Y, Matsumiya H, Mori M, Kanayama M, et al. Prognostic factors of advanced or postoperative recurrent non-small cell lung cancer targeted with immune check point inhibitors. *J Thorac Dis*. (2019) 11:1117–23. doi: 10.21037/jtd.2019.04.41
28. Pai SI, Faivre S, Licitra L, Machiels JP, Vermorken JB, Bruzzi P, et al. Comparative analysis of the phase III clinical trials of anti-PD1 monotherapy in head and neck squamous cell carcinoma patients (CheckMate 141 and KEYNOTE 040). *J ImmunoTher Cancer*. (2019) 7:1–4. doi: 10.1186/s40425-019-0578-0
29. Robert Koch-Institut. *Krebs in Deutschland für 2013/2014*. Berlin: Robert Koch-Institut (2017).
30. Wienecke A, Kraywinkel K. Epidemiologie von Kopf-Hals-Tumoren in Deutschland. *Der Onkologe*. (2019) 25:190–200. doi: 10.1007/s00761-019-0534-0
31. Mehanna H, Beech T, Nicholson T, El-Hariry I, McConkey C, Paleri V, et al. Prevalence of human papillomavirus in oropharyngeal and nonoropharyngeal head and neck cancer–systematic review and meta-analysis of trends by time and region. *Head Neck*. (2013) 35:747–55. doi: 10.1002/hed.22015
32. Quabius ES, Haag J, Kühnel A, Henry H, Hoffmann AS, Görögh T, et al. Geographical and anatomical influences on human papillomavirus prevalence diversity in head and neck squamous cell carcinoma in Germany. *Intern J Oncol*. (2015) 46:414–22. doi: 10.3892/ijo.2014.2697
33. Kreimer AR, Clifford GM, Boyle P, Franceschi S. Human papillomavirus types in head and neck squamous cell carcinomas worldwide: a systematic review. *Cancer Epidemiol. Biomarkers Prev*. (2005) 14:467–75. doi: 10.1158/1055-9965.EPI-04-0551
34. Tinhofer I, Jöhrens K, Keilholz U, Kaufmann A, Lehmann A, Weichert W, et al. Contribution of human papilloma virus to the incidence of squamous cell carcinoma of the head and neck in a European population with high smoking prevalence. *Eur J Cancer*. (2015) 51:514–21. doi: 10.1016/j.ejca.2014.12.018
35. EuroCare Database. *Survival of Cancer Patients in Europe* (2019). Available online at: http://www.eurocare.it/Database/tabid/77/Default.aspx (accessed November 14, 2019).
36. Xu W, Atkinson VG, Menzies AM. Intratumoural immunotherapies in oncology. *Eur J Cancer*. (2020) 127:1–11. doi: 10.1016/j.ejca.2019.12.007
37. de Ruiter EJ, Ooft ML, Devriese LA, Willems SM. The prognostic role of tumor infiltrating T-lymphocytes in squamous cell carcinoma of the head and neck: a systematic review and meta-analysis. *Oncoimmunology*. (2017) 6:e135614. doi: 10.1080/2162402X.2017.1356148
38. Vassilakopoulou M, Avgeris M, Velcheti V, Kotoula V, Rampias T, Chatzopoulos K, et al. Evaluation of PD-L1 expression and associated tumor-infiltrating lymphocytes in laryngeal squamous cell carcinoma. *Clin Cancer Res*. (2016) 22:704–13. doi: 10.1158/1078-0432.CCR-15-1543
39. Li B, Cui Y, Nambiar DK, Sunwoo JB, Li R. The immune subtypes and landscape of squamous cell carcinoma. *Clin Cancer Res*. (2019) 25:clincanres.4085.2018. doi: 10.1158/1078-0432.CCR-18-4085
40. Romagosa C, Simonetti S, López-Vicente L, Mazo A, Lleonart ME, Castellvi J, et al. p16(Ink4a) overexpression in cancer: a tumor suppressor gene associated with senescence and high-grade tumors. *Oncogene*. (2011) 30:2087–97. doi: 10.1038/onc.2010.614
41. Idel C, Ribbat-Idel J, Kuppler P, Krupar R, Offermann A, Vogel W, et al. EVI1 as a marker for lymph node metastasis in HNSCC. *Int J Mol Sci*. (2020) 21:854. doi: 10.3390/ijms21030854
42. McShane LM, Altman DG, Sauerbrei W, Taube SE, Gion M, Clark GM, et al. Reporting recommendations for tumor marker prognostic studies (REMARK). *J Natl Cancer Inst*. (2005) 97:1180–4. doi: 10.1093/jnci/dji237
43. *ICD-10 Version:2014*. Available online at: https://icd.who.int/browse10/2014/en#/II

Conflict of Interest: The authors declare that the research was conducted in the absence of any commercial or financial relationships that could be construed as a potential conflict of interest.

frontiers in Medicine

ORIGINAL RESEARCH
published: 27 April 2021
doi: 10.3389/fmed.2021.640515

Performance of Different Diagnostic PD-L1 Clones in Head and Neck Squamous Cell Carcinoma

Julika Ribbat-Idel[1†], Franz F. Dressler[1†], Rosemarie Krupar[2], Christian Watermann[1], Finn-Ole Paulsen[1], Patrick Kuppler[1], Luise Klapper[1], Anne Offermann[1], Barbara Wollenberg[3], Dirk Rades[4], Simon Laban[5], Markus Reischl[6], Karl-Ludwig Bruchhage[7], Christian Idel[7†] and Sven Perner[1,2†]*

[1] Institute of Pathology, University of Luebeck and University Hospital Schleswig-Holstein, Luebeck, Germany, [2] Pathology, Research Center Borstel, Leibniz Lung Center, Borstel, Germany, [3] Department of Otorhinolaryngology, MRI Technical University Munich, Munich, Germany, [4] Department of Radiation Oncology, University of Luebeck, Luebeck, Germany, [5] Department of Otorhinolaryngology, Head and Neck Surgery, University of Ulm, Ulm, Germany, [6] Karlsruhe Institute of Technology, Institute for Automation and Applied Informatics, Eggenstein-Leopoldshafen, Germany, [7] Department of Otorhinolaryngology, University of Luebeck, Luebeck, Germany

OPEN ACCESS

Edited by:
Arndt Hartmann, Pathological Institute, Germany

Reviewed by:
Markus Eckstein, University of Erlangen Nuremberg, Germany
Korinna Joehrens, Technische Universität Dresden, Germany

***Correspondence:**
Julika Ribbat-Idel
Julika.Ribbat-Idel@uksh.de

[†] These authors have contributed equally to this work

Specialty section:
This article was submitted to Pathology, a section of the journal Frontiers in Medicine

Received: *11 December 2020*
Accepted: *29 March 2021*
Published: *27 April 2021*

Citation:
Ribbat-Idel J, Dressler FF, Krupar R, Watermann C, Paulsen F-O, Kuppler P, Klapper L, Offermann A, Wollenberg B, Rades D, Laban S, Reischl M, Bruchhage K-L, Idel C and Perner S (2021) Performance of Different Diagnostic PD-L1 Clones in Head and Neck Squamous Cell Carcinoma. Front. Med. 8:640515. doi: 10.3389/fmed.2021.640515

Background: The approval of immune checkpoint inhibitors in combination with specific diagnostic biomarkers presents new challenges to pathologists as tumor tissue needs to be tested for expression of programmed death-ligand 1 (PD-L1) for a variety of indications. As there is currently no requirement to use companion diagnostic assays for PD-L1 testing in Germany different clones are used in daily routine. While the correlation of staining results has been tested in various entities, there is no data for head and neck squamous cell carcinomas (HNSCC) so far.

Methods: We tested five different PD-L1 clones (SP263, SP142, E1L3N, 22-8, 22C3) on primary HNSCC tumor tissue of 75 patients in the form of tissue microarrays. Stainings of both immune and tumor cells were then assessed and quantified by pathologists to simulate real-world routine diagnostics. The results were analyzed descriptively and the resulting staining pattern across patients was further investigated by principal component analysis and non-negative matrix factorization clustering.

Results: Percentages of positive immune and tumor cells varied greatly. Both the resulting combined positive score as well as the eligibility for certain checkpoint inhibitor regimens was therefore strongly dependent on the choice of the antibody. No relevant co-clustering and low similarity of relative staining patterns across patients was found for the different antibodies.

Conclusions: Performance of different diagnostic anti PD-L1 antibody clones in HNSCC is less robust and interchangeable compared to reported data from other tumor entities. Determination of PD-L1 expression is critical for therapeutic decision making and may be aided by back-to-back testing of different PD-L1 clones.

Keywords: HNSCC, PD-L1, checkpoint inhibitors, TMA, harmonization, therapy prediction, protein quantitation

INTRODUCTION

In a growing number of solid tumors, immunotherapy by checkpoint blockage targeting programmed death receptor 1 (PD-1) or its ligand programmed death-ligand 1 (PD-L1) has become a standard treatment (1–9). The response to the administration of most PD-1 or PD-L1 inhibitors often correlates with PD-L1 expression determined before therapy using specific companion diagnostics for immunohistochemistry (IHC) resulting in approval in combination with PD-L1 expression as a diagnostic biomarker (8, 9). In HNSCC, this does not hold good for nivolumab which is approved for administration after cisplatin failure, regardless of PD-L1 status determined by IHC. For pembrolizumab, though, it is still necessary to specify PD-L1 status by IHC. Interestingly, most tumor boards still request PD-L1 status from the pathologists to decide for or against a checkpoint inhibitor therapy regime. While IHC is a routine tool in modern pathology to investigate diagnostic and predictive markers in tissue samples, its use in PD-L1 expression analysis has raised several issues: (a) There are different PD-L1 assays each specific to a therapeutic antibody without a common standard. (b) Different scoring systems are applied to different tumor types and indications. (c) Problems of tumor heterogeneity, inter-institutional preanalytics, and inter-/intra-observer variability are being addressed but are difficult to solve (10). Several attempts have been made to compare commercially available PD-L1 clones (11–14). For example, clone 22C3 (Agilent Dako Omnis, Santa Clara, CA, USA) showed high concordance with SP263 (Ventana Medical Systems Roche, Oro Valley, AZ, USA). For non-small cell lung cancer (NSCLC), it was therefore recently CE-marked for interchangeable use with 22C3 and 28-8 (Abcam, Cambridge, UK) (10). Some pathology laboratories use less expensive PD-L1 clones such as 22C3 and E1L3N for different reasons. Like many hospitals, they are dedicated to the economically efficient use of reagents and resources. Similarly, some lack access to the specific immunostainer platform that is necessary to carry out clone-specific stains (e.g., Ventana Benchmark immunostainer for SP263, both Ventana Roche), and there are no commercially available ready to use kits for PD-L1 clones for the widely used Leica Bond platform (Leica Biosystems, Wetzlar, Germany) (10).

Checkpoint and PD-L1 inhibitors like pembrolizumab, atezolizumab, and durvalumab have been approved for first or second-line treatment of PD-L1 positive advanced cancers [e.g., NSCLC (2, 3, 15)], urothelial cancer (16), and triple-negative breast cancer (17). Since then, pathologists are required to report the PD-L1 status, which comprises one or more PD-L1 scores depending on the tumor entity. The tumor positivity score (TPS) is defined as the estimated percentage of tumor cells showing partial or complete membrane staining for PD-L1. It was developed for clone 22C3 as a biomarker for pembrolizumab (9, 18). The immune cell score (IC) is based on the estimated area of PD-L1 positive tumor immune cells in relation to all tumor immune cells. It was developed for SP142 in urothelial carcinoma, NSCLC (15), and TNBC. The combined positivity score (CPS) is supposed to reflect both tumor cell and immune cell PD-L1 expression. It was also developed as a biomarker for pembrolizumab.

In the USA, the Federal Drug Administration (FDA) restricted the application of pembrolizumab for advanced NSCLC to those patients whose tumor samples had been tested using the DAKO 22C3 pharmDx assay (the so-called companion diagnostic assay) (18). In Europe though, the DAKO platform is not as widely used, and the European Medicines Agency (EMA) does not demand a mandatory specific PD-L1 IHC platform or clone (10).

For recurrent HNSCC, two therapeutic anti-PD-1 antibodies are currently used: Nivolumab after cisplatin failure without PD-L1 expression as a biomarker and Pembrolizumab after cisplatin failure and with a TPS $\geq$50%. Pembrolizumab is also approved for palliative first-line treatment of HNSCC with a CPS$\geq$1 with or without platinum-based chemotherapy. Thus, targeting the same molecule, Pembrolizumab requires PD-L1 expression to be demonstrated by IHC, while the use of Nivolumab is not restricted.

MATERIALS AND METHODS

Tumor Material and Patient Data

The study was conducted according the Declaration of Helsinki. Approval by the University of Luebeck Ethics Committee was obtained (project code AZ 16-277). Tissue samples were routinely fixated in 4% buffered neutral formalin for 12–24 h. After paraffin embedding the preserved tissue blocks were stored at room temperature in our archives until they were retrieved. We accessed our large and comprehensively clinicopathologically characterized HNSCC cohort, as described before (19, 20). For the study at hand, we selected those TMAs from our cohort that contained tumor tissue of recurrent disease and matching primary tumors ($n = 75$ patients). For patient details please refer to **Supplementary Table 1**.

TMA Construction

H&E slides were annotated for regions of interest (ROI) containing representative squamous cell carcinoma areas. Corresponding paraffin blocks were matched. Manual Tissue Arrayer 1 (Estigen AlphaMetrix Biotech, Rödermark, Germany) was used to construct TMAs as seen in **Figure 1**. Briefly, 2 mm diameter cores were punched out of the donor block's ROI and embedded into a paraffin recipient block. This was repeated three times for each tumor sample resulting in three cores per patient. One recipient block holds up to 60 triplets. Whenever possible, meaning whenever enough representative tumor tissue could be yielded, we created two more replicas of each TMA.

Immunohistochemistry and Evaluation of Stains

3 µm thin slices were cut from the TMA recipients' blocks and put on glass slides (**Figure 1**). All immunohistochemical stainings were performed on a Ventana BenchMark automated staining system (Roche, Basel, Switzerland), as previously described (21). Deparaffinization protocol according to EZ Prep was followed by heat-mediated antigen retrieval (pH 8.4 buffer for up to 32 min; both Ventana Medical Systems Roche, Oro

Valley, AZ, USA). Primary antibody was titrated and incubated as follows.

- SP263: incubation for 20 min at 36° (rabbit monoclonal antibody with OptiView DAB IHC Detection Kit, both Ventana Medical Systems Roche)
- SP142: incubation for 8 min at 37° (rabbit monoclonal antibody with OptiView DAB IHC Detection Kit, both Ventana Medical Systems Roche)
- E1L3N: incubation for 60 min at 36° (rabbit monoclonal antibody, RTU, Cell Signaling, Danvers, MA, USA). Counterstaining with haematoxylin (Ventana Medical Systems, Tucson, AZ, USA) and the proper alkalinity was ensured by washing with Bluing reagent, pH = 8.0.
- 28-8: incubation for 40 minutes at 37° (ab205921, rabbit monoclonal antibody, Abcam, Cambridge, UK with OptiView IHC Detection Kit, Ventana Medical Systems Roche)
- 22C3: incubation for 40 min at 37° (mouse monoclonal antibody, Agilent Dako Omnis, Santa Clara, CA, USA with OptiView DAB IHC Detection Kit, Ventana Medical Systems Roche)

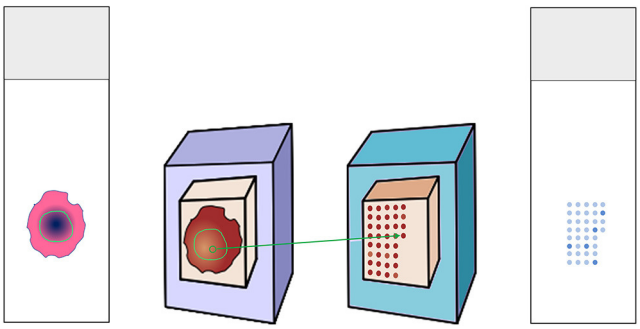

FIGURE 1 | Construction of tissue microarray. Donor H&E slides were annotated for the tumor region. The matching donor blocks were identified and annotated as well. Three cores from the region of interest were punched out and embedded in the recipient paraffin block. The recipient block could then serve for multiple analyses, e.g., immunohistochemical stainings.

Tonsil tissue was employed as positive control (**Supplementary Figure 1**). PD-L1 IHC stains were then evaluated by two independent pathologists. Tumors were represented by three cores to address tumor heterogeneity. PD-L1 scores were reported separately for each core. Mean values of the three cores were calculated and used as input for score calculation. The resulting expression data contained the number and area shares of tumor and immune cells with the expression as well as the ratio of tumor to immune cell number [necessary to calculate the combined positive score (CPS)]. The latter was calculated as the number of positive immune and tumor cells divided by the number of viable tumor cells, multiplied by and capped at 100. The total positive score (TPS) was calculated as the percentage of tumor cells with positive membrane staining, regardless of staining intensity and continuance. The immune cell score (IC) is the percentage of tumor area occupied by tumor immune cells.

Statistical Analysis and Visualization

All statistical analyses were performed by custom scripts in Python 2.7 (Enthought, Austin, USA, Canopy distribution 1.1.0.1371) including the scipy, numpy, sklearn, matplotlib, seaborn and pandas packages. Non-negative matrix factorization was performed based on the nimfa package (22). Briefly, the data were z-score transformed, shifted by the minimum value to turn negative into positive values without changing data patterns, and factorized with random seed, rank * 100 iterations and 100 runs. The resulting data was further analyzed and visualized with the scipy.cluster.hierarchy module.

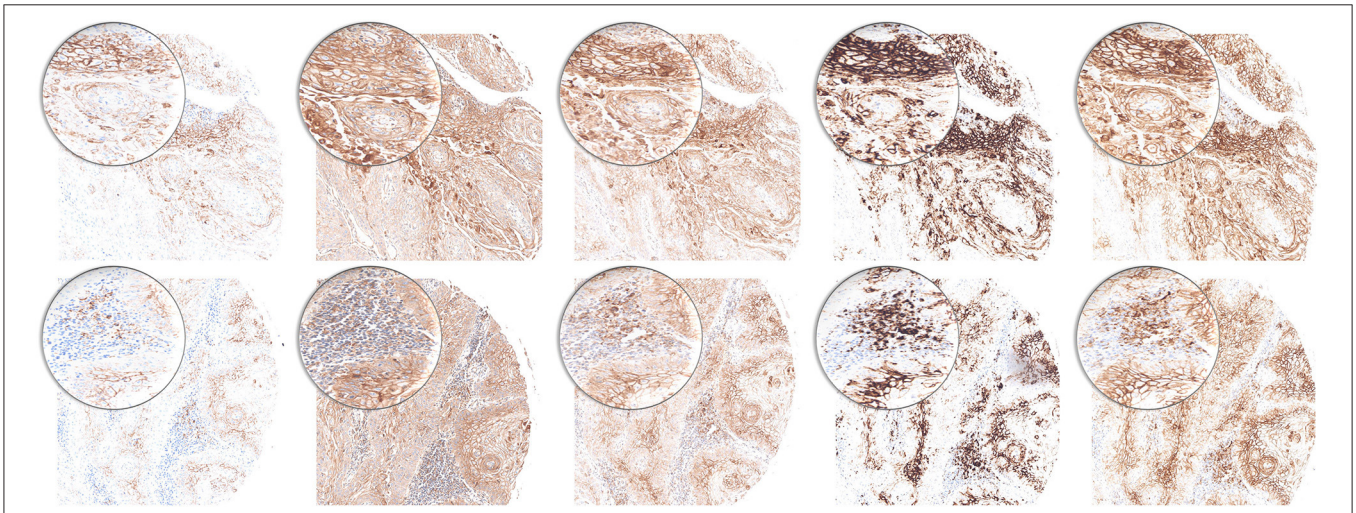

FIGURE 2 | PD-L1 staining pattern in HNSCC. Upper row: tumor cells. Lower row: immune cells. From left to right: 22C3, 28-8, E1L3N, SP142, and SP263. Original magnification x100. Inlay magnification x200.

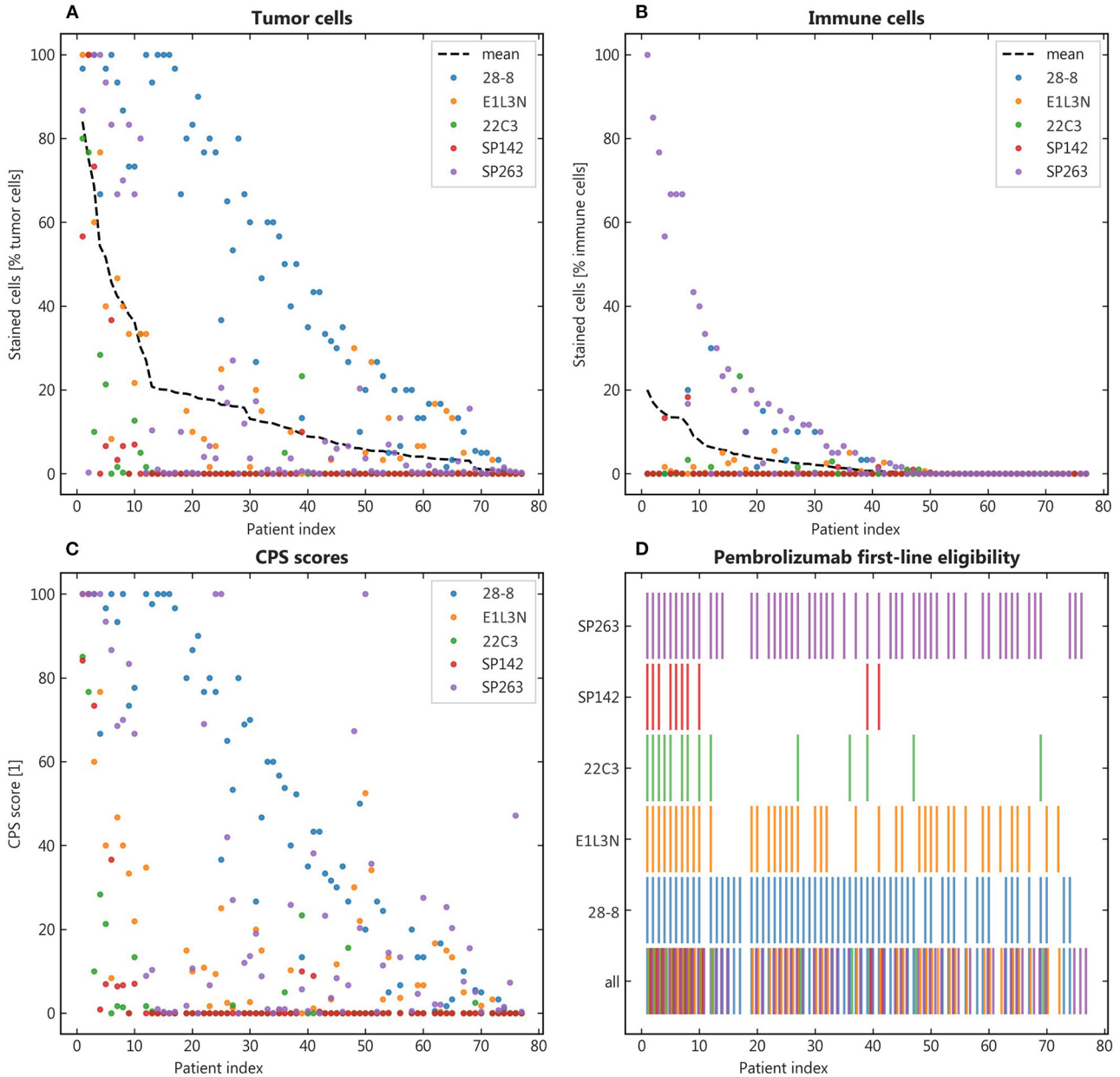

FIGURE 3 | Qualitative results. **(A,B)**: Patients were ranked by their mean positive tumor and immune cells respectively to facilitate comparison across the different antibody clones; **(C)**: The combined positive score (CPS) was calculated for each patient and the resulting eligibility for pembrolizumab portrayed in binary representation (color = eligible) **(D)**.

Apart from Python visualization packages, we used the following software to create artwork and edit photomicrographs. Inkspace (version 0.92.4, The Inkscape Project c/o Software Freedom Conservancy, Brooklyn, NY, USA, https://inkscape.org/), Krita (version 4.2.8, Stichting Krita Foundation, Deventer, The Netherlands, https://krita.org), GIMP (version 2.10.14, The GIMP Project c/o GNOME Foundation, Orinda, CA, USA, https://www.gimp.org).

RESULTS

Tumor Material and Patient Data

As described previously, our cohort is well-representative for HNSCCs and well-reflects the aggressive tumor behavior (19). Briefly, our cohort mirrors the typical characteristics for HNSCC patients: three-quarters were men with smoking and alcohol as common nutritive-toxic pathogens. A little <1/3 were p16 positive. The majority offered advanced stages (UICC III/IV) at first-time diagnosis. About 25% of patients experienced a cancer

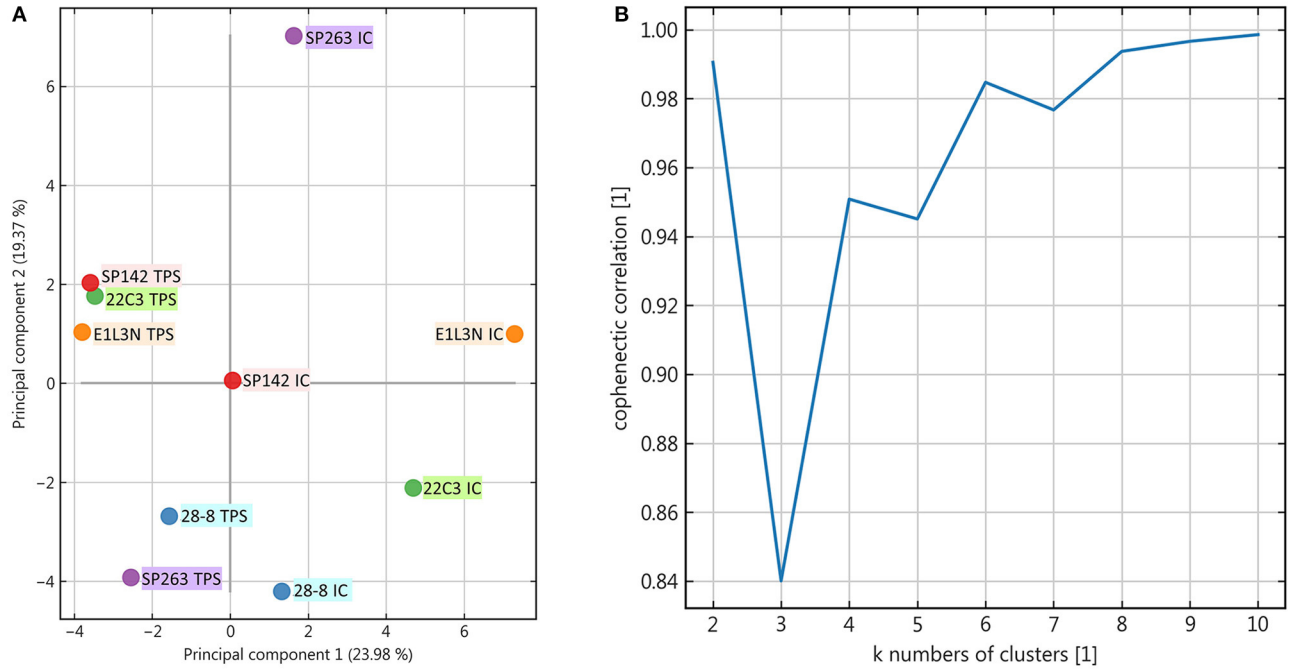

FIGURE 4 | Principal component analysis and rank estimate for non-negative matrix factorization (NMF) consensus clustering. **(A)**: Principal components were calculated for the dataset and the individual clones visualized two-dimensionally according to their relative correlation with the two main components; **(B)**: In NMF the cophenetic correlation was calculated to find the number of clusters that reduced dimensionality best.

relapse, half of which passed away within 5 years. The 5-year survival for the whole cohort was about 60%.

Immunohistochemistry and Evaluation of Stains

We performed immunohistochemical PD-L1 stains for five clones (22C3, 28-2, E1L3N, SP142, and SP263) and estimated TPS, IC, and CPS. All five clones delivered satisfactory staining quality with 22C3 being the most discreet. SP142 offered a more grainy aspect. E1L3N, SP263, and 28-8 showed a robust pattern (**Figure 2**). Positive controls demonstrate staining success (tonsil tissue, **Supplementary Figure 1**).

Statistical Analysis

To illustrate the variety of staining with different clones, the mean share of positive stainings across clones was calculated and the patient samples ranked by this order (**Figures 3A,B**). The resulting distribution showed marked dispersion, which was also mirrored by the resulting CPS (**Figure 3C**). As a relevant clinical consequence, the individual eligibility of patients for first-line pembrolizumab was assessed by CPS $\geq$ 1 (**Figure 3D**). Thereby, relevant differences between clones were observed with eligible patients ranging from SP142 with 14%, 22C3 with 18% to E1L3N with 48%, SP263 with 68%, and 28-8 with 78% of patients. As other cutoffs are used in clinical trials we also calculated alternative eligibility cutoffs for CPS1, CPS20, CPD50, and TPS50 (**Supplementary Figure 2**).

Apart from this qualitative assessment, the identification of underlying staining patterns was approached by principal component analysis (PCA) and non-negative matrix factorization-based consensus clustering (NMF). While PCA showed similarity between the tumor stainings of SP142, 22C3, and E1L3N (**Figure 4A**), no stable and relevant reduction of dimensionality could be observed by NMF clustering (**Figure 5**) indicated by maximum cophenetic correlation for k = 10 clusters (with $n = 10$ input samples (clones); **Figure 4B**). Some co-clustering of SP142/22C3 tumor staining was observed as well as less stable co-clustering of SP263 and E1L3N tumor staining. SP263 and 28-8 co-clustered relatively strongly for k = 2 clusters, mirrored by similar correlations in PCA and similar quantitative results of the staining raw data. However, the cluster did not prove to be stable in higher ranks (compare to quick drop in cophenetic correlation, **Figure 4B**).

DISCUSSION

The introduction of immune checkpoint inhibitors in cancer therapy considerably improved survival in several entities, e.g., melanoma and lung cancer (23, 24). For HNSCC, survival improved compared to the previous standard of care. However, the high hopes remained hitherto unfulfilled in large part. While overall survival for recurrent disease is still significantly increased in comparison with previous therapy regimens, the effect size seems to be smaller than in melanoma (8, 25). Adverse effects were significantly less severe than with chemotherapy. No more

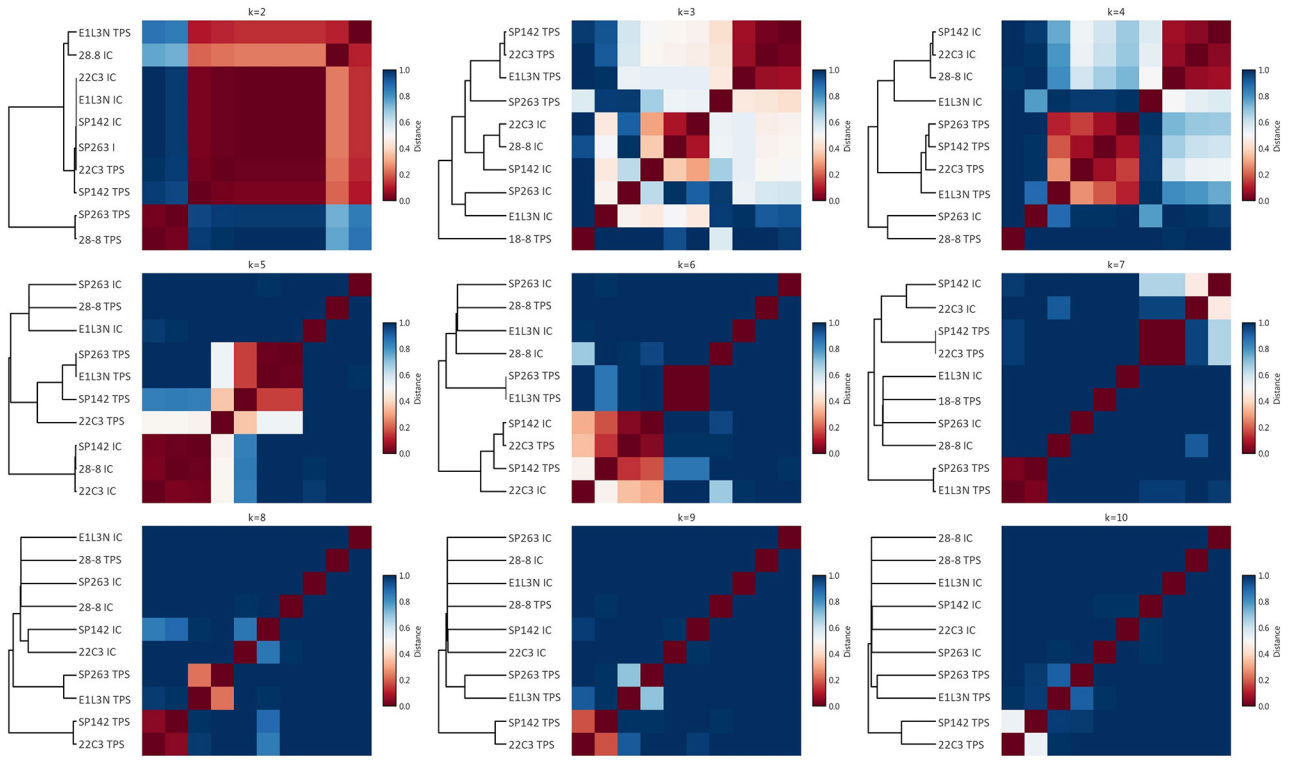

FIGURE 5 | NMF consensus clustering. For varying numbers of clusters (ranks; subplots), NMF consensus clustering was performed; for each rank, the consensus matrix as a measure of cluster stability is shown as a heat plot with red indicating perfect consensus for a given pair of clones across stochastic runs (the clones end up in the same cluster all the time); the dendrogram on the left indicates relative cluster similarity by the respective lengths of the horizontal lines.

grade IV/V side effects were observed than with the comparator. Still, checkpoint inhibitors do offer side effects, some of which can be quite severe (e.g., pneumonitis, myocarditis). Against this background accurate checkpoint inhibitor response prediction in HNSCC patients is important.

Our data show a marked variation of staining results based on the diagnostic antibody used. Both descriptive analyses such as the basic share of positive cells as well as more comprehensive statistical approaches reveal only weak staining similarity, mostly between SP263 and 28-8 tumor staining. Taken altogether this translates into considerably different shares of patients being identified as eligible for second-line monotherapy.

Several harmonization studies for the diagnostic detection of PD-L1 expression were performed in different solid cancer entities with most studies focusing on non-small cell lung cancer (12, 14, 26–30). The results of the study presented here are only partially mirrored by investigations in other tumor entities. In two large studies of PD-L1 staining in lung cancer, three out of four assays showed interchangeable results (11, 31). In urothelial carcinoma, the different antibodies directed against PD-L1 showed different staining positivities but variance was still confined to an acceptable level. Here, too, three out of four assays were virtually interchangeable (32). In the above-mentioned studies, SP142 stained fewer samples, which was also observed in our data with SP142 identifying the fewest patients to be eligible for Pembrolizumab with CPS $\geq$ 1. In our study, the 22C3 clone showed CPS$>=1$ in surprisingly much <85% reported in the KEYNOTE-048 (8) study. This may be due to tumor heterogeneity, selection bias, different pre-analytics, or staining platform protocols. Whatever the reason, this stark contrast further encourages to be cautions upon PD-L1 scoring results. Other comparative studies in non-small cell lung cancer found a high concordance in tumor cell scores for PD-L1 but apoor concordance in immune cells. Similarly, our results demonstrate slightly better concordance in tumor cell scoring compared to immune cells, which might affect CPS variance overproportionally. Overall comparability of scoring performance, however, was much lower in our data regardless of cell type than described in other entities.

The deviation of our results may in part root in the approach taken: To stay as close to real-world routine diagnostics as possible we did not average the results by multiple reviewing pathologists. The pronounced staining heterogeneity nonetheless suggests further systemic differences compared to other tumor entities. In this context, a potentially relevant aspect has been addressed by Lee et al. showing differences in the binding of Dako 28-8 before and after deglycosylation of FFPE samples (33). They concluded that the binding of a diagnostic antibody directed

against PD-L1 is affected by the glycosylation state of the PD-L1 molecule itself. Since every antibody binds to a different epitope of the PD-L1 molecule, binding can be differentially affected by the glycosylation status of PD-L1 in each sample. Different levels of the inter-tumor variance of glycosylation patterns in HNSCC and other tumors might explain our observations—at least for the diagnostic antibodies that bind to the N-terminal extracellular domain [28-8 and 22C3; (34)].

Apart from discussing fixed diagnostic/therapeutic antibody pairs as companion diagnostic assays, it might be necessary to take a closer look at preanalytical optimization. Different glycosylation patterns in turn might not only be relevant in blurring formal eligibility criteria but also in better prediction of actual tumor biological behavior (33, 35). The different diagnostic scores in use add further complexity but only the CPS is currently applied clinically in HNSCC. We therefore restricted our primary comparisons to the CPS, with similar results for the TPS (**Supplementary Figure 1**). Given our present data, CPS determination in HNSCC should be interpreted with caution for therapeutic decisions. As CPS is crucial for therapeutic decision making a conceivable solution may be to establish an algorithm of testing various PD-L1 clones in succession to determine the CPS. In a back-to-back testing sequence, different PD-L1 clones could compensate for each other's "blind spots."

DATA AVAILABILITY STATEMENT

The raw data supporting the conclusions of this article will be made available by the authors, without undue reservation.

ETHICS STATEMENT

The studies involving human participants were reviewed and approved by University of Luebeck Ethics Committee (Ethikkommission der Universität zu Lübeck), Universität zu Lübeck, Ratzeburger Allee 160, 23538 Lübeck/Germany. Written informed consent for participation was not required for this study in accordance with the national legislation and the institutional requirements.

AUTHOR CONTRIBUTIONS

SP designed the study. Conceptualization by SP and SL. TMAs were constructed by JR-I, CI, and PK. RK, LK, CI, and CW maintained the cohort. JR-I, AO, and FD read the IHC slides and scored the stains. Statistical analyses were performed by FD supported by MR. BW, K-LB, and DR provided anonymized clinical data. JR-I, CI, FD, SL, and SP wrote the manuscript. Artwork was created by JR-I and F-OP. Graphs were created by FD. All authors contributed to the article and approved the submitted version.

FUNDING

CI received a grant clinical scientist fellowship from the Medical Faculty of the University of Lübeck (J26-2018). Fellowships of the Mildred Scheel doctoral program of the German Cancer Aid awarded to LK and F-OP (grant numbers 70113940 and 70112679, respectively). FD received funding from the Else Kröner-Fresenius Foundation (2018_A84) and the German Federal Ministry of Education and Research. All those institutions provide public research funding.

ACKNOWLEDGMENTS

Our special thanks go to Eva Dreyer and Wenzel Vogel for their excellent technical contribution in TMA construction and for performing immunohistochemical stains.

SUPPLEMENTARY MATERIAL

The Supplementary Material for this article can be found online at: https://www.frontiersin.org/articles/10.3389/fmed.2021.640515/full#supplementary-material

Supplementary Figure 1 | Positive control for PD-L1 immunohistochemistry. Tonsil tissue, from top to bottom: 22C3, 28-8, E1L3N, SP142, and SP263. Original magnification x100. Inlay magnification x400.

Supplementary Figure 2 | Clinical eligibility for alternative CPS and TPS cutoffs. **(A)** CPS 1 eligibility. **(B)** CPS 20 eligibility. **(C)** CPD50 eligibility. **(D)** TPS 50 eligibility.

Supplementary Table 1 | Patient Data.

REFERENCES

1. Wolchok JD, Weber JS, Maio M, Neyns B, Harmankaya K, Chin K. Four-year survival rates for patients with metastatic melanoma who received ipilimumab in phase II clinical trials. *Ann Oncol*. (2013) 24:2174–80. doi: 10.1093/annonc/mdt161
2. Borghaei H, Paz-Ares L, Horn L, Spigel DR, Steins M, Ready NE. Nivolumab versus docetaxel in advanced nonsquamous non-small-cell lung cancer. *N Engl J Med*. (2015) 373:1627–39. doi: 10.1056/NEJMoa1507643
3. Garon EB, Rizvi NA, Hui R, Leighl N, Balmanoukian AS, Eder JP. Pembrolizumab for the treatment of non-small-cell lung cancer. *N Engl J Med*. (2015) 372:2018–28. doi: 10.1056/NEJMoa1501824
4. Larkin J, Chiarion-Sileni V, Gonzalez R, Grob JJ, Cowey CL, Lao CD. Combined nivolumab and ipilimumab or monotherapy in untreated melanoma. *N Engl J Med*. (2015) 373:23–34. doi: 10.1056/NEJMc1509660
5. Robert C, Long GV, Brady B, Dutriaux C, Maio M, Mortier L. Nivolumab in previously untreated melanoma without BRAF mutation. *N Engl J Med*. (2015) 372:320–30. doi: 10.1056/NEJMoa1412082
6. Robert C, Schachter J, Long GV, Arance A, Grob JJ, Mortier L. Pembrolizumab versus Ipilimumab in advanced melanoma. *N Engl J Med*. (2015) 372:2521–32. doi: 10.1056/NEJMoa1503093
7. Ferris RL, Blumenschein G, Fayette J, Guigay J, Colevas AD, Licitra L. Nivolumab for recurrent squamous-cell carcinoma of the head and neck. *N Engl J Med*. (2016) 375:1856–67. doi: 10.1056/NEJMoa1602252
8. Burtness B, Harrington KJ, Greil R, Soulières D, Tahara M, de Castro G. Pembrolizumab alone or with chemotherapy versus cetuximab with chemotherapy for recurrent or metastatic squamous cell carcinoma of the head and neck (KEYNOTE-048): a randomised, open-label, phase 3 study. *Lancet*. (2019) 394:1915–28. doi: 10.1016/S0140-6736(19)32591-7
9. Cohen EEW, Bell RB, Bifulco CB, Burtness B, Gillison ML, Harrington KJ. The Society for Immunotherapy of Cancer consensus statement

on immunotherapy for the treatment of squamous cell carcinoma of the head and neck (HNSCC). *J Immunother Cancer*. (2019) 7:184. doi: 10.1186/s40425-019-0662-5
10. Savic S, Berezowska S, Eppenberger-Castori S, Cathomas G, Diebold J, Fleischmann A. PD-L1 testing of non-small cell lung cancer using different antibodies and platforms: a Swiss cross-validation study. *Virchows Archiv*. (2019) 475:67–76. doi: 10.1007/s00428-019-02582-0
11. Hirsch FR, McElhinny A, Stanforth D, Ranger-Moore J, Jansson M, Kulangara K. PD-L1 immunohistochemistry assays for lung cancer: results from Phase 1 of the blueprint PD-L1 IHC assay comparison project. *J Thorac Oncol*. (2017) 12:208–22. doi: 10.1016/j.jtho.2016.11.2228
12. Tsao MS, Kerr KM, Kockx M, Beasley M-B, Borczuk AC, Botling J. PD-L1 Immunohistochemistry comparability study in real-life clinical samples: results of blueprint Phase 2 project. *J Thorac Oncol*. (2018) 13:1302–11. doi: 10.1016/j.jtho.2017.09.100
13. Ratcliffe MJ, Sharpe A, Midha A, Barker C, Scott M, Scorer P. Agreement between programmed cell death ligand-1 diagnostic assays across multiple protein expression cutoffs in non–small cell lung cancer. *Clin Cancer Res*. (2017) 23:3585–91. doi: 10.1158/1078-0432.CCR-16-2375
14. Adam J, Le Stang N, Rouquette I, Cazes A, Badoual C, Pinot-Roussel H. Multicenter harmonization study for PD-L1 IHC testing in non-small-cell lung cancer. *Ann Oncol*. (2018) 29:953–8. doi: 10.1093/annonc/mdy014
15. Herbst RS, Giaccone G, de Marinis F, Reinmuth N, Vergnenegre A, Barrios CH. Atezolizumab for first-line treatment of PD-L1-selected patients with NSCLC. *N Engl J Med*. (2020) 383:1328–39. doi: 10.1056/NEJMoa1917346
16. Balar AV, Castellano D, O'Donnell PH, Grivas P, Vuky J, Powles T. First-line pembrolizumab in cisplatin-ineligible patients with locally advanced and unresectable or metastatic urothelial cancer (KEYNOTE-052): a multicentre, single-arm, phase 2 study. *Lancet Oncol*. (2017) 18:1483–92. doi: 10.1016/S1470-2045(17)30616-2
17. Narayan P, Wahby S, Gao JJ, Amiri-Kordestani L, Ibrahim A, Bloomquist E. FDA approval summary: atezolizumab plus paclitaxel protein-bound for the treatment of patients with advanced or metastatic TNBC whose tumors express PD-L1. *Clin Cancer Res*. (2020) 26:2284–9. doi: 10.1158/1078-0432.CCR-19-3545
18. Reck M, Rodríguez-Abreu D, Robinson AG, Hui R, Csőszi T, Fülöp A, et al. Pembrolizumab versus Chemotherapy for PD-L1-Positive Non-Small-Cell Lung Cancer. *N Engl J Med*. (2016) 375:1823–33. doi: 10.1056/NEJMoa1606774
19. Ribbat-Idel J, Perner S, Kuppler P, Klapper L, Krupar R, Watermann C. Immunologic "cold" squamous cell carcinomas of the head and neck are associated with an unfavorable prognosis. *Front Med*. (2021) 8:622330. doi: 10.3389/fmed.2021.622330
20. Idel C, Ribbat-Idel J, Kuppler P, Krupar R, Offermann A, Vogel W. EVI1 as a Marker for lymph node metastasis in HNSCC. *Int J Mol Sci*. (2020) 21:854. doi: 10.3390/ijms21030854
21. Queisser A, Hagedorn S, Wang H, Schaefer T, Konantz M, Alavi S. Ecotropic viral integration site 1, a novel oncogene in prostate cancer. *Oncogene*. (2017) 36:1573–84. doi: 10.1038/onc.2016.325
22. Žitnik M, Zupan B. NIMFA: a python library for nonnegative matrix factorization. *J Mach Learn Res*. (2012) 13:849–53. Available online at: http://jmlr.org/papers/v13/zitnik12a.html
23. Moreira RS, Bicker J, Musicco F, Persichetti A, Pereira AMPT. Anti-PD-1 immunotherapy in advanced metastatic melanoma: State of the art and future challenges. *Life Sci*. (2020) 240:117093. doi: 10.1016/j.lfs.2019.117093
24. Sui H, Ma N, Wang Y, Li H, Liu X, Su Y. Anti-PD-1/PD-L1 therapy for non-small-cell lung cancer: toward personalized medicine and combination strategies. *J Immunol Res*. (2018) 2018:6984948. doi: 10.1155/2018/6984948
25. Ferris RL, Blumenschein G, Fayette J, Guigay J, Colevas AD, Licitra L. Nivolumab vs investigator's choice in recurrent or metastatic squamous cell carcinoma of the head and neck: 2-year long-term survival update of CheckMate 141 with analyses by tumor PD-L1 expression. *Oral Oncol*. (2018) 81:45–51. doi: 10.1016/j.oraloncology.2018.04.008
26. Munari E, Zamboni G, Lunardi G, Marchionni L, Marconi M, Sommaggio M. PD-L1 expression heterogeneity in non-small cell lung cancer: defining criteria for harmonization between biopsy specimens and whole sections. *J Thorac Oncol*. (2018) 13:1113–20. doi: 10.1016/j.jtho.2018.04.017
27. Lantuejoul S, Damiola F, Adam J. Selected highlights of the 2019 pulmonary pathology society biennial meeting: PD-L1 test harmonization studies. *Transl Lung Cancer Res*. (2020) 9:906–16. doi: 10.21037/tlcr.2020.03.23
28. Scheel AH, Dietel M, Heukamp LC, Jöhrens K, Kirchner T, Reu S. Harmonized PD-L1 immunohistochemistry for pulmonary squamous-cell and adenocarcinomas. *Mod Pathol*. (2016) 29:1165–72. doi: 10.1038/modpathol.2016.117
29. Scheel AH, Baenfer G, Baretton G, Dietel M, Diezko R, Henkel T. Interlaboratory concordance of PD-L1 immunohistochemistry for non-small-cell lung cancer. *Histopathology*. (2018) 72:449–59. doi: 10.1111/his.13375
30. Shimabukuro Ho R, Mioti Sebastião M, Venezian de Carvalho JP, Neves T, Nussbaum M. Cost-effectiveness analysis of the SP142 versus 22C3 PD-L1 assays in the treatment of atezolizumab plus nab-paclitaxel for patients with advanced triple negative breast cancer in the Brazilian private healthcare system. *J Med Econ*. (2020) 23:1340–4. doi: 10.1080/13696998.2020.1821039
31. Tsao MS, Kerr KM, Kockx M, Beasley M-B, Borczuk AC, Botling J. PD-L1 Immunohistochemistry comparability study in real-life clinical samples: results of blueprint Phase 2 project. *J Thorac Oncol*. (2018) 13:1302–11. doi: 10.1016/j.jtho.2018.05.013
32. Eckstein M, Erben P, Kriegmair MC, Worst TS, Weiß C-A, Wirtz RM. Performance of the Food and Drug Administration/EMA-approved programmed cell death ligand-1 assays in urothelial carcinoma with emphasis on therapy stratification for first-line use of atezolizumab and pembrolizumab. *Eur J Cancer*. (2019) 106:234–43. doi: 10.1016/j.ejca.2018.11.007
33. Lee H-H, Wang Y-N, Xia W, Chen C-H, Rau K-M, Ye L. Removal of N-linked glycosylation enhances PD-L1 detection and predicts anti-PD-1/PD-L1 therapeutic efficacy. *Cancer Cell*. (2019) 36:168–78.e4. doi: 10.1016/j.ccell.2019.06.008
34. Lawson NL, Dix CI, Scorer PW, Stubbs CJ, Wong E, Hutchinson L. Mapping the binding sites of antibodies utilized in programmed cell death ligand-1 predictive immunohistochemical assays for use with immuno-oncology therapies. *Mod Pathol*. (2020) 33:518–30. doi: 10.1038/s41379-019-0372-z
35. De Bousser E, Meuris L, Callewaert N, Festjens N. Human T cell glycosylation and implications on immune therapy for cancer. *Hum Vaccin Immunother*. (2020) 16:2374–88. doi: 10.1080/21645515.2020.1730658

Conflict of Interest: The authors declare that the research was conducted in the absence of any commercial or financial relationships that could be construed as a potential conflict of interest.

Recurrent HNSCC Harbor an Immunosuppressive Tumor Immune Microenvironment Suggesting Successful Tumor Immune Evasion

Christian Watermann[1], Helen Pasternack[1], Christian Idel[2], Julika Ribbat-Idel[1], Johannes Brägelmann[3,4,5], Patrick Kuppler[1], Anne Offermann[1], Danny Jonigk[6,7], Mark Philipp Kühnel[6,7], Andreas Schröck[8], Eva Dreyer[1], Christian Rosero[9], Jacqueline Nathansen[10,11], Anna Dubrovska[10,11,12,13,14], Lars Tharun[1], Jutta Kirfel[1], Barbara Wollenberg[15], Sven Perner[1,9], and Rosemarie Krupar[1,9]

ABSTRACT

Purpose: Recurrent tumors (RT) of head and neck squamous cell carcinoma (HNSCC) occur in up to 60%, with poor therapeutic response and detrimental prognosis. We hypothesized that HNSCC RTs successfully evade antitumor immune response and aimed to reveal tumor immune microenvironment (TIME) changes of primary tumors (PT) and corresponding RTs.

Experimental Design: Tumor-infiltrating leukocytes (TIL) of 300 PTs and 108 RTs from two large independent and clinically well-characterized HNSCC cohorts [discovery cohort (DC), validation cohort (VD)] were compared by IHC. mRNA expression analysis of 730 immune-related genes was performed for 18 PTs and RTs after adjuvant chemoradiotherapy (CRT). The effect of chemotherapy and radiation resistance was assessed with an *in vitro* spheroid/immunocyte coculture model.

Results: TIME analysis revealed overall decrease of TILs with significant loss of $CD8^+$ T cells (DC $P = 0.045$/VC $P < 0.0001$) and B lymphocytes (DC $P = 0.036$/VC $P < 0.0001$) in RTs compared with PTs in both cohorts. Decrease predominantly occurred in RTs after CRT. Gene expression analysis confirmed loss of TILs ($P = 0.0004$) and B lymphocytes ($P < 0.0001$) and showed relative increase of neutrophils ($P = 0.018$), macrophages ($P < 0.0001$), dendritic cells ($P = 0.0002$), and mast cells ($P = 0.0057$) as well as lower overall expression of immune-related genes ($P = 0.018$) in RTs after CRT. Genes involved in B-lymphocyte functions and number of tertiary lymphoid structures showed the strongest decrease. *SPP1* and *MAPK1* were upregulated *in vivo* and *in vitro*, indicating their potential suitability as therapeutic targets in CRT resistance.

Conclusions: HNSCC RTs have an immunosuppressive TIME, which is particularly apparent after adjuvant CRT and might substantially contribute to poor therapeutic response and prognosis.

[1]Institute of Pathology, University Hospital Schleswig-Holstein, Campus Lübeck, Lübeck, Germany. [2]Department of Otorhinolaryngology, University Hospital Schleswig-Holstein, Campus Lübeck, Lübeck, Germany. [3]Molecular Pathology, Institute of Pathology, University Hospital of Cologne, Cologne, Germany. [4]Department of Translational Genomics, Center of Integrated Oncology Cologne-Bonn, Medical Faculty, University of Cologne, Cologne, Germany. [5]Mildred Scheel School of Oncology, Cologne, University Hospital Cologne, Medical Faculty, Cologne, Germany. [6]Institute for Pathology, Hannover Medical School, Hannover, Germany. [7]Biomedical Research in Endstage and Obstructive Lung Disease (BREATH), German Center for Lung Research, Hannover, Germany. [8]Department of Otorhinolaryngology, Head and Neck Surgery, Johanniter Hospital Bonn, Bonn, Germany. [9]Pathology, Research Center Borstel, Leibniz Lung Center, Borstel, Germany. [10]OncoRay–National Center for Radiation Research in Oncology, Faculty of Medicine, University Hospital Carl Gustav Carus, Technical University Dresden, Helmholtz-Zentrum Dresden-Rossendorf, Dresden, Germany. [11]Institute of Radiooncology-OncoRay, Helmholtz-Zentrum Dresden-Rossendorf (HZDR), Dresden, Germany. [12]German Cancer Consortium (DKTK), Partner Site Dresden, Dresden, Germany. [13]German Cancer Research Center (DKFZ), Heidelberg, Germany. [14]National Center for Tumor Diseases (NCT) Partner Site Dresden, Dresden, Germany. [15]Clinic for Otorhinolaryngology, Head and Neck Surgery, MRI TUM, Technical University Munich, Munich, Germany.

Note: Supplementary data for this article are available at Clinical Cancer Research Online (http://clincancerres.aacrjournals.org/).

S. Perner and R. Kruper contributed equally to this article.

Corresponding Author: Rosemarie Krupar, Institute of Pathology, University Hospital Schleswig-Holstein, Campus Lübeck, Pathology, Research Center Borstel, Leibniz Lung Center, Lübeck 23562, Germany. Phone: 49–4537–188–6290; Fax: 49045371882290; E-mail: rkrupar@fz-borstel.de

Clin Cancer Res 2020;XX:XX–XX

doi: 10.1158/1078-0432.CCR-20-0197

Introduction

Head and neck squamous cell carcinoma (HNSCC) is the sixth most common cancer worldwide accounting for more than 600,000 cases and 380,000 deaths annually (1, 2). In the United States, more than two-thirds of patients are diagnosed at advanced stages of disease leading to poor prognosis with 5-year survival rates ranging between 39% and 65% (3). A major factor contributing to poor prognosis is the development of local recurrent tumors (RT) in up to 60% of patients (4).

Standard-of-care treatment of HNSCC primary tumors (PT) in a locally advanced setting consists of surgical resection of PT and draining lymph nodes in combination with risk-adapted adjuvant radiotherapy, with or without platinum-based chemotherapy. Alternatively, standalone definitive concurrent chemoradiotherapy (CRT) is administered (5, 6). Those treatment options are quite effective in the primary disease setting, but cannot prevent high RT rates (7). Treatment of recurrent HNSCC, which are often not accessible to surgery or radiotherapy, has for a long time been limited to platinum-based doublet chemotherapy in combination with the anti-EGFR antibody cetuximab with a low median overall survival of 10.1 months (8, 9). Recently, the two immunotherapeutic agents nivolumab and pembrolizumab, mAbs targeting the immune checkpoint molecule programmed cell death protein 1 (PD1), have been proven to contribute to longer overall survival in comparison with standard chemotherapy in pretreated recurrent or metastatic HNSCC in the two randomized phase III trials CHECKMATE-141 and KEYNOTE-040 (10, 11). Furthermore, pembrolizumab has shown prolonged overall survival as first line treatment for recurrent or metastatic HNSCC, either in combination with standard therapy or as single-agent therapy for

Translational Relevance

The development of locoregional recurrences is one main reason for the poor prognosis of head and neck squamous cell carcinoma (HNSCC). Recurrent HNSCC shows low response rates to conventional chemoradiotherapy (CRT) as well as immunotherapy. Particularly, the administration of immunotherapy depends on a favorable preexisting tumor immune microenvironment (TIME). This study demonstrates an unfavorable, immunosuppressive, and protumor TIME in HNSCC recurrences compared with corresponding primary tumors on protein and mRNA expression levels in two independent and clinically well-characterized patient cohorts. Immunosuppression predominantly occurs in recurrences of patients who received CRT after resection of their primary tumor and was associated with a decrease of tertiary lymphoid structures. These results suggest an immunosuppressive TIME as one major factor promoting HNSCC recurrences. Furthermore, they support inclusion of immunotherapies at an early stage of treatment to fully exploit its antitumor immune capacities and avoid an immunosuppressive TIME.

patients with IHC-proven programmed cell death protein ligand 1 (PDL1) overexpression (PDL1 combined positive score: ≥1; ref. 12). Therefore, pembrolizumab and nivolumab have been included into the latest treatment guidelines for recurrent and metastatic HNSCC (13). Nevertheless, relative response rates stay below 15% and benefit to median overall survival of 1.4 to 2.4 months is still poor (14).

Success of immunotherapies and of standard CRT is strongly influenced by the preexisting tumor immune microenvironment (TIME) and its alterations during therapy (15). Despite high variability across different cancer entities, solid tumors such as HNSCC are usually classified into three different TIME types according their prognostic and predictive impact (16–21):

(i) Hot (inflamed) tumors with high numbers of effector immune cells such as $CD8^+$ and $CD4^+$ T cells as well as natural killer (NK) cells.
(ii) Cold (noninflamed) tumors with enrichment of immunosuppressive cytokines, presence of regulatory T cells (Tregs) and myeloid-derived suppressor cells (MDSC) as well as scarcity of $CD8^+$, $CD4^+$, and NK cells.
(iii) Immune-excluded tumors with absence of all types of immunocytes.

Best response rates to immune checkpoint inhibitors are observed for patients with an active antitumoral immune response of the first type (22).

Considering high rates of RTs after successful eradication of PTs as well as poor response rates and survival benefits of immune checkpoint inhibitors in the recurrent setting, we hypothesize that RTs have successfully escaped antitumor immune response, which is characterized by a decrease of antitumor immune cells and activity and an increase of protumor and immunosuppressive immune cells. Furthermore, we think that adjuvant CRT contributes to the immunosuppressive TIME of RTs.

To elucidate immunologic changes in recurrent HNSCC, we performed *in vivo* characterization of the TIME of PTs and corresponding RTs in two independent HNSCC cohorts via IHC and immune-specific gene expression profiling. Furthermore, we compared the immunologic changes with an *in vitro* model of chemotherapy- and radiotherapy-resistant HNSCC spheroids cocultured with immune cells.

Materials and Methods

Patient data and tumor material

Two large, independent, and clinically well-characterized HNSCC cohorts were used for this study. The discovery cohort (Lübeck cohort) consists of 63 patients with HNSCC, who were treated according to local treatment guidelines at the Department for Otorhinolaryngology of the University Hospital Schleswig-Holstein, Campus Lübeck, Germany, between 2001 and 2016. All patients developed a local RT (RT1) between 4 months to 11 years after clinically or radiologically proven eradication of their PT. A total of 13 patients developed a second RT (RT2). Overall survival data, patient characteristics, and social histories were obtained from the Department for Otorhinolaryngology of the University Hospital Schleswig-Holstein, Campus Lübeck, Germany. Formalin-fixed paraffin-embedded (FFPE) tumor tissues were retrieved from the archives of the Pathology of the University Hospital Schleswig-Holstein, Campus Lübeck, Germany and tissue microarrays (TMA) were constructed from representative tumor areas. Three 0.6 mm cores of each tumor specimen were assembled into TMA blocks. Human papillomavirus (HPV)-status was assessed by p16 IHC staining and HPV-DNA PCR testing.

The second cohort was an independent validation cohort (Bonn cohort) consisting of 237 PTs and 45 unmatched RTs established as a TMA-based cohort with three 0.6 mm cores for each tumor specimen at the Institute of Pathology of the University Hospital Bonn (Bonn, Germany). An overview of the two independent cohorts and the setup of the study is displayed in Supplementary Fig. S1. The study was approved by the Institutional Review Board (IRB) of the University Lübeck (Lübeck, Germany) and the University Hospital of Bonn (Bonn, Germany), which follow the declaration of Helsinki. Included patients signed a hospital-internal general consent form to participate in research and education, which dispensed with additional written consents for this study according to the IRB, as patient data were anonymized at the source.

IHC

IHC was performed on 4-μm-thick paraffin-embedded TMA sections as described previously (23). The OptiView DAB IHC Detection Kit was used on a Ventana BenchMark Ultra (Roche) for the following antibodies: CD4 (SP35, Ventana), CD8 (SP57, Ventana), CD20 (L26, Ventana), CD1A (EP3622, Cell Marque), CD68 (KP-1, Ventana), CD56 (MRQ-42, Cell Marque), FOXP3 (236A/E7, Invitrogen), PD1 (NAT105, Cell Marque), PDL1 (E1L3N, Cell Signaling Technology), Tryptase (G3, Cell Marque) CD15 (MMA, Ventana), and DC-LAMP (101E1.01, Novus Biologicals). Quantitative analysis of immune cell infiltration was determined using a semiautomated image analysis software (Definiens Developer XD 2.0, Definiens). For each immune cell subtype infiltration, intensity was measured as count of immune cells per mm^2 tumor tissue. Intratumoral immune cells as well as immune cells at the tumor margin were considered. An experienced pathologist blinded to clinical information manually quantified the percentages of PDL1-expressing tumor cells. Mean values from up to three TMA cores for each tumor specimen were calculated. On average, 2.6 cores for PTs and RTs and 2.7 cores for RT2 were analyzed. *In vitro* spheroid experiments, as described below, were analyzed in the same manner using QuPath 0.1.2 (24). IHC double staining against CD20 in red (alkaline-phosphatase-reaction) and ERG (EPR3864, Abcam) in brown (3,3′-Diaminobenzidine) was performed on whole

slides and analyzed using QuPath 0.1.2 (24). Representative areas containing tumor and peritumoral stroma were annotated on the digitized slide and an experienced, board-certified pathologist, blinded to the data, counted the number of tertiary lymphoid structures (TLS), defined as $CD20^+$ B-lymphocyte aggregates around ERG^+ venules. Afterward, the number of TLS per mm^2 tumor was calculated.

RNA extraction

RNA from FFPE tissue was extracted using six to eight 8-μm-thick sections on a glass slide. Sections were deparaffinized with Xylene. An experienced pathologist marked representative areas containing only tumor tissue on an hematoxylin and eosin slide, which was then used for microdissection. Representative tumor tissue was scratched from the glass slide using a 11× feather disposable scalpel. RNA isolation was performed using the Maxwell RSC RNA FFPE Kit on the Maxwell RSC Instrument (Promega) according to manufacturer' instructions without using mineral oil because samples have already been deparaffinized. RNA from *in vitro* experiments was isolated using the RNeasy Mini Kit (Qiagen) as indicated by the manufacturer. RNA concentration and purity were assessed with a NanoDrop 1000 spectrophotometer (NanoDrop Technologies) and the Qubit RNA HS Assay Kit on the Qubit 2.0 fluorometer (Invitrogen).

Gene expression analysis

RNA from 18 PTs and their corresponding RTs from the discovery cohort was used for gene expression profiling via the nCounter PanCancer Immune Profiling Panel (NanoString Technologies) as described previously (25). All patients received CRT between resection of the primary tumor and development of recurrence. Digital data acquisition via the nCounter Digital Analyzer (NanoString Technologies) was performed at the Institute of Pathology of the Hannover Medical School. NSolver 4.0 Analysis Software (NanoString Technologies) as well as R 3.5.0 were used for data analysis. Gene expression analysis of *in vitro* experiments was performed in the same manner.

Cell lines and culture conditions

FaDu cell line (26) was purchased from the Leibniz Institute DSMZ - German Collection of Microorganisms and Cell Cultures (DSMZ) and was grown in a 5% CO_2 incubator at 37°C and 85% humidity. FaDu cells were maintained in DMEM (Thermo Fisher Scientific) containing 10% FBS (Biochrom), 1% penicillin–streptomycin antibiotics (Thermo Fisher Scientific), and 1% L-Glutamine (Thermo Fisher Scientific).

The cisplatin-resistant cell line FaDu/CR was developed by continuously exposing FaDu cells to increasing doses (0.1–0.7 μg/mL) of cisplatin NeoCorp (Hexal) for over 6 months. Methyl-thiazolyl-tetrazolium bromide (MTT) assay as originally described by Mosmann and colleagues was performed to assess cisplatin resistance of FaDu/CR cells compared with untreated FaDu/WT cells (27). The radiation-resistant cell line FaDu/RR was generously provided by the research group of Professor Anna Dubrovska and tested for radiation resistance by clonogenic assay as described previously (28).

Peripheral blood mononuclear cell isolation and activation

Peripheral blood mononuclear cells (PBMC) were isolated from fresh heparinized blood of healthy donors using Ficoll-Paque Plus (GE Healthcare) density gradient centrifugation and activated as described in Supplementary Fig. S2.

Spheroid immune cell cocultures

Spheroids were created by the hanging drop method and further processed as displayed in Supplementary Fig. S2. Briefly, 20,000 FaDu/WT cells, FaDu/CR cells, or FaDu/RR cells were suspended in 20 μL of complete culture medium and placed on the lid of a 24-well plate. After 5 days, hanging drops were transferred into agarose-coated wells containing 1 mL of complete culture medium. Activated PBMCs were added. Two healthy donors were used for all PBMC experiments. FaDu/WT and FaDu/CR or FaDu/RR were treated with the same PBMCs of one donor for each experiment. Spheroid immune cell cocultures were incubated for 72 hours. After harvest, spheroids were fixed in 4% formaldehyde and embedded in paraffine. Histologic specimens were analyzed by IHC as described above. Three independent experiments were performed.

Statistical analysis

Paired two-tailed *t* test was applied for discrimination of immune cell markers of IHC analysis of the discovery cohort. Welsh *t* test was used for discrimination of IHC analysis of the validation cohort. Multivariate ANOVA was used to test correlations between clinicopathologic parameters and TIME characteristics in both cohorts. Fisher exact test was applied for clustering of PTs and RTs after CRT in $k = 2$ cluster via Euclidean distance based on mRNA expression. Unpaired two-tailed *t* test was performed for discriminating mRNA-based immune cell infiltration scores and mRNA expression scores of immune-related genes between PTs and RTs after CRT as well as for comparing resistance to cisplatin of cell lines in MTT test and to radiotherapy in clonogenic assay. *P* values less than 0.05 were considered statistically significant. For mRNA-based analysis, *P* values adjusted for multiple testing by the Benjamini–Hochberg procedure ($Q = 0.05$) are listed in Supplementary Table S1. IBM SPSS Statistics version 25.0 for Windows (IBM Corp.) and GraphPad Prism version 8.3.0 for Windows (GraphPad Software) were used for statistical analysis.

Results

Clinicopathologic characteristics of the two independent HNSCC cohorts

TIME studies of primary and recurrent HNSCC were based on two independent patient cohorts. Patient and tumor features of the discovery cohort (Luebeck cohort) are listed in **Table 1**. This cohort consists of 63 patients (oral cavity, oropharynx, hypopharynx, larynx) with available PT, corresponding first recurrence (RT1) and for 13 patients also corresponding second recurrence (RT2). A total of 58 RTs (92%) were locoregional recurrences (52 local RTs, 6 regional lymph node RTs) and 5 RTs (8%) were distant metastases. A total of 51 patients (81%) underwent surgical resection of PT with complete resection in 95.2% of cases. Radiotherapy was performed in 31 (49.2%) patients with an average total radiation dose of 61.7 Gray (Gy; SD = 6.7 Gy). In addition, 20 (64.5%) patients with radiotherapy also received platinum-based chemotherapy. Mean 5-year overall survival rate was 41.4%.

A second independent patient cohort (Bonn cohort) was used as a validation cohort, consisting of 237 PTs and 45 RTs. Details of the second cohort are displayed in Supplementary Table S2.

Characterization of the TIME of HNSCC PTs and RTs reveals immunosuppression in RTs

First, we aimed to define differences between the TIME of primary and recurrent HNSCC by analyzing the number and subtype composition of tumor-infiltrating leukocytes (TIL). The following immune cells were characterized on the basis of IHC marker expressions: $CD8^+$ cytotoxic T cells, $CD20^+$ B lymphocytes, $CD4^+$ Th cells, $FOXP3^+$

Table 1. Clinical and pathologic characteristics of the HNSCC discovery cohort (Lübeck).

***N* = 63 (%)**					
Mean age (y) [SD]	60.7 [10.8]	**T Stage PT (*n* = 62)**		**T Stage RT (*n* = 53)**	
Sex	44 (69.8) male	T1	10 (16.1)	T1	8 (15.1)
p16 status	8 (12.7) positive	T2	21 (33.9)	T2	10 (18.9)
HPV DNA status	8 (12.7) positive	T3	20 (32.3)	T3	11 (20.8)
Anatomic site		T4	11 (17.7)	T4	24 (45.3)
Oral cavity	17 (27)				
Oropharynx	17 (27)	**N Stage PT (*n* = 62)**		**N Stage RT (*n* = 56)**	
Hypopharynx	6 (9.5)	0	37 (59.7)	0	35 (62.5)
Larynx	23 (36.5)	1	6 (9.7)	1	7 (12.5)
Differentiation PT (*n* = 58)		2	16 (25.8)	2	14 (25)
Well	5 (8.6)	3	3 (4.8)	3	0 (0)
Moderate	41 (70.7)				
Poor	12 (20.7)	**M Stage PT (*n* = 62)**		**M Stage RT (*n* = 49)**	
Surgery of PT	51 (81)	0	61 (98.4)	0	42 (85.7)
Time between PT and RT (m) [SD]	31 [35.8]	1	2 (1.6)	1	7 (14.3)
Patients with second RT	13 (20.6)				
Radiotherapy ± chemotherapy between PT and RT	31 (49.2)				

Abbreviations: m, months; PT, primary tumor; RT, recurrent tumor; y, year.

Tregs, $PD1^+$ cells, $CD56^+$ NK cells, $CD1A^+$ dendritic cells, DC-LAMP+ mature dendritic cells, $CD68^+$ macrophages, $CD15^+$ neutrophil granulocytes, tryptase+ mast cells, and PDL1 expression.

In the discovery cohort, a general trend toward a decrease of TILs from PTs to first and especially to second corresponding RTs was observed for various lymphocyte subtypes (**Fig. 1A** and **B**). The highest change was observed for $CD20^+$ B lymphocytes. They showed a subtotal depletion in RTs with an average of 488.5 cells/mm^2 in PTs and 20.6 cells/mm^2 in RT2 ($P = 0.036$). $CD8^+$ T cells, as one of the major antitumor immunocyte types, also strongly decreased from 383.4 cells/mm^2 in PTs to 152 cells/mm^2 in RT2 ($P = 0.045$). $CD56^+$ NK cells significantly decreased from 54.3 cells/mm^2 in RT1 to 37.4 cells/mm^2 in RT2 ($P = 0.036$). $FOXP3^+$ Tregs decreased from an average of 32.2 cells/mm^2 in PTs to 16.9 cells/mm^2 in RT2 ($P = 0.047$). The loss of antitumor $CD8^+$ T cells relatively outweighed the absolute loss of $FOXP3^+$ Tregs, demonstrated by a trend toward a decreased $CD8^+/FOXP3^+$ T-cell ratio from 142.3 in PTs to 24.2 in RT2 ($P = 0.39$; Supplementary Fig. S3). The average absolute count of immunosuppressive $PD1^+$ cells was not substantially altered between PTs (37.1 cells/mm^2), RT1 (44.4 cells/mm^2) and RT2 (28.4 cells/mm^2). The CD8/PD1 ratio, however, decreased in analogy to the $CD8^+/FOXP3^+$ ratio from 16.6 in PTs to 5.9 in RT2 ($P = 0.058$). PDL1 expression did not significantly change between PTs, RT1, or RT2.

$CD68^+$ macrophages, $CD15^+$ neutrophil granulocytes, and tryptase+ mast cells did not show significant changes between PTs, RT1, or RT2 (**Fig. 1C** and **D**). Corresponding to previous ratios, $CD8^+/CD15^+$ ratio also decreased from 6.6 in PTs to 2.1 in RT2s ($P = 0.3375$) and CD8/CD68 ratio from 6.1 in PTs to 4.8 in RT1s and 2.7 in RT2s ($P = 0.2932$; Supplementary Fig. S3). $CD1A^+$ dendritic cells were the only immunocyte subtype, which significantly increased from a mean count of 96.9 cells/mm^2 in PTs to 149.9 cells/mm^2 in RT1 ($P = 0.013$) and 219.6 cells/mm^2 in RT2 ($P = 0.036$). DC-LAMP+ mature dendritic cells in contrast decreased from a mean count of 50.5 cells/mm^2 in PTs to 29.2 cells/mm^2 in RT1 ($P = 0.0023$) and 17.1 cells/mm^2 in RT2 ($P = 0.0719$). Correspondingly, the CD1A/DC-LAMP ratio significantly increased from 4.6 in PTs to 15.0 in RT1 ($P = 0.0013$; Supplementary Fig. S3).

To validate our observations of the discovery cohort, we performed similar analyses in our independent validation cohort (Bonn cohort). Here, we could confirm the strong loss of $CD20^+$ B lymphocytes with a decrease from an average of 345.9 cells/mm^2 in PTs to 84.7 cells/mm^2 in RTs ($P < 0.0001$) as well as a loss of $CD8^+$ T cells from 733.2 cells/mm^2 in PTs to 347.3 cells/mm^2 in RTs ($P < 0.0001$; **Fig. 1E**). $CD1A^+$ dendritic cells were not increased, but slightly decreased from average 235.2 cells/mm^2 in PTs to 207.1 cells/mm^2 in RTs ($P = 0.50$). $FOXP3^+$ Tregs tended to decrease from 66 cells/mm^2 in PTs to 46.7 cells/mm^2 in RTs ($P = 0.14$) and the CD8/FOXP3 ratio showed a comparable decrease to the discovery cohort from 85.8 in PTs to 26.3 in RTs ($P = 0.062$). A display of TIME changes via dot plot diagrams reflecting the distribution of immunocyte types across patients of the two cohorts as well as a display for matched tumor samples only is listed in Supplementary Fig. S4. In addition, a correlation of the immune cell infiltration of PTs to clinicopathologic parameters for the discovery cohort and the validation cohort can be found in Supplementary Table S3A and S3B.

Adjuvant CRT contributes to loss of $CD20^+$ B lymphocytes in RTs

Because adjuvant CRT is known to have a wide range of immunemodulatory effects, we aimed to evaluate its impact on the TIME of RTs with previous CRT (15). To further elucidate the effect of CRT on the TIME, the discovery cohort was therefore divided into two subgroups: (i) Patients with CRT before development of first or second RT [CRT-treated (CRT-t) RTs, $n = 35$]. (ii) Patients with surgical resection only before development of RT ($n = 28$).

Our analysis revealed that loss of $CD20^+$ B lymphocytes was CRT dependent. In patients with CRT after resection of PT, subtotal depletion of B lymphocytes from an average of 471.3 cells/mm^2 in CRT-naïve (CRT-n) PTs to 23.5 cells/mm^2 in corresponding CRT-t RTs was observed ($P = 0.0006$; **Fig. 2A**). Patients with surgical resection only showed no significant change in B-lymphocyte counts (432.6 cells/mm^2 in preoperative PTs to 576.8 cells/mm^2 in postoperative RTs, $P = 0.59$; **Fig. 2B**). While $CD8^+$ T cells did not change, $CD4^+$ T cells tended to decrease in CRT-t RTs ($P = 0.092$) and tended to increase in postoperative RTs after surgery only ($P = 0.099$). An

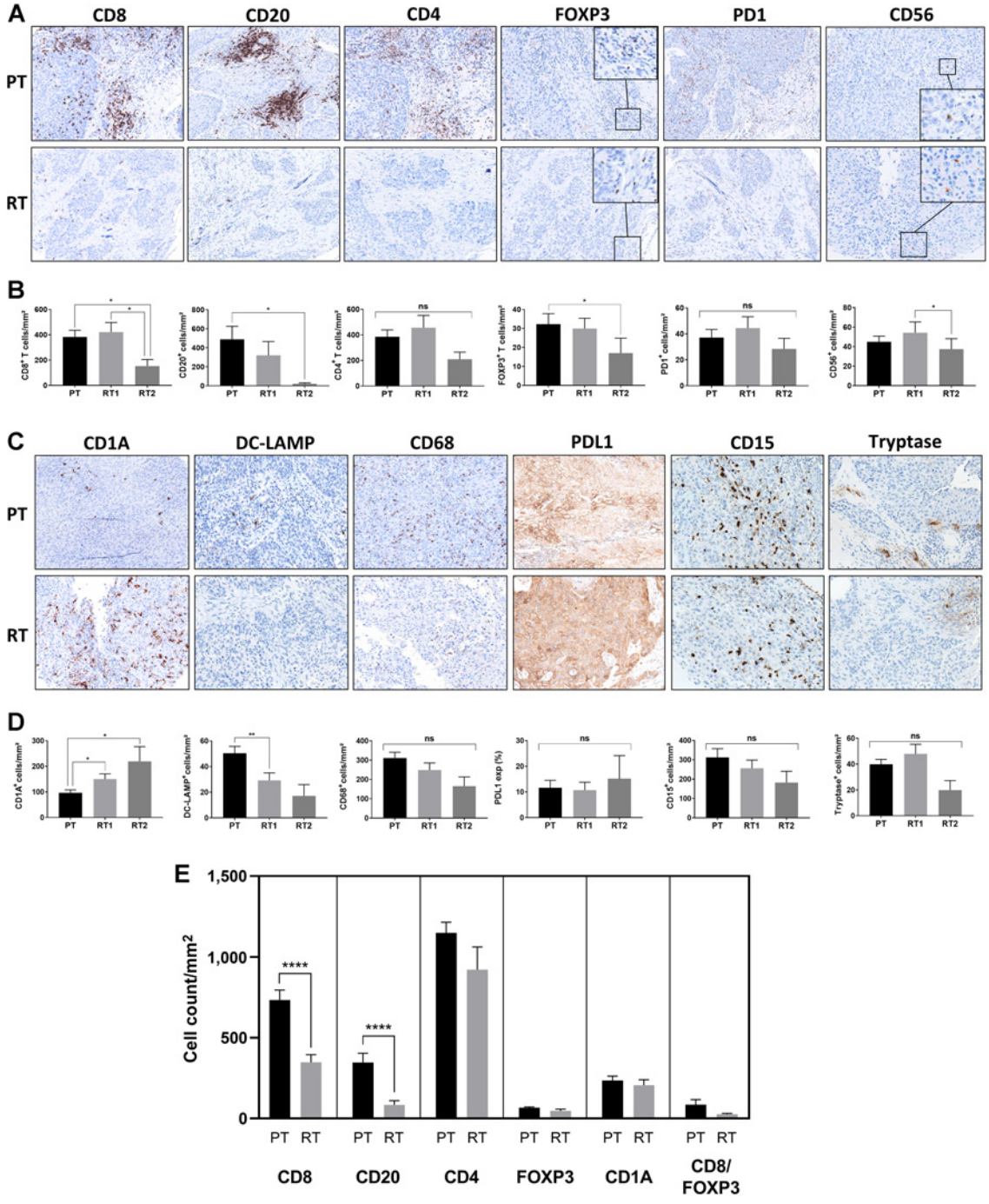

Figure 1.

Protein expression analysis by IHC evaluation of the TIME of HNSCC PTs and RTs with loss of antitumor immunity in RTs in two independent cohorts. **A** and **C,** Representative IHC TMA pictures of the discovery cohort comparing tissue from PTs (top) to corresponding RTs (bottom) with lymphocyte lineage markers in **A** and myeloid lineage markers as well as PDL1 in **C**. Selected TMA pictures show three representative patients of the cohort with matched PT and RT pictures (patient 1: CD8, CD20, CD4, FOXP3, PD1, Tryptase, DC-LAMP; patient 2: CD1A, CD68, CD56, CD15; patient 3: PDL1). **B** and **D,** Chart diagrams of the average count of indicated immune cell subtypes per mm^2 tumor tissue in PT ($n = 63$), corresponding first RT (RT1, $n = 63$), and corresponding second RT (RT2, $n = 13$). General trend toward less immune cell infiltration in RT2 compared with PT with significant decreases for $CD8^+$ T cells, $CD20^+$ B lymphocytes, and $FOXP3^+$ T cells. $CD1A^+$ dendritic cells were the only immune cell subtype with a significant increase from PT to RT1 and from PT to RT2, while DC-LAMP+ mature dendritic cells decreased in RT1. (*, $P < 0.05$; **, $P < 0.01$). **E,** Chart diagrams of an independent validation cohort (Bonn) confirming loss of antitumor immunity in RTs via IHC-based analysis of protein expression with average count of indicated immune cell subtypes per mm^2 tumor tissue in PTs ($n = 265$) and RTs ($n = 47$). General tendency toward less immune cell infiltration in RTs and significant decrease of $CD8^+$ T cells and $CD20^+$ B lymphocytes as well as a strong trend toward decrease of CD8/FOXP3 ratio. In contrast to the discovery cohort, the count of $CD1A^+$ dendritic cells was not altered in RTs in the validation cohort. (****, $P < 0.0001$).

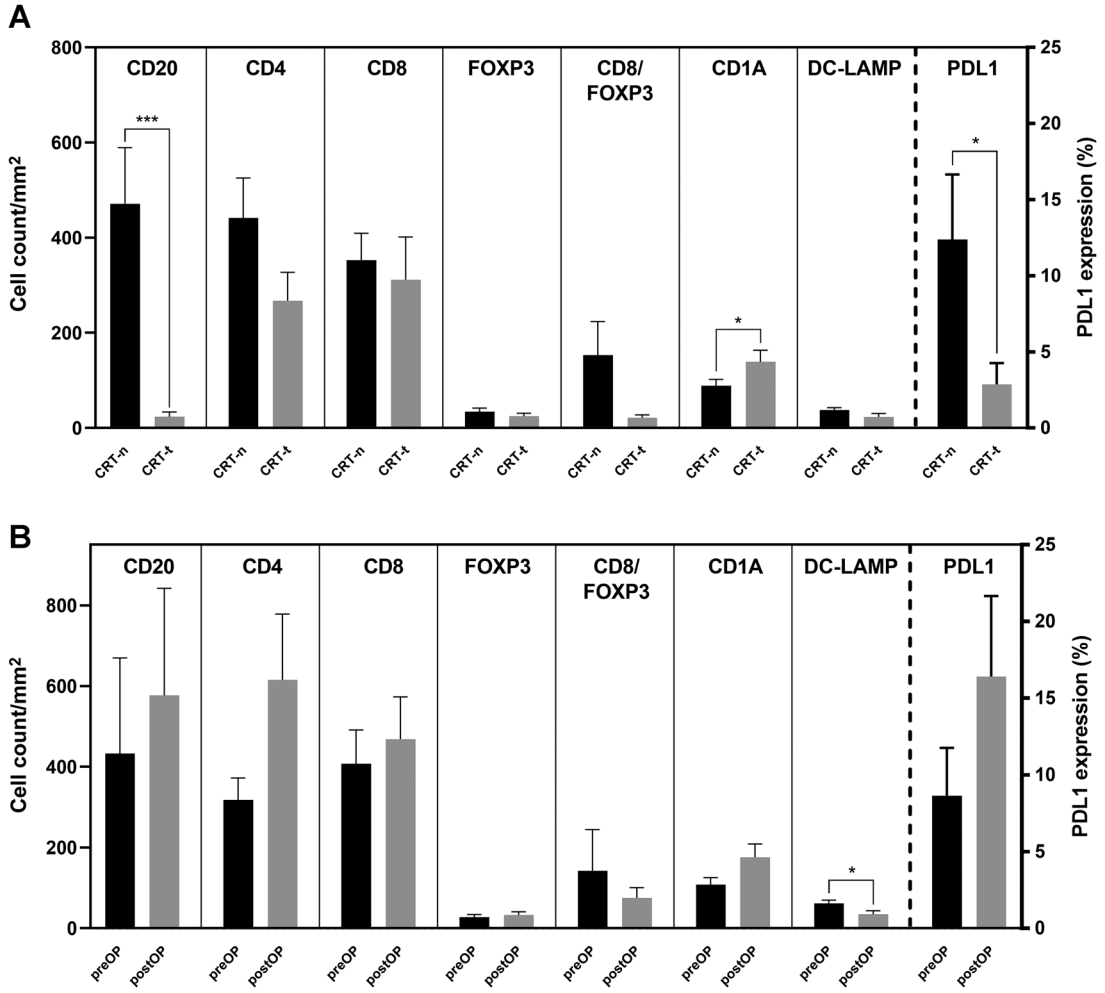

Figure 2.

The TIME of patients with recurrent HNSCC after adjuvant CRT is immunosuppressed in comparison with the TIME of patients without adjuvant CRT. **A,** Chart diagrams of the mean count of indicated immune cell subtypes per mm^2 tumor tissue or percentage of expressing tumor cells (PDL1) in corresponding CRT-n PTs and CRT-t RTs of the discovery cohort with a subtotal depletion of CD20$^+$ B lymphocytes as well as a significant increase of CD1A$^+$ dendritic cells, significant decrease of PDL1 expression, and a trend toward decreased CD4$^+$ T cells and CD8/FOXP3 ratio in CRT-t RTs ($n = 35$; ***, $P < 0.001$; *, $P < 0.05$). **B,** Chart diagrams of the mean count of indicated immune cell subtypes per mm^2 tumor tissue in preoperative (preOP) PTs and corresponding postoperative (postOP) RTs from patients who only had surgical resection of the tumor ($n = 28$).

increase of CD1A$^+$ dendritic cells and a decrease of the CD8/FOXP3 ratio in RTs was also more pronounced after CRT exposure. DC-LAMP+ mature dendritic cells, on the other hand, had a stronger decrease in postoperative RTs ($P = 0.0203$) than in CRT-t RTs ($P = 0.0653$). In addition, CRT-t RTs had a significant decrease of PDL1 expression from 12.4% in CRT-n PTs to 2.9% in CRT-t RTs ($P = 0.049$).

PTs and RTs after CRT show distinct mRNA expression profiles of immune-related genes

To elucidate differences in the TIME of PTs and RTs after CRT on transcriptomic level, we performed mRNA expression analysis of 730 immune-related genes for 18 patients from our discovery cohort using nCounter PanCancer Immune Profiling Panel (NanoString Technologies). Only patients from the subgroup with adjuvant CRT after resection of PT were selected for transcriptomic analysis.

Unsupervised hierarchical clustering via Euclidean distance, as shown in **Fig. 3A**, showed a significant separation of PTs and RTs after CRT, instead of a patient-specific clustering of PTs and their corresponding RTs ($k = 2$, $P = 0.018$). The clustering of PTs was based on an overall higher normalized expression score of immune-related genes than in RTs after CRT. This is remarkable, as it demonstrates that the TIME of different PTs and RTs after CRT is more similar than the TIME of the PT and RT of the same patient.

Next, we used NSolver 4.0 Analysis Software (NanoString Technologies) to create immune cell infiltration scores for various immunocyte subtypes based on mRNA expression of marker genes as implemented in the nanostring panel (Supplementary Table S4). Here, we confirmed the decrease of total TILs ($P = 0.0004$), loss of B lymphocytes/TILs ($P < 0.0001$) and increase of dendritic cells/TILs ($P = 0.0002$) from PTs to RTs after CRT on transcriptomic level (**Fig. 3B**). In addition, we discovered a significant increase of mast cells ($P = 0.0057$), macrophages ($P < 0.0001$), and neutrophils ($P = 0.018$) relative to total TIL count in RTs. Interestingly, all the former cell types belong to the myeloid lineage, which have variable roles in cancer

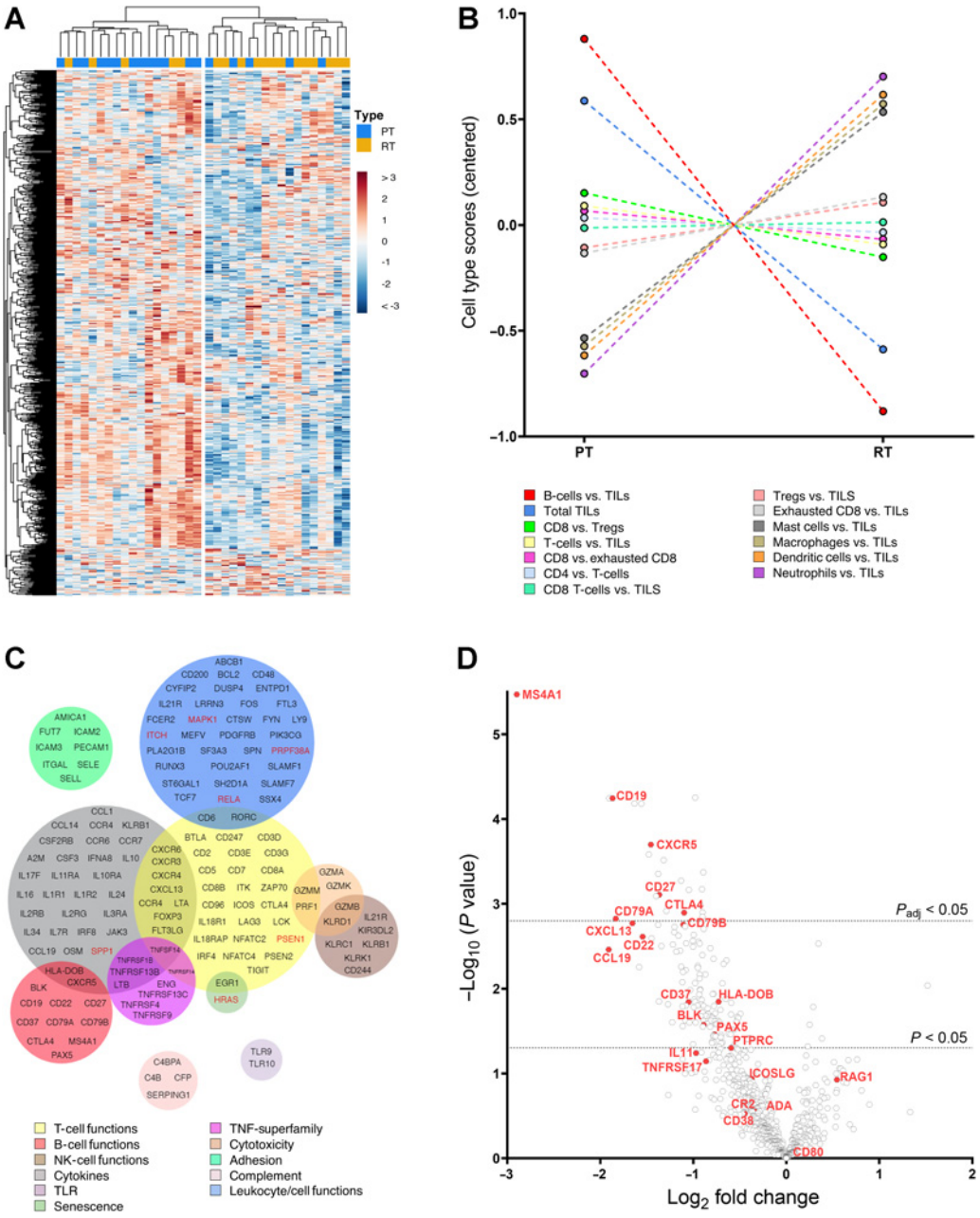

Figure 3.

Analysis of mRNA expression levels of immune-related genes in PTs and RTs after CRT. **A,** Hierarchical clustering of matched PTs and corresponding RTs after CRT ($n = 18$) of the discovery cohort, displayed as a heatmap with row wise z-scores of $\log_2$ transformed normalized read counts (nanostring) for 730 immune-related genes. Close clustering of PTs with mostly high expression levels of immune-related genes on the left and RTs after CRT with mostly low expression levels on the right side. **B,** Immune cell infiltration based on mRNA expression profiles in PTs and RTs after CRT. Decrease of the total count of TILs and B-lymphocyte fraction as well as increase of dendritic cell, mast cell, macrophage, and neutrophil fraction in RTs. **C,** Venn diagram of all genes from the nanostring PanCancer Immune Profiling Panel with significantly differential expression levels in PTs and RTs after CRT. Significantly downregulated genes are displayed in black and upregulated genes in red. Genes are arranged according to their immune functions as color coded in the annotations below. **D,** Volcano plot of normalized RNA-expression scores in PTs and RTs after CRT, displaying genes involved in B-lymphocyte functions in red (P_{adj}: adjusted P value by Benjamini–Hochberg procedure).

immunity including antitumor, but also protumor inflammation-promoting functions (29).

We also assessed additional genes with significantly differential expression between PTs and RTs after CRT (**Fig. 4C**). A set of 7 genes was found to be significantly upregulated in RTs: *SPP1, HRAS, MAPK1, PSEN1, RELA, ITCH*, and *PRPF38A*. Strongest upregulation was observed for *SPP1*, as measured by $\log_2$ fold change ($\log_2$FC: 1.52). On the other hand, 160 genes appeared to be significantly down-regulated in CRT-t RTs. Downregulated genes were predominantly cytokines, genes from the TNF family and genes involved in cellular

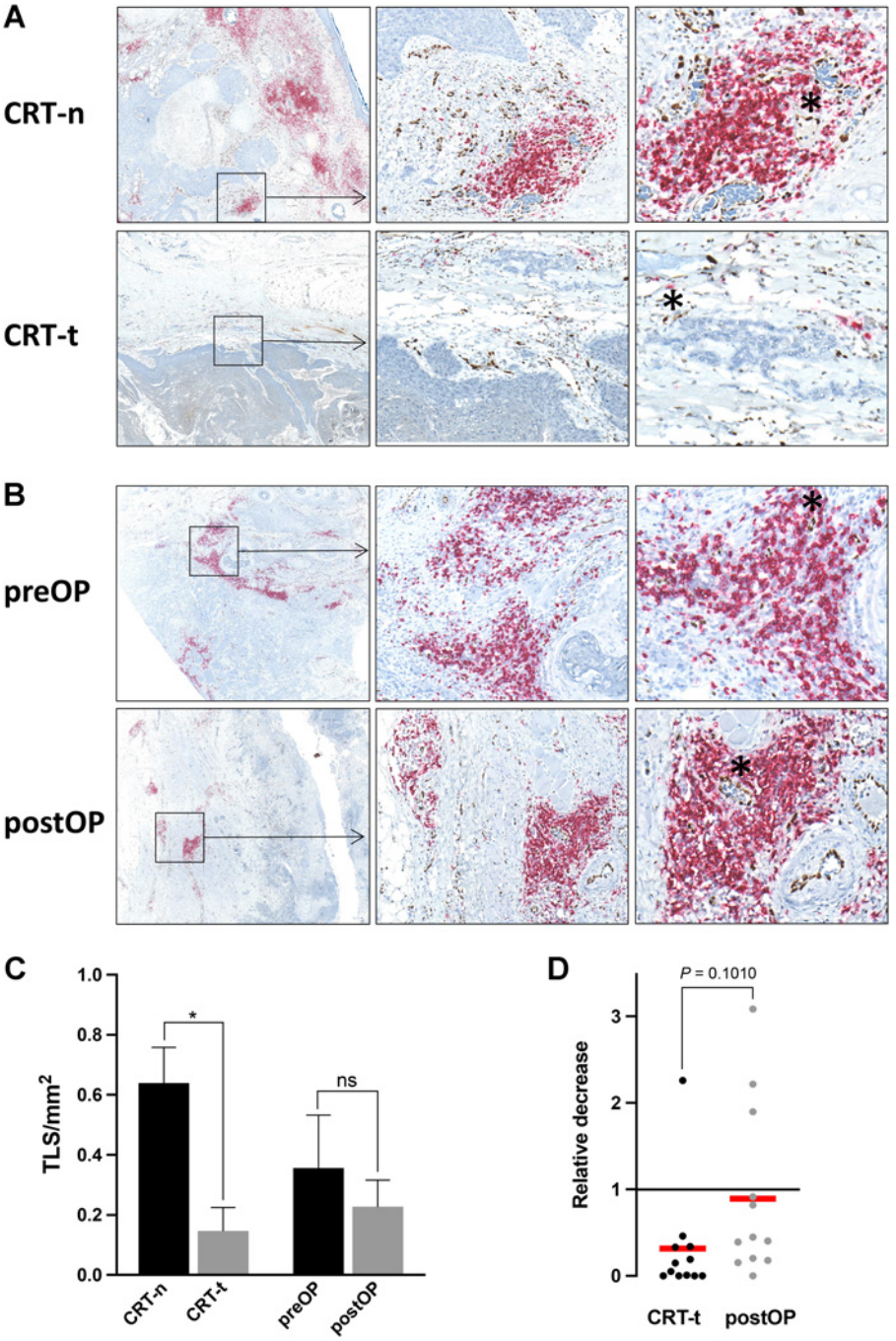

Figure 4.

The number of TLS significantly decreases after adjuvant CRT. **A,** Representative whole slide, IHC pictures of a CRT-n PT and the corresponding CRT-t RT of one patient. TLS are displayed as $CD20^+$ lymphoid aggregates (red) around ERG^+ venules (brown, asterisk). The CRT-n PT shows several TLS in the vicinity of tumor infiltrates. The CRT-t RT has only a few $CD20^+$ B lymphocytes without TLS formation. **B,** Representative whole slide, IHC pictures of a preOP PT and the corresponding postOP RT with formation of several TLS within and around the tumor and no significant change in the postOP RT. **C,** Chart diagrams of the average count of TLS per mm^2 tumor tissue in CRT-n PT and corresponding CRT-t RT ($n = 12$) as well as preOP PT and corresponding postOP RT ($n = 12$). TLS are significantly decreased in CRT-t RTs in comparison with CRT-n PTs, while there is no significant differences between preOP PTs and postOP RTs. **D,** Scatter plot of relative decreases in TLS frequencies for CRT-t RTs (corresponding CRT-n RT = 1) and for postOP RTs (corresponding preOP PT = 1). CRT-t RTs tend to have a more pronounced loss of TLS in comparison with postOP RTs. Red line marks mean (*, $P < 0.05$).

adhesion as well as genes important for T-cell, B-lymphocyte, and NK-cell functions and their cytotoxic capacities (**Fig. 3C** and **D**). The strongest downregulation was observed for *MS4A1* (log_2FC: −2.90), respectively *CD20*, as well as *CD19* (log_2FC: −1.87), *CD79A* (log_2FC: −1.83), and *CD22* (log_2FC: −1.54), which are all components of B-lymphocyte receptor signaling (30). Furthermore, the ligands and receptors *CCL19* (log_2FC: −1.91), *CCR7* (log_2FC: −1.90), *CXCL13* (log_2FC: −1.65), *CXCR5* (log_2FC: −1.46), *CCL14* (log_2FC: −1.45), and *LTB* (log_2FC: −1.22), which play crucial roles in the formation of TLS and in chemotaxis of B lymphocytes, as well as *ICAM-2* (log_2FC: −0.82) and *ICAM-3* (log_2FC: −0.56), which are essential to retain leukocytes in TLS through specialized high endothelial venules (HEV), were also strongly downregulated in RTs after CRT (31).

As the pattern of strongly downregulated genes was mostly associated with B lymphocytes and TLS, we aimed to further define the presence of TLS and their dependency of CRT. An IHC double stain labeling $CD20^+$ B lymphocytes (red) and ERG^+ venules (brown) was used to detect TLS on whole slides of 12 matched preoperative PTs and postoperative RTs without CRT as well as 12 matched CRT-n and CRT-t tumors. $CD20^+$ B-lymphocyte aggregates around ERG+ venules as marker for TLS were found in intratumoral fibrous bands and in the peritumoral desmoplastic stroma (**Fig. 4A** and **B**). While

mean TLS numbers per mm^2 were significantly lower in CRT-t RTs (0.14 TLS/mm^2) than in CRT-n PTs (0.64 TLS/mm^2, $P = 0.0113$), only small changes were observed after surgery from an average of 0.36 TLS/mm^2 in preoperative PTs to 0.23 TLS/mm^2 in postoperative RTs ($P = 0.5548$; **Fig. 4C**). Although the mean TLS number per mm^2 tended to be slightly lower in the preoperative PTs compared with CRT-n PTs, this difference was not significant ($P = 0.1950$) and is considered to be within the range of pathophysiologic variations of the TIME across different patients with HNSCC. Relative changes of TLS frequencies in CRT-t RTs normalized to their matched CRT-n PTs in comparison with postoperative RTs normalized to their matched preoperative PTs also demonstrated a trend toward a more pronounced TLS loss in CRT-t RTs (0.32) as compared with postoperative RTs (0.91, $P = 0.1010$; **Fig. 4D**).

Effect of chemotherapy and radiation resistance on the TIME in an *in vitro* spheroid model reveals both differences from and similarities to CRT-t RTs *in vivo*

Because our *in vivo* studies showed striking changes of the TIME after exposure to CRT, we aimed to further investigate whether tumor cell resistance to cytotoxic therapy plays a role for these immunologic changes.

First, we created a chemotherapy-resistant HNSCC cell line via long-term treatment of the hypopharyngeal squamous cell carcinoma cell line FaDu with cisplatin (FaDu/CR). A radiation-resistant FaDu cell line (Fadu/RR) was provided by the research group of Anna Dubrovska. Cisplatin and radiation resistance in comparison with wildtype FaDus (FaDu/WT) were determined via MTT assay and survival colony formation assay (**Fig. 5A** and **B**). As we hypothesized that cytotoxic therapy resistance leads to differences in antitumor immune response, we created an *in vitro* model of tumor cell spheroids, which can be cocultured with immunocytes, to subsequently analyze quantity and quality of spheroid-infiltrating immunocytes (Supplementary Fig. S2).

Coincubation of FaDu/WT and FaDu/CR spheroids with activated PBMCS of healthy donors showed significant differences in immunocyte infiltrations. Importantly, coincubation of spheroids with immune cells was performed in the absence of cisplatin to avoid direct cytotoxic effects on PBMCs. In contrast to the previously observed lower immune infiltration of CRT-t RTs *in vivo*, FaDu/CR spheroids were characterized by a significantly higher immune cell infiltrate than FaDu/WT spheroids as indicated by an increase of $CD45^+$ leukocytes from an average of 11.8 cells/mm^2 in FaDu/WT spheroids to 133 cells/mm^2 in FaDu/R spheroids ($P < 0.0001$; **Fig. 5C** and **E**). Because of previous activation of T cells with anti-CD3 and anti-CD28 incubation of isolated PBMCs, most spheroid infiltrating leukocytes were $CD4^+$ Th cells with a mean increase from 5.2 cells/mm^2 in FaDu/WT spheroids to 33.5 cells/mm^2 in FaDu/R spheroids ($P < 0.0001$) or $CD8^+$ cytotoxic T cells with a mean increase from 8.1 cells/mm^2 in FaDu/WT spheroids to 70.8 cells/mm^2 in FaDu/CR spheroids ($P < 0.0001$). Moreover, in contrast to the HNSCC cohort, PDL1 expression was significantly increased from a mean relative score of 0.05 in FaDu/WT spheroids to 0.32 in FaDu/CR spheroids ($P < 0.0001$). Spheroid-infiltrating leukocytes also tended to be higher in FaDu/RR spheroids with the strongest increase for $CD8^+$ cytotoxic T cells from 31.3 to 84.8 cells/mm^2 ($P = 0.0557$). Analogous to FaDu/CR spheroids PDL1 expression was significantly upregulated in FaDu/RR with a mean relative score of 0.30 in FaDu/WT to 0.40 in FaDu/RR ($P < 0.05$).

In summary, the *in vitro* experiments indicated a higher immunogenicity of tumor cells after gaining cisplatin resistance in contrast to the immunosuppressive TIME in CRT-t RTs of the *in vivo* cohort. Radiation resistance caused a similar, but weaker effect in the *in vitro* experiments. To still analyze overlapping molecular changes between the cohort and the *in vitro* model, we also performed mRNA expression analysis of FaDu/WT spheroids and FaDu/CR spheroids. Comparison with PTs and RTs after CRT revealed five genes, which were simultaneously significantly upregulated in CRT-t RTs as well as in FaDu/R spheroids: *SPP1, MAPK1, PSEN1, RELA*, and *ITCH* (**Fig. 5D**). On the other hand, 16 genes were simultaneously downregulated *in vivo* and *in vitro* with highest *in vitro* downregulation of *ENG* (log_2FC: −2.18) and *IL24* (log_2FC: −1.27).

Discussion

High rates of RTs are still a major factor leading to poor prognosis of HNSCC. Although immune checkpoint inhibitors have been included in the latest treatment guidelines of recurrent HNSCC, response rates, and overall survival benefit stay low (14). As the TIME is one main factor influencing CRT response as well as efficacy of immune checkpoint inhibitors, there is an urgent need to better define the TIME of HNSCC RTs (13, 32).

Comparative immune cell infiltration analyses of PTs and RTs in two independent cohorts revealed major differences. Significant loss of $CD8^+$ cytotoxic T cells and $CD20^+$ B lymphocytes in RTs as well as general trend toward less immune infiltration of RTs was observed in both cohorts and indicates a shift from antitumor immune response in PTs to immunosuppression in RTs (17, 33). This conclusion is supported by multiple studies demonstrating improved overall survival and local tumor control of HNSCC and other solid malignancies, which are highly infiltrated by $CD8^+$ cytotoxic T cells and $CD20^+$ B lymphocytes (16, 18, 19). From a therapeutic perspective, a CD8-dominant T-cell infiltration is considered to be one key factor for successful immune checkpoint therapy (22, 32). An additional hint for local immunosuppression in RTs was the increase of CD8/FOXP3 and CD8/PD-1 ratio, as $FOXP3^+$ Tregs and $PD\text{-}1^+$ cells are both known for dampening the antitumoral immune response (14, 34). According to the discovery cohort, the decrease of TILs ($CD8^+$, $CD20^+$, $FOXP3^+$, $CD56^+$ TILs) was particularly evident in RT2s. We think that this suggests a stepwise development of an immunosuppressive TIME in HNSCC over the course of repeated recurrence development. In addition, we found a significant increase of $CD1A^+$ dendritic cells in RTs in our discovery cohort, which was not confirmed in our validation cohort. Dendritic cells generally form a heterogenous group of different subtypes harboring both antitumor and protumor capacities (35, 36). A selective assessment of DC-LAMP+ mature dendritic cells, in contrast, showed a significant decrease in RTs. DC-LAMP+ dendritic cells support an efficient T cell–mediated antitumor immune response as well as a close interaction with B lymphocytes in the context of TLS and are of prognostic and predictive significance in different tumor entities, including HNSCC (37, 38).

The direct impact of CRT on immunologic functions is known to harbor immune-stimulating as well as immunosuppressive effects (15). Most relevant immune-stimulating effects include attraction and activation of dendritic cells, which can activate tumor antigen-specific $CD8^+$ CTLs (39, 40). Nevertheless, CRT also impedes the development of an effective antitumor immune response and can lead to long-term immune dysfunction in HNSCC (41). E.g., CRT kills not only tumor cells, but also immunocytes over the course of treatment. Furthermore, it has been shown to increase the number of circulating Tregs, PD-1–expressing cells, and MDSCs in HNSCC (42, 43).

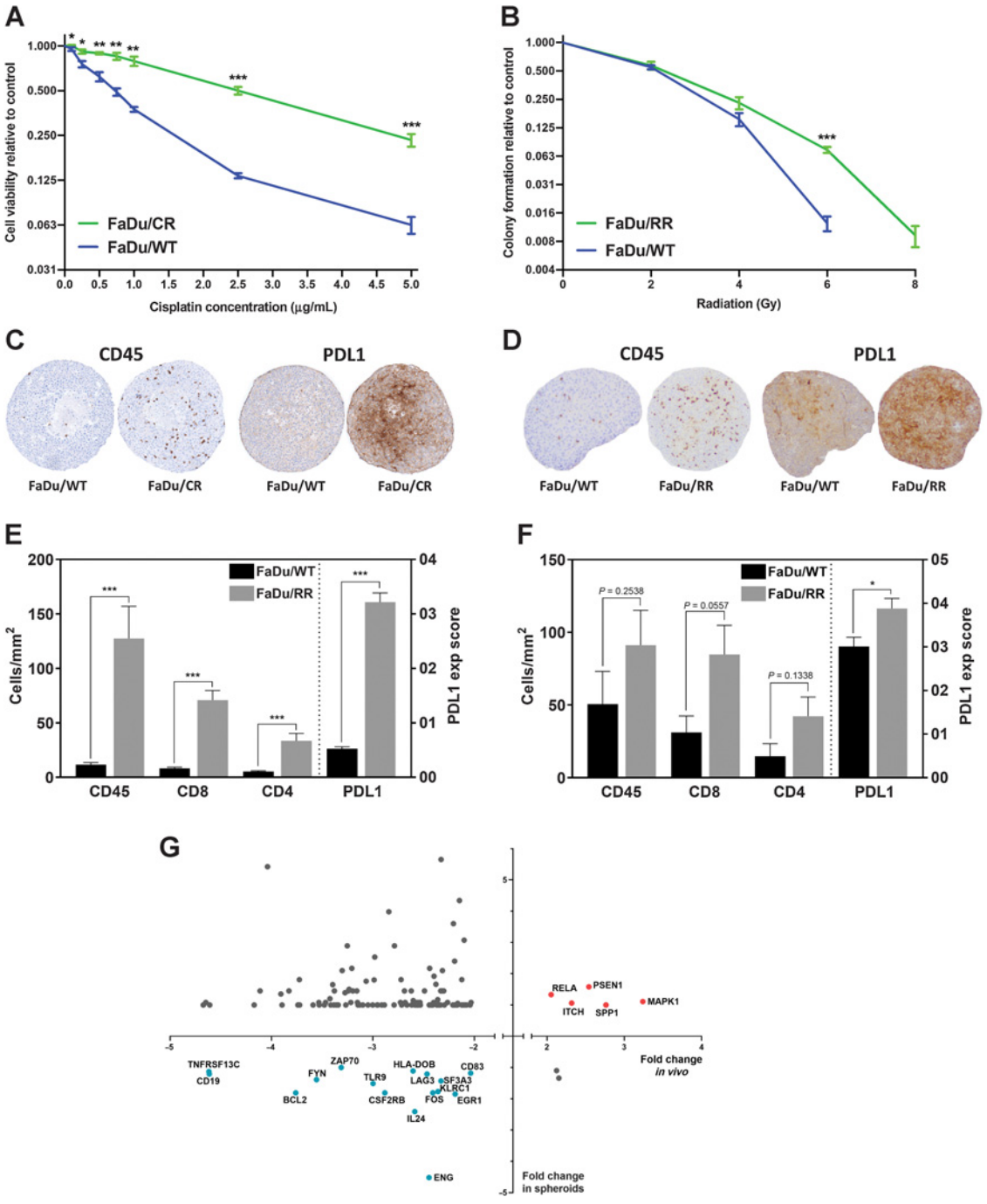

Figure 5.

Immunocyte infiltration in cisplatin- or radiation-resistant FaDu spheroids and correlation of immune-related gene expression to CRT-t RTs. **A,** Concentration-dependent gain of resistance to cisplatin according to MTT assay after exposing FaDu/WT to increasing concentrations of cisplatin for over 6 months and thereby selecting cisplatin-resistant FaDu cells (FaDu/CR). **B,** Survival colony formation assay for FaDu/WT and FaDu/RR to increasing doses of radiation. **C** and **D,** Representative pictures of $CD45^+$ cell infiltration and PDL1 expression in FaDu/WT versus FaDu/CR spheroids and FaDu/WT versus FaDu/RR spheroids. **E,** Mean count of indicated immune cell subtypes per mm^2 spheroid tissue with significant increases of $CD45^+$, $CD8^+$, and $CD4^+$ cells and PDL1 expression in FaDu/CR spheroids compared with FaDu/WT spheroids. **F,** Analogous evaluation to (**E**) for FaDu/RR with significant upregulation of PDL1 expression and trends toward higher numbers of $CD45^+$, $CD8^+$, and $CD4^+$ cells for FaDu/RR spheroids. **G,** Comparison of fold changes of immune-related genes based on mRNA expression scores between *in vivo* CRT-n PTs and CRT-t RTs and *in vitro* FaDu/WT and FaDu/CR spheroids. Only significantly upregulated or downregulated genes are displayed. Simultaneously upregulated genes of *in vivo* and *in vitro* studies are in the upper right quadrant (red), simultaneously downregulated genes in the lower left quadrant (blue; ***, $P < 0.001$; **, $P < 0.01$; *, $P < 0.05$).

Consecutively, we wondered, if the deprivation of antitumor immune response in RTs is related to CRT. Therefore, we selectively analyzed the subcohort of patients, who were exposed to adjuvant CRT before development of their RT (CRT-t RT) and compared them with patients, who had no CRT prior to RT development (postOP RTs). Here, the significant decrease of immunocytes with antitumor capacities was reserved to CRT-t RTs, but not observed in postOP RTs. Correspondingly, we assume that the shift toward an immunosuppressive TIME is related to the previous CRT exposure. Most remarkably, $CD20^+$ B lymphocytes showed a nearly complete depletion in CRT-t RTs, whereas patients with resection only had no significant changes of $CD20^+$ B lymphocytes. Intratumoral B lymphocytes account for up to 25% of all TIL-subtypes across different cancer entities and are mostly associated with prolonged survival (20, 44, 45). Functional mechanisms of the antitumor capacity of B lymphocytes include long-term antigen presentation, which supports formation of $CD4^+$ and $CD8^+$ memory T cells at the tumor site, tumor-reactive autoantibodies, recruitment of other antitumor leukocytes via cytokine release and direct tumor cell killing via granzyme or TNF-related apoptosis-inducing ligand (TRAIL) signaling (45–47). Some subtypes of B lymphocytes, on the other hand, especially lately described regulatory B cells (Bregs), have pro-tumor effects, such as IL10–mediated suppression of cytotoxic immune responses and TGFß-mediated modulation of $CD4^+$ T cells to immunosuppressive Tregs (46, 48).

To further elucidate CRT-associated shift to a more protumor and immunosuppressive TIME in RTs and to better specify depletion of B lymphocytes, we performed mRNA expression analysis of 730 immune-related genes via nanostring profiling. According to unsupervised hierarchical clustering, the TIMEs within the group of PTs or CRT-t RTs were closer related than the TIMEs of a PT and its corresponding CRT-t RT. This observation ties in with recent findings revealing that RTs after CRT often seem to be unrelated to their corresponding PT when compared for copy-number alterations (49).

Subtype-specific immune cell infiltration scores based on mRNA expression of marker genes confirmed the significant decrease of total TILs and B lymphocytes as well as the significant increase of dendritic cells from PTs to RTs. Furthermore, mRNA-based analysis revealed a significant increase of neutrophils, mast cells, and macrophages relative to total TILs in RTs. The later immune cell types are all associated with an immunosuppressive TIME leading to reduced survival in various cancer entities and have also been found to be increased in patients plasma after CRT (29, 42, 50).

In the next step, we evaluated genes, which were significantly differentially expressed between PTs and RTs after CRT. Overall, most genes of the immune panel were downregulated with only a few exclusions demonstrating upregulation in RTs. Corresponding to our previous results, strongest downregulation could be observed for genes, which are involved in B-lymphocyte receptor signaling. Highly significant loss of *CD27*, which is predominantly known as a marker for memory B cells, in combination with nearly no alteration of *CD38*, which is known as a marker of early stages of B-cell development and of Bregs, indicated that depletion affects particularly long-lasting memory B cells (51). On the other hand, *IL10*, a major protumor mediator of Bregs, was also significantly downregulated in CRT-t RTs (46). In addition, we found that many of the highly downregulated genes are crucially involved in the initiation and growth of TLSs as well as in the retention of leukocytes to TLS through specialized HEVs (31, 52, 53). TLSs are ectopic lymphoid formations, which occur at sites of chronic inflammation, as in autoimmunity disease or cancer, and share common characteristics with secondary lymphoid organs (31). They mostly develop at the tumor margin and recent studies could demonstrate that they essentially contribute to a long-lasting and tumor-specific immune response by an interplay of follicular dendritic cells, $CD8^+$ and $CD4^+$ T cells, as well as $CD20^+$ B lymphocytes (31, 52). Thus, the existence of TLS at the tumor sites is associated with prolonged survival and local tumor control in various entities including HNSCC (31, 54). In our subsequent analyses, we could confirm a significant decrease of TLS in RTs after CRT using IHC-based whole slide evaluations. This decrease was insubstantial in postoperative RTs, who had not yet received CRT.

As we could reveal that an immunosuppressed TIME of RTs is highly associated with previous CRT treatment of the PT, we wanted to further investigate the role of cytotoxic therapy on the TIME *in vitro*. Our aim was to examine, if tumor cell resistance to cancer therapies *per se* leads to changes in the T cell–mediated cytotoxic immune response as the common final path of antitumor immune response. Our cell culture studies focused on chemotherapy resistance to cisplatin and resistance to radiation, which regularly occurs in HNSCC RTs. We used a three-dimensional spheroid/immune cell coculture model of wildtype FaDu cells (FaDu/WT) and compared it with cisplatin-resistant FaDu cells (FaDu/CR) or radiation-resistant FaDu cells (FaDu/RR) coincubated with PBMCs of healthy donors. Here, we observed significantly higher infiltration with $CD45^+$ leukocytes, which were predominantly $CD4^+$ and $CD8^+$ T cells, and higher levels of PDL1 expression in FaDu/CR spheroids. FaDu/RR also had a higher PDL1 expression and tended to have higher lymphocyte infiltrates, in particular, $CD8^+$ T cells. These results indicate overall higher immunogenicity of FaDu spheroids resistant to cytotoxic therapies. We assume that the higher immune infiltration in resistant FaDu cells can be explained by their accumulation of genetic alterations elicited by DNA damages. Although we did not know the HLA subtype of our healthy PBMC donors and therefore have to assume that it might oftentimes not have matched the HLA subtype of FaDu cells (HLA-A*01:01), this systematic error does not affect our results as we analyzed relative differences. In summary, our cell culture results form a contrast to our *in vivo* results with an immunosuppressive TIME in CRT-t RTs. Our *in vitro* results support the stimulating effects of cisplatin and radiation on antitumor immune response and exclude a direct immunosuppressive effect of tumor cells on immunocytes *in vitro*. In addition, the spheroid/immunocyte coculture make clear that the multidimensional impact of cytotoxic therapy is more complex in patients with HNSCC. The local and systemic immune response as well as the role of stromal components, which interact with the local immune response and are highly affected by radiotherapy, probably lead to an immunosuppressed TIME in RTs *in vivo*.

Because resistance to cytotoxic therapy and changes in immune cell infiltration were more pronounced in FaDu/CR spheroids, these were used for further molecular analyses. Our aim was to discover potential relevant therapeutic targets contributing to cisplatin resistance and RT development by elaborating specific genes showing significant mRNA upregulation or downregulation *in vivo* after CRT as well as *in vitro* after cisplatin exposure. Mutually upregulated genes *in vivo* and *in vitro* include *SPP1, MAPK1*, and *PSEN1*. *SPP1*, also known as osteopontin, represents a cytokine, which is mostly secreted by tumor or stroma cells and substantially modulates the TIME by attracting protumor myeloid cells as well as facilitating tumor progression and metastasis (55). Consequently, its upregulation might be a major functional mechanism leading to the increase of myeloid cells in CRT-t RTs *in vivo*. Lou and colleagues furthermore showed that *SPP1* is frequently upregulated in cisplatin-resistant HNSCC and leads to

poor prognosis (56). RAS/MAPK activation has recently been associated with reduced TILs in patients with breast cancer (57) and with disease relapse as well as therapeutic resistance in HNSCC (58).

In summary, we could for the first time demonstrate that HNSCC RTs are characterized by an immunosuppressive TIME suggesting tumor immune evasion as one major factor promoting tumor recurrence. In addition, we elaborated that an immunosuppressive TIME predominantly occurs in CRT-t RTs, but not in RTs after surgical resection only. $CD20^+$ B lymphocytes as well as chemokines involved in B-lymphocyte chemotaxis and formation of tertiary lymphoid structures seem to be particularly subjected to the immunosuppressive TIME in CRT-t RTs. Finally, our mRNA expression analyses revealed new potential targets, as *SPP1*, which could help minimize the immunosuppressive effect of CRT. Our results are of particular therapeutic relevance, considering the rising application of immune checkpoint inhibitors in RTs on the one hand and the immunosuppressive TIME in RTs on the other hand. Our studies support the inclusion of immunotherapies at an early stage of treatment to fully exploit the antitumor immune activity and to avoid therapy resistance due to an immunosuppressive TIME.

Authors' Disclosures

No disclosures were reported.

Authors' Contributions

C. Watermann: Formal analysis, validation, investigation, writing-original draft, writing-review and editing. **H. Pasternack:** Data curation, software, investigation, visualization, methodology. **C. Idel:** Conceptualization, resources, data curation, project administration, writing-review and editing. **J. Ribbat-Idel:** Conceptualization, resources, writing-review and editing. **J. Brägelmann:** Data curation, software, formal analysis, writing-review and editing. **P. Kuppler:** Resources, data curation, formal analysis. **A. Offermann:** Data curation, methodology, writing-review and editing. **D. Jonigk:** Resources, data curation, software, writing-review and editing. **M.P. Kühnel:** Resources, software, writing-review and editing. **A. Schröck:** Conceptualization, resources, project administration. **E. Dreyer:** Data curation, methodology. **C. Rosero:** Formal analysis, validation. **J. Nathansen:** Resources, data curation, validation. **A. Dubrovska:** Resources, validation, writing-review and editing. **L. Tharun:** Resources, data curation, writing-review and editing. **J. Kirfel:** Conceptualization, data curation, software, supervision, writing-review and editing. **B. Wollenberg:** Conceptualization, resources, writing-review and editing. **S. Perner:** Conceptualization, resources, funding acquisition, project administration, writing-review and editing. **R. Krupar:** Conceptualization, resources, data curation, software, formal analysis, supervision, investigation, visualization, methodology, writing-original draft, project administration, writing-review and editing.

Acknowledgments

J. Brägelmann was supported by the Else Kröner-Fresenius Stiftung Memorial Grant (2018_EKMS.35) and the Deutsche Krebshilfe through a Mildred Scheel Nachwuchszentrum Grant (70113307).

The costs of publication of this article were defrayed in part by the payment of page charges. This article must therefore be hereby marked *advertisement* in accordance with 18 U.S.C. Section 1734 solely to indicate this fact.

Received February 12, 2020; revised July 24, 2020; accepted October 23, 2020; published first October 27, 2020.

References

1. Bray F, Ferlay J, Soerjomataram I, Siegel RL, Torre LA, Jemal A. Global cancer statistics 2018: GLOBOCAN estimates of incidence and mortality worldwide for 36 cancers in 185 countries. CA Cancer J Clin 2018;68:394–424.
2. Global Burden of Disease Cancer Collaboration, Fitzmaurice C, Allen C, Barber RM, Barregard L, Bhutta ZA, et al. Global, regional, and national cancer incidence, mortality, years of life lost, years lived with disability, and disability-adjusted life-years for 32 cancer groups, 1990 to 2015: a systematic analysis for the global burden of disease study. JAMA Oncol 2017;3:524–48.
3. Siegel RL, Miller KD, Jemal A. Cancer statistics, 2019. CA Cancer J Clin 2019;69:7–34.
4. Sacco AG, Cohen EE. Current treatment options for recurrent or metastatic head and neck squamous cell carcinoma. J Clin Oncol 2015;33:3305–13.
5. Seiwert TY, Cohen EEW. State-of-the-art management of locally advanced head and neck cancer. Br J Cancer 2005;92:1341–8.
6. Oosting SF, Haddad RI. Best practice in systemic therapy for head and neck squamous cell carcinoma. Front Oncol 2019;9:815.
7. Foster CC, Melotek JM, Brisson RJ, Seiwert TY, Cohen EEW, Stenson KM, et al. Definitive chemoradiation for locally-advanced oral cavity cancer: a 20-year experience. Oral Oncol 2018;80:16–22.
8. Vermorken JB, Mesia R, Rivera F, Remenar E, Kawecki A, Rottey S, et al. Platinum-based chemotherapy plus cetuximab in head and neck cancer. N Engl J Med 2008;359:1116–27.
9. Marur S, Forastiere AA. Head and neck cancer: changing epidemiology, diagnosis, and treatment. Mayo Clin Proc 2008;83:489–501.
10. Ferris RL, Blumenschein G, Fayette J, Guigay J, Colevas AD, Licitra L, et al. Nivolumab for recurrent squamous-cell carcinoma of the head and neck. N Engl J Med 2016;375:1856–67.
11. Cohen EEW, Soulières D, Le Tourneau C, Dinis J, Licitra L, Ahn M-J, et al. Pembrolizumab versus methotrexate, docetaxel, or cetuximab for recurrent or metastatic head-and-neck squamous cell carcinoma (KEYNOTE-040): a randomised, open-label, phase 3 study. Lancet 2019;393:156–67.
12. Rischin D, Harrington KJ, Greil R, Soulieres D, Tahara M, de Castro G, et al. Protocol-specified final analysis of the phase 3 KEYNOTE-048 trial of pembrolizumab (pembro) as first-line therapy for recurrent/metastatic head and neck squamous cell carcinoma (R/M HNSCC). J Clin Oncol 37:15s, 2019 (suppl; abstr 6000).
13. Cohen EEW, Bell RB, Bifulco CB, Burtness B, Gillison ML, Harrington KJ, et al. The Society for Immunotherapy of Cancer consensus statement on immunotherapy for the treatment of squamous cell carcinoma of the head and neck (HNSCC). J Immunother Cancer 2019;7:184.
14. Forster MD, Devlin M-J. Immune checkpoint inhibition in head and neck cancer. Front Oncol 2018;8:310.
15. Miyauchi S, Kim SS, Pang J, Gold KA, Gutkind JS, Califano JA, et al. Immune modulation of head and neck squamous cell carcinoma and the tumor microenvironment by conventional therapeutics. Clin Cancer Res 2019;25:4211–23.
16. Rooney MS, Shukla SA, Wu CJ, Getz G, Hacohen N. Molecular and genetic properties of tumors associated with local immune cytolytic activity. Cell 2015;160:48–61.
17. Turan T, Kannan D, Patel M, Matthew Barnes J, Tanlimco SG, Lu R, et al. Immune oncology, immune responsiveness and the theory of everything. J Immunother Cancer 2018;6:50.
18. Mandal R, Şenbabaoğlu Y, Desrichard A, Havel JJ, Dalin MG, Riaz N, et al. The head and neck cancer immune landscape and its immunotherapeutic implications. JCI Insight 2016;1:e89829.
19. Russell S, Angell T, Lechner M, Liebertz D, Correa A, Sinha U, et al. Immune cell infiltration patterns and survival in head and neck squamous cell carcinoma. Head Neck Oncol 2013;5:24.
20. Bindea G, Mlecnik B, Tosolini M, Kirilovsky A, Waldner M, Obenauf AC, et al. Spatiotemporal dynamics of intratumoral immune cells reveal the immune landscape in human cancer. Immunity 2013;39:782–95.
21. Nagarsheth N, Wicha MS, Zou W. Chemokines in the cancer microenvironment and their relevance in cancer immunotherapy. Nat Rev Immunol 2017;17:559–72.
22. Herbst RS, Soria J-C, Kowanetz M, Fine GD, Hamid O, Gordon MS, et al. Predictive correlates of response to the anti-PD-L1 antibody MPDL3280A in cancer patients. Nature 2014;515:563–7.
23. Krupar R, Robold K, Gaag D, Spanier G, Kreutz M, Renner K, et al. Immunologic and metabolic characteristics of HPV-negative and HPV-positive head and neck

squamous cell carcinomas are strikingly different. Virchows Arch 2014;465:299–312.
24. Bankhead P, Loughrey MB, Fernández JA, Dombrowski Y, McArt DG, Dunne PD, et al. QuPath: open source software for digital pathology image analysis. Sci Rep 2017;7:16878.
25. Geiss GK, Bumgarner RE, Birditt B, Dahl T, Dowidar N, Dunaway DL, et al. Direct multiplexed measurement of gene expression with color-coded probe pairs. Nat Biotechnol 2008;26:317–25.
26. Rangan SR. A new human cell line (FaDu) from a hypopharyngeal carcinoma. Cancer 1972;29:117–21.
27. Mosmann T. Rapid colorimetric assay for cellular growth and survival: application to proliferation and cytotoxicity assays. J Immunol Methods 1983;65:55–63.
28. Kurth I, Hein L, Mäbert K, Peitzsch C, Koi L, Cojoc M, et al. Cancer stem cell related markers of radioresistance in head and neck squamous cell carcinoma. Oncotarget 2015;6:34494–509.
29. Engblom C, Pfirschke C, Pittet MJ. The role of myeloid cells in cancer therapies. Nat Rev Cancer 2016;16:447–62.
30. Pieper K, Grimbacher B, Eibel H. B-cell biology and development. J Allergy Clin Immunol 2013;131:959–71.
31. Sautès-Fridman C, Petitprez F, Calderaro J, Fridman WH. Tertiary lymphoid structures in the era of cancer immunotherapy. Nat Rev Cancer 2019;19:307–25.
32. Hegde PS, Karanikas V, Evers S. The where, the when, and the how of immune monitoring for cancer immunotherapies in the era of checkpoint inhibition. Clin Cancer Res 2016;22:1865–74.
33. Schreiber RD, Old LJ, Smyth MJ. Cancer immunoediting: integrating immunity's roles in cancer suppression and promotion. Science 2011;331:1565–70.
34. Jie H-B, Gildener-Leapman N, Li J, Srivastava RM, Gibson SP, Whiteside TL, et al. Intratumoral regulatory T cells upregulate immunosuppressive molecules in head and neck cancer patients. Br J Cancer 2013;109:2629–35.
35. Wculek SK, Cueto FJ, Mujal AM, Melero I, Krummel MF, Sancho D. Dendritic cells in cancer immunology and immunotherapy. Nat Rev Immunol 2020;20:7–24.
36. Tran Janco JM, Lamichhane P, Karyampudi L, Knutson KL. Tumor-infiltrating dendritic cells in cancer pathogenesis. J Immunol 2015;194:2985–91.
37. Truxova I, Kasikova L, Hensler M, Skapa P, Laco J, Pecen L, et al. Mature dendritic cells correlate with favorable immune infiltrate and improved prognosis in ovarian carcinoma patients. J Immunother Cancer 2018;6:139.
38. Ladányi A, Kapuvári B, Papp E, Tóth E, Lövey J, Horváth K, et al. Local immune parameters as potential predictive markers in head and neck squamous cell carcinoma patients receiving induction chemotherapy and cetuximab. Head Neck 2019;41:1237–45.
39. Golden EB, Apetoh L. Radiotherapy and immunogenic cell death. Semin Radiat Oncol 2015;25:11–7.
40. Demaria S, Golden EB, Formenti SC. Role of local radiation therapy in cancer immunotherapy. JAMA Oncol 2015;1:1325–32.
41. Verastegui EL, Morales RB, Barrera-Franco JL, Poitevin AC, Hadden J. Long-term immune dysfunction after radiotherapy to the head and neck area. Int Immunopharmacol 2003;3:1093–104.
42. Sridharan V, Margalit DN, Lynch SA, Severgnini M, Zhou J, Chau NG, et al. Definitive chemoradiation alters the immunologic landscape and immune checkpoints in head and neck cancer. Br J Cancer 2016;115:252–60.
43. Parikh F, Duluc D, Imai N, Clark A, Misiukiewicz K, Bonomi M, et al. Chemoradiotherapy-induced upregulation of PD-1 antagonizes immunity to HPV-related oropharyngeal cancer. Cancer Res 2014;74:7205–16.
44. Lechner A, Schlößer HA, Thelen M, Wennhold K, Rothschild SI, Gilles R, et al. Tumor-associated B cells and humoral immune response in head and neck squamous cell carcinoma. Oncoimmunology 2019;8:1535293.
45. Nelson BH. CD20+ B cells: the other tumor-infiltrating lymphocytes. J Immunol 2010;185:4977–82.
46. Tsou P, Katayama H, Ostrin EJ, Hanash SM. The emerging role of B cells in tumor immunity. Cancer Res 2016;76:5597–601.
47. Yuen GJ, Demissie E, Pillai S. B lymphocytes and cancer: a love-hate relationship. Trends Cancer 2016;2:747–57.
48. Sarvaria A, Madrigal JA, Saudemont A. B cell regulation in cancer and anti-tumor immunity. Cell Mol Immunol 2017;14:662–74.
49. de Roest RH, Mes S, Brink A, Poell JB, van de Wiel MA, Bloemena E, et al. Molecular characterization of locally relapsed head and neck cancer after concomitant chemoradiotherapy. Clin Cancer Res 2019;25:7256–65.
50. Tong CCL, Kao J, Sikora AG. Recognizing and reversing the immunosuppressive tumor microenvironment of head and neck cancer. Immunol Res 2012;54:266–74.
51. Clavarino G, Delouche N, Vettier C, Laurin D, Pernollet M, Raskovalova T, et al. Novel strategy for phenotypic characterization of human B lymphocytes from precursors to effector cells by flow cytometry. PLoS One 2016;11:e0162209.
52. Colbeck EJ, Ager A, Gallimore A, Jones GW. Tertiary lymphoid structures in cancer: drivers of antitumor immunity, immunosuppression, or bystander sentinels in disease? Front Immunol 2017;8:1830.
53. Jing F, Choi EY. Potential of cells and cytokines/chemokines to regulate tertiary lymphoid structures in human diseases. Immune Netw 2016;16:271–80.
54. Wirsing AM, Rikardsen OG, Steigen SE, Uhlin-Hansen L, Hadler-Olsen E. Characterisation and prognostic value of tertiary lymphoid structures in oral squamous cell carcinoma. BMC Clin Pathol 2014;14:38.
55. Castello LM, Raineri D, Salmi L, Clemente N, Vaschetto R, Quaglia M, et al. Osteopontin at the crossroads of inflammation and tumor progression. Mediators Inflamm 2017;2017:4049098.
56. Luo S-D, Chen Y-J, Liu C-T, Rau K-M, Chen Y-C, Tsai H-T, et al. Osteopontin involves cisplatin resistance and poor prognosis in oral squamous cell carcinoma. BioMed Res Int 2015;2015:508587.
57. Loi S, Dushyanthen S, Beavis PA, Salgado R, Denkert C, Savas P, et al. RAS/MAPK activation is associated with reduced tumor-infiltrating lymphocytes in triple-negative breast cancer: therapeutic cooperation between MEK and PD-1/PD-L1 immune checkpoint inhibitors. Clin Cancer Res 2016;22:1499–509.
58. Roy S, Roy S, Kar M, Padhi S, Saha A, Anuja K, et al. Role of p38 MAPK in disease relapse and therapeutic resistance by maintenance of cancer stem cells in head and neck squamous cell carcinoma. J Oral Pathol Med 2018;47:492–501.

Clinical Cancer Research

Recurrent HNSCC Harbor an Immunosuppressive Tumor Immune Microenvironment Suggesting Successful Tumor Immune Evasion

Christian Watermann, Helen Pasternack, Christian Idel, et al.

Clin Cancer Res Published OnlineFirst October 27, 2020.

SCIENTIFIC REPORTS
nature research

OPEN

In silico analysis reveals EP300 as a panCancer inhibitor of anti-tumor immune response via metabolic modulation

Rosemarie Krupar[1,2,5]✉, Christian Watermann[2,5], Christian Idel[3], Julika Ribbat-Idel[2], Anne Offermann[2], Helen Pasternack[2], Jutta Kirfel[2], Andrew G. Sikora[4] & Sven Perner[1,2]

The tumor immune microenvironment (TIME) of head and neck squamous cell carcinomas (HNSCC) and other solid malignancies is a key determinant of therapy response and prognosis. Among other factors, it is shaped by the tumor mutational burden and defects in DNA repair enzymes. Based on the TCGA database we aimed to define specific, altered genes associated with different TIME types, which might represent new predictive markers or targets for immuno-therapeutic approaches. The HNSCC cohort of the TCGA database was used to define 3 TIME types (immune-activated, immune-suppressed, immune-absent) according to expression of immune-related genes. Mutation frequencies were correlated to the 3 TIME types. Overall survival was best in the immune-activated group. 9 genes were significantly differentially mutated in the 3 TIME types with strongest differences for *TP53* and the histone-acetyltransferase *EP300*. Mutations in *EP300* correlated with an immune-activated TIME. In panCancer analyses anti-tumor immune activity was increased in *EP300* mutated esophageal, stomach and prostate cancers. Downregulation of EP300 gene expression was associated with higher anti-tumor immunity in most solid malignancies. Since EP300 is a promoter of glycolysis, which negatively affects anti-tumor immune response, we analyzed the association of EP300 with tumor metabolism. PanCancer tumor metabolism was strongly shifted towards oxidative phosphorylation in EP300 downregulated tumors. *In silico* analyses of of publicly available *in vitro* data showed a decrease of glycolysis-associated genes after treatment with the EP300 inhibitor C646. Our study reveals associations of specific gene alterations with different TIME types. In detail, we defined EP300 as a panCancer inhibitor of the TIME most likely via metabolic modulation. In this context EP300 represents a promising predictive biomarker and an immuno-therapeutic target.

The tumor immune microenvironment (TIME) has emerged as a critical factor determining prognosis and therapy response across most solid tumors. In immunogenic tumors, such as breast and colon cancers or non-small cell lung cancers, the quantity and quality of tumor infiltrating lymphocytes has prognostic significance comparable to the TNM-classification[1]. The TIME is highly variable across different cancer entities and cancer subtypes as well as over the course of cancer progression and treatment[2,3]. Nevertheless, solid tumors can generally be classified into different categories according to their specific TIME profiles. We can distinguish at least three different TIME types in solid tumors, considering their prognostic impact and the quantity and quality of tumor infiltrating leukocytes[2,4]:

I. Tumors with a predominantly anti-tumor TIME, characterized, among other factors, by a high number of CD8 + cytotoxic T cells (CTLs) and other lymphocytes such as CD4 T helper cells, natural killer (NK) cells, regulatory T cells (Tregs), B lymphocytes, plasmocytoid dendritic cells as well as elevated levels of granzyme and perforin.

[1]Pathology of the Research Center Borstel, Leibniz Lung Center, Borstel, Germany. [2]Pathology of the University Hospital Schleswig-Holstein, Campus Luebeck, Luebeck, Germany. [3]Department of Otorhinolaryngology, University Hospital Schleswig-Holstein, Luebeck, Germany. [4]Department of Otorhinolarygology – Head and Neck Surgery, Baylor College of Medicine, Houston, USA. [5]These authors contributed equally: Rosemarie Krupar and Christian Watermann. ✉e-mail: rkrupar@fz-borstel.de

II. Tumors with a predominantly pro-tumor TIME, characterized by few infiltrating lymphocytes and a high number of infiltrating myeloid cells, in particular M2 macrophages and myeloid derived suppressor cells (MDSC).

III. Tumors with an immune-absent TIME, characterized by an overall absence of tumor infiltrating leukocytes.

Factors regulating the TIME composition are not understood in a detailed fashion. The attraction of tumor infiltrating myeloid cells is considered to depend on the production of chemokines such as VEGF, GM-CSF and TGF-β by tumor immune and stromal cells[5]. The amount of tumor infiltrating CD8 CTLs and their cytolytic activity, in contrast, is primarily influenced by the immunogenicity of the tumor. Tumor cells express antigens, which can induce a targeted anti-tumor immune response, when presented to T cells via major histocompatibility complexes (MHC) by antigen presenting cells (APC). Several mechanisms can lead to the formation of tumor antigens. One mechanism is the expression of germ-line genes ("cancer-testis antigens"). In healthy persons these are only expressed by male germ line cells and are usually not presented by MHC to induce T cell tolerance during thymic maturation. Another source of tumor antigens are oncogenic viruses, such as Human Papilloma Virus (HPV) or Epstein-Barr Virus (EBV), which can encode antigenic peptides. Over the last years tumor mutations (mostly non-synonymous point mutations) have been brought into focus as another source of tumor antigens. These lead to modified peptide sequences ("mutational neoantigens"), which can induce a T cell response, when presented by MHC[6]. The amount of non-synonymous mutations (tumor mutational burden/TMB) has been shown to correlate with anti-tumor immunity, outcome and response to treatment with immune checkpoint inhibitors[4,7]. Further investigations have elaborated the role of a functional antigen presenting machinery, to make optimal use of the TMB for an anti-tumor immune response[8]. Tobacco- and alcohol-induced squamous cell carcinomas of the head and neck, the esophagus and the lung are among the cancers with a high mutational load[9]. A high TMB and high CD8 CTL infiltrates predict particularly in head and neck squamous cell carcinoma (HNSCC) a benefit from PDL-1 inhibitor treatment[10]. In this study we aimed to discover specific mutations associated with specific TIME profiles and therefore constituting predictors for response to immune checkpoint inhibition or as potential adjuncts to improve efficacy of current immunotherapeutic agents.

Materials and Methods

The Cancer Genome Atlas (TCGA) database analysis. TCGA data bank analysis was performed on the cBioPortal for Cancer Genomics website (http://www.cbioportal.org) with access to clinical data, gene mutations and gene expression levels. All analyses were based on TCGA data provided by cBioPortal until December 2018. HPV status were deduced from a previous extensive characterization of the TCGA database by Rooney et *al.*[4].

Characterization of tumor immune microenvironment (TIME) types. Molecular TIME types were defined according to mean expression levels of transcriptomic cell markers (z-Score = 0), as outlined in Fig. 1A. Genes used for transcriptomic cell type markers were selected from the TCGA database study by Rooney et *al.*[4]. A focus was put on genes with established immunohistochemical markers in diagnostic pathology work-up (CD45, CD8A, FOXP3, CD79A, CD68, Granzyme, Perforin). Based on an additional study, S100A9 was included as a gene expression marker for myeloid derived suppressor cells[11]. Correlation of molecular TIME types with histological tumor appearances was performed using the digital slide archive (DSA, https://cancer.digitalslidearchive.org), which provides scanned Hematoxilin- and Eosin- (H&E-) stained tumor tissue slides of the TCGA cohorts[12]. One board-certified pathologist (R. K.), experienced in head and neck pathology, performed slide evaluations. The following criteria were applied to assign the histological tumor slides to the 3 TIME types:

- Immune-activated: Rich lymphoplasmocytic infiltrate in the desmoplastic peritumoral stroma and at least occasional presence of tumor infiltrating lymphocytes (TILs)
- Immune-suppressed: Presence of neutrophils, eosinophils, macrophages or mast cells in the desmoplastic peritumoral stroma and at least occasional presence of tumor infiltrating neutrophils, eosinophils, macrophages or mast cells
- Immune-absent: Few immunocytes in the desmoplastic peritumoral stroma and mostly absence of tumor infiltrating immunocytes.

Cytolytic activity was used as a measurement of anti-tumor immune response. Analogous to Rooney *et al.* cytolytic activity was based on simultaneous upregulation of GZMB (granzyme) and PFN1 (perforin) according to mean gene expression levels (z-Score = 0). EP300 upregulation was determined according to mean EP300 expression with a z-Score = 1.

The tumor immune subtypes C1- C6 were downloaded from the Supplementary Files of the publication by Thorsson *et al.* for further correlations[13].

Annotation of mean total mutation count and specific non-synonymous gene mutations in the TCGA database. The total number of non-synonymous gene mutations per HNSCC patient were accessed via cBioPortal, in order to compare the mean total mutation count in different TIME types. In the next step, only genes with a mutation frequency of at least 10x in the HNSCC TCGA cohort were selected for further analysis. This represents a mutation frequency of 1.95% and could include several non-synonymous mutations in one gene of one patient as well as one mutation in one gene of several different patients.

Metabolic characterization of the TCGA database. Metabolic characterizations of tumors were executed via analyses of gene expression levels involved in energy metabolism. The Glucose Metabolism RT[2] Profiler PCR array and the Mitochondrial Energy Metabolism RT[2] Profiler PCR array by Qiagen (Hilden, Germany) served as configuration standards to compile lists of relevant genes for metabolism studies. Based on genes represented in these arrays a glycolysis-dependent and an oxidative phosphorylation- (OXPHOS-) dependent tumor

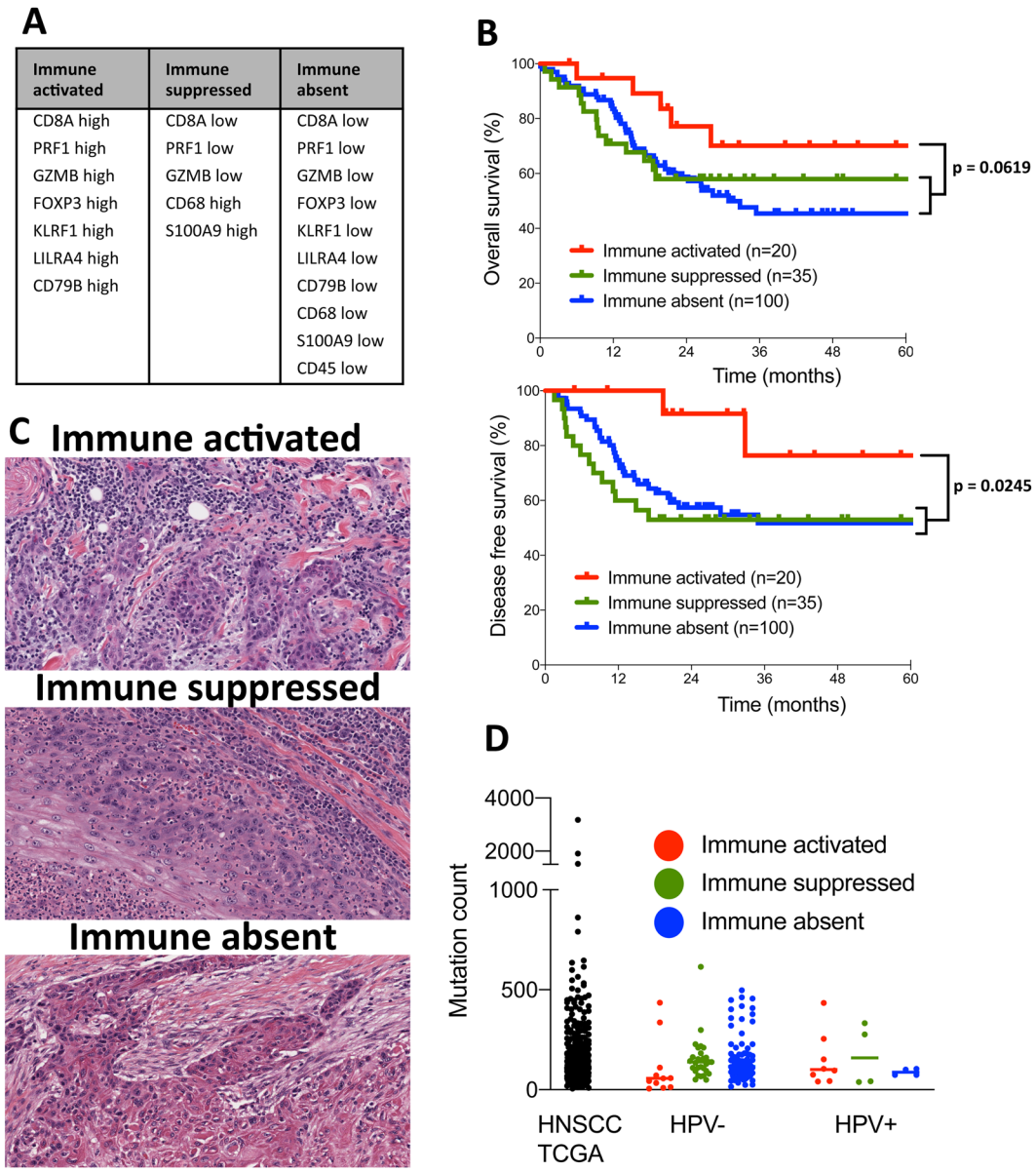

Figure 1. Gene expression-based tumor immune microenvironment (TIME) subtypes in HNSCC are clinically relevant and reflect histological phenotypes, but do not correlate with tumor mutational burden. (**A**) List of genes defining different TIME subtypes. (**B**) Patient subgroups with immune-activated, immune-suppressed and immune-absent TIMEs with best overall and disease free survival for immune-activated TIME patients. (**C**) Histological pictures of one representative immune-activated tumor with strong lymphocytic immune cell infiltrate (patient TCGA-CV-A468), one immune-suppressed tumor with a background of eosinophils and neutrophils (patient TCGA-BA-A6DA) and one immune-absent tumor without any immunocytes (patient TCGA-CN-5376). (**D**) Non-synonymous mutation counts for all HNSCC TCGA patients and for the three TIME subtypes subdived by HPV status with no signficant differenes between the groups.

metabolism were defined (z-Score = 0). Based on our own previous studies the glucose transporter 1 (GLUT1) as well as lactate dehydrogenase A and B (LDHA, LDHB) were added to the glycolysis-dominant gene list[14,15].

In summary the glycolysis-dominant list consisted of 24 enzymes and transporters involved in glucose and pyruvate/lactate metabolism: ALDOA, ALDOB, ALDOC, BPGM, ENO1, ENO2, ENO3, GALM, GCK, GPI, HK2, HK3, PFKL, PGAM2, PGK1, PGK2, PGM1, PGM2, PGM3, PKLR, TPI1, GLUT1, LDHA, LDHB.

The OXPHOS-dominant list was composed of 31 mitochondrial proteins necessary for the formation of complex I – V of the respiratory chain: ATP12A, ATP5A1, ATP5F1, ATP5G3, ATP5J, ATP5O, ATP6V1C2, LHPP, OXA1L, PPA1, COX4I1, COX5B, COX6B1, COX7A2, COX8A, BCS1L, UQCRC1, UQCRH, SDHA, SDHC, NDUFA1, NDUFA2, NDUFA5, NDUFA8, NDUFB2, NDUFB5, NDUFB8, NDUFC2, NDUFS3, NDUFS6, NDUFV1.

The Visualization of metabolic tumor phenotypes was achieved by the word cloud generator www.wortwolken.com.

Metabolic characterization of cell lines after EP300 inhibition. The L1000 Connectivity Map data (L1000 CMap), provided by the Broad Institute, was used to study the effects of EP300 inhibition on cell metabolism in different cell lines[16]. The analyses were performed with Genevestigator (Nebion AG, Zurich, Switzerland). The following experiments of the L1000 CMap were included into the study: 1. Controls: Cell lines treated with DMSO for 24 hours (10 replicates for each cell line). 2. Cell lines treated with 10 μM C646 for 24 hours (3–6 replicates for each cell line). Matched data was available for 8 different cell lines (A375, A549, HA1E, HCC515, HEPG2, HT29, MCF7, PC3). EP300 mutation and baseline expression status was extracted from cBioPortal. The glycolysis-dominant list of genes was expanded by an addition of 30 glycolysis genes provided by Genevestigator. This led to a total of 52 genes with available L1000 CMap gene expression data to characterize a glycolysis-associated metabolism. 112 OXPHOS-related genes provided by Genevestigator were added to the OXPHOS-dominant gene list yielding a total of 116 genes with available gene expression data.

Statistical analysis. Disease free and overall survival of different TIME types were calculated by Kaplan-Meyer method and Wilcoxon test for statistical significances. Fisher's exact test was applied to compare gene mutation frequencies between different TIME groups. Additionally, the distribution of cases with upregulated and downregulated anti-tumor immunity in *EP300* mutated and *EP300* wildtype tumors were tested for statistical significance by Fisher's exact test. Upregulation frequency of each metabolic gene in EP300 high and low tumors was also compared by Fisher's exact test. Unpaired two-tailed t-test was used to compare means of all upregulated genes of one metabolic phenotype in the panCancer analyses. The metabolic phenotype of cell lines after C646 treatment was compared by paired t-test. P values less than 0.05 were considered statistically significant. Statistical analyses and graph creations were performed with Prism 8 (GraphPad, San Diego, CA).

Précis. The lysine-acetyltransferase EP300 inhibits anti-tumor immune response via modulation of tumor metabolism and might therefore represent a new target for combinatory immuno-therapeutic approaches.

Results

Tumor immune microenvironment subtypes in head and neck squamous cell carcinomas are associated with specific gene mutations. First, we aimed to identify gene mutations associated with different TIME subtypes within the HNSCC cohort of the TCGA database. At the time of the computational analyses (last updated 12/2018) the TCGA HNSCC cohort consisted of 530 patients with available clinical, proteomic and genomic data. We started the evaluation with the creation of three TIME subtypes based on gene expression profiles of immune-related genes as outlined in Fig. 1A:

1. An immune-activated TIME with high expressions of genes involved in cytotoxic T cell response.
2. An immune-suppressed TIME with low expression of genes involved in cytotoxic T cell response and high expression of the macrophage defining gene CD68 and S100A9, a gene with good specificity for myeloid derived suppressor cells[11].
3. An immune-absent TIME with downregulation of all immune-related genes used for subtype stratification.

Patients with upregulation or downregulation of genes as outlined in Fig. 1A (z-Score = 0) were included into the respective TIME subtypes. In summary, this yielded 20 patients for the immune-activated group, 35 patients for the immune-suppressed group and 100 patients for the immune-absent group. The remaining 375 patients of the TCGA HNSCC cohort were excluded from further analyses, as they did not consistently fit into one of the immune gene profiles of Fig. 1A. In order to ensure clinical relevance of the gene expression-based TIME classification, we tested its impact on overall and disease free survival of the three groups (Fig. 1B). This resulted in a well-defined segmentation with best overall ($p = 0.0619$) and disease free ($p = 0.0245$) survival for the immune-activated group compared to the combination of the immune-suppressed and immune-absent group. A further comparison of clinical and tumor characteristics for the three different TIME types and the complete TCGA cohort is summarized in Table 1. The TCGA HNSCC cohort contained significantly more patients with immune-absent TIME than with immune-activated TIME (100 versus 20). The number of HPV-positive patients was significantly higher in the immune-activated group as in the other groups (45% versus 15% in the immune-suppressed and 6% in the immune absent group). Correspondingly, the immune-activated group also contained significantly more oropharyngeal squamous cell carcinomas. Furthermore patients of the immune-activated group had a lower average number of cigarette pack years. These findings of the immune-activated group reflect to a large extent the features of HPV-induced HNSCC, which are typically located in the oropharynx, frequently show a strong anti-tumor immune infiltrate and are not necessarily associated with a history of tobacco abuse[14,17]. Regarding tumor stage patients with stage IV tumors accumulated in the immune-suppressed group (75% of immune suppressed tumors versus 48% of immune-absent tumors). We also evaluated the scanned tumor tissue slides, as provided by cBioPortal and the Digital Slide Archive (DSA, www. https://cancer.digitalslidearchive.org), for histological representativeness of each TIME subset. Overall the molecular TIME types were well reflected by their histological appearances (Fig. 1C). The histological appearances matched for 18 of 20 tumors in the immune-activated group (1 tumor had an immune-absent histological appearance, 1 tumor was not evaluable). 20 of 35 tumors had matching histological appearances in the immune-suppressed group (7 tumors had an immune-activated histological appearance, 5 tumors an immune-absent histological appearance, 3 tumors were not evaluable). The immune absent group showed matching histological appearances in 46 of 100 cases (47 tumors of this group demonstrated an immune-suppressed histological appearance, 5 tumors an immune-activated histological appearance, 2 tumors were not evaluable).

	TCGA HNSCC	Immune activated	Immune suppressed	Immune absent	
Number	530	**20 (4%)**	35 (7%)	**100 (19%)**	**p < 0.0001**
Mean age (y)	60.9	58.55	60.2	61.5	ns
Male sex	386 (73%)	18 (90%)	28 (80%)	81 (81%)	ns
HPV positive	**77 (15%)**	**9 (45%)**	**5 (14%)**	**6 (6%)**	**p < 0.03**
Anatomical site					
Oropharynx	**82 (16%)**	**12 (60%)**	**4 (11%)**	**8 (8%)**	**p < 0.0001**
Oral cavity	**320 (60%)**	**7 (35%)**	20 (57%)	**62 (62%)**	**p < 0.05**
Hypopharynx	10 (2%)	0	2 (5.7%)	1 (1%)	ns
Larynx	117 (22%)	**1 (5%)**	9 (26%)	**29 (29%)**	**p < 0.03**
Stage					
I	21 (4%)	3 (15%)	1 (3%)	4 (4%)	ns
II	**99 (19%)**	2 (10%)	**2 (6%)**	20 (20%)	**p < 0.05**
III	107 (21%)	4 (20%)	5 (16%)	26 (26%)	ns
IV	288 (56%)	11 (55%)	**24 (75%)**	**48 (48%)**	**p < 0.05**
Differentiation					
G1	64 (13%)	0 (0%)	2 (6%)	9 (9%)	ns
G2	311 (61%)	9 (53%)	21 (64%)	63 (64%)	ns
G3	125 (25%)	7 (41%)	10 (30%)	25 (26%)	ns
G4	7 (1%)	1 (6%)	0 (0%)	1 (1%)	ns
Social history					
Smoking (pack years)	46 (n = 299)	**27 (n = 9)**	**50 (n = 18)**	**48 (n = 61)**	**p < 0.03**
Drinks/day	3.2 (n = 222)	2.8 (n = 8)	3.8 (n = 11)	3.6 (n = 45)	ns
Recurrence/Progression	145 (36%, n = 398)	3 (21%, n = 14)	14 (47%, n = 30)	32 (42%, n = 77)	ns

Table 1. Patient and tumor characteristics of the complete TCGA HNSCC cohort and the three different TIME subtypes (signifcant differences compared to underlined values are marked with bold type). ns = not significant.

Next, we investigated, if there were differences between the tumor mutational burden of the complete TCGA HNSCC cohort and the different TIME subtypes. The overall number of non-synonymous mutations was, however, very heterogeneous and did not significantly differ between the TIME subtypes. Consideration of HPV status did also not significantly affect the mutational count distribution (Fig. 1D).

Afterwards, we wanted to find out, if the different TIME subtypes accumulate distinct mutations. For this purpose, a list of mutated genes within the HNSCC cohort was compiled. This included only non-synonymous mutations as annotated by cBioPortal. At least 10 mutations had to be annotated for one gene across 512 profiled HNSCC samples to be included into the gene list. This represents a mutation frequency of 1.95%, to ensure feasibility of statistical work-up and clinical relevance. A total of 1519 mutated genes were included into the analysis. *TP53* had the highest mutational load with 446 mutations (mutation frequency 71.48%), followed by *TTN a*nd *FAT1 w*ith 379 (mutation frequency 41.60%) and 144 (mutation frequency 22.46%) mutations, respectively. Next, the list of 1529 mutated genes was used for a patient database query among the three different TIME subtypes (Fig. 2). Since HPV-positive HNSCC are considered a distinct molecular HNSCC entity, gene mutations were correlated for all HNSCC patients as well as for the subsets of HPV-positive and HPV-negative patients. A total of 9 and 11 mutated genes were significantly associated with one specific TIME subtype for all HNSCC and the subset of HPV-negative HNSCC, respectively. In HPV-positive HNSCC, 8 mutated genes tended to associate with specific TIME subtypes. Only 2 genes (*TP53 a*nd *TTN*), however, were found to be significantly enriched in one TIME subtype. In general, most genes were significantly associated with an immune-activated TIME, except for *TP53* mutations. Mutated *TP53* strongly correlated with an immune-absent TIME in all HNSCC subsets. This serves as a good internal control, as *TP53* mutations are known to inhibit anti-tumor immune response[18,19]. Another mutated gene, which was significantly associated with an immune-suppressed TIME in all HNSCC as well as in HPV-positive HNSCC, was *FBXW7*. Additional gene mutations with tendencies towards an immune-suppressed TIME in the HPV-positive subset were M*AP3K13*, *MYO9A* and *NBPF1*. *EP300* was together with *TP53* the only mutated gene, which was associated with one TIME subtype across all HNSCC, HPV-negative HNSCC and HPV–positive HNSCC. Its mutational status correlated with an immune-activated TIME. *EP300* is a lysine acetyltransferase similar to CREB binding protein (CBP) serving as a cofactor for the expression of numerous genes. Hence, it regulates many different processes including proliferation, cell cycle, cell differentiation and DNA damage response[20].

***In silico* analyses suggest lysine acetyltransferase EP300 as a panCancer modulator of anti-tumor immune response.** Based on the association of *EP300* mutations with an immune-activated TIME in HNSCC, we consequently, wondered, if we could confirm this in other tumor types. Most of the common solid malignancies of the TCGA database were included for the analysis: Esophageal adeno- and squamous cell carcinoma, lung adeno- and squamous cell carcinoma, breast carcinoma, gastric adenocarcinoma, cholangiocellular adenocarcinoma, pancreatic adenocarcinoma, hepatocellular carcinoma, colorectal adenocarcinoma,

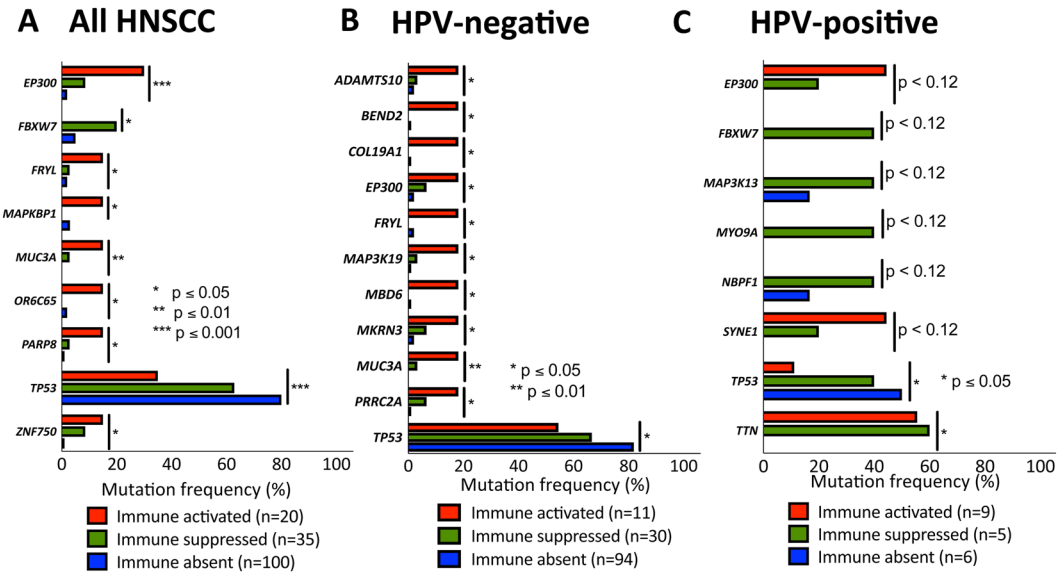

Figure 2. Correlation of gene mutation frequencies with TIME subtypes revealing EP300 mutation as significantly associated with an immune-activated TIME: Significant association of gene mutation frequencies with specific TIME subtypes for 9 genes of all HNSCC (**A**), 11 genes of HPV-negative HNSCC (**B**) and 8 genes of HPV-positive HNSCC. Mutations in *TP53* and *EP300* are found in all three groups.

renal clear cell carcinoma, adrenal carcinoma, bladder carcinoma, prostate adenocarcinoma, endometrial carcinoma, cervical carcinoma, melanoma. The analysis included a total of 7564 patients with an overall *EP300* mutation prevalence of 3.1% (277 patients). The highest mutation frequency was found in HPV-associated carcinomas (15.4% of HPV-positive HNSCCs and 11.8% of uterine cervical carcinomas). Lung adenocarcinomas, breast carcinomas and prostate carcinomas had the lowest mutation frequency with 0.3%, 1.1% and 1.2%, respectively (Fig. 3A). Next, we compared the anti-tumor immunity with the mutational status of *EP300*. We used gene expression profiles of the pore-forming and proteolytic proteins perforin (PFN1) and granzyme (GZMB), to define the anti-tumor immune response. The simultaneous upregulation of PFN1 and GZMB, which are secreted by CD8 + CTLs, has been defined as cytolytic activity by Rooney *et al.* and has been shown to correlate with neoantigen load[4]. We defined tumors with simultaneous upregulation of PRF1 and GZMB (CytAct Up, z-Score = 0) as tumors with increased anti-tumor immunity. Tumors with a simultaneous downregulation of PRF1 and GZMB (CytAct Down) were defined as tumors with downregulated anti-tumor immunity. Besides HNSCC, upregulation of cytolytic activity significantly correlated with *EP300* mutation in esophageal squamous cell carcinomas, gastric carcinomas and prostate carcinomas (Fig. 3A).

Since we hypothesized that mutation-associated functional limitations of *EP300* lead to an immune-activated TIME, we wondered, how EP300 expression correlates with anti-tumor immune response. We divided patients of all 18 solid malignancies in EP300 low and high expressers according to a z-Score = 1. This yielded a total of 916 patients with downregulated EP300 and 1181 patients with upregulated EP300. Assessing all tumor entities separately, EP300 downregulation was strongly associated with increased cytolytic activity in almost all cancer entities, except for carcinomas of the breast (Fig. 3A).

We also correlated EP300 expression with the recently described tumor immune profiles by Thorsson *et al.*[13]. These are based on TCGA data of more than 10000 tumors and stratify tumors into six different subtypes: C1 (wound-healing), C2 (Interferon-γ dominant), C3 (inflammatory), C4 (lymphocyte-depleted), C5 (immunologically quiet), C6 (TGF-β dominant). Immune subtype C2 is characterized by the highest M1/M2 macrophage polarization and the highest CD8 count. Consistent with our analyses, *EP300* mutated tumors and tumors with decreased EP300 expression showed significantly more frequently a C2 immune subtype (Suppl. Fig. 1). The C3 immune subtype, in contrast, was more frequently present in *EP300* wildtype tumors and tumors with high EP300 expression. The C3 subtype is defined by elevated Th1 and Th17 genes.

Overall distribution of *EP300* mutations within the TCGA panCancer cohort correlated with results of previous studies[20]. The histone acetyltransferase domain KAT carried the most mutations with a total of 62 non-synonymous mutations (22.2% of all *EP300* mutations). The other functional domains had low mutation frequencies ranging from 8 in the TAZ1 domain (transcriptional adapter zinc finger 1, 2.9% of all *EP300* mutations) to 15 in the BR-PHD domain (bromodomain-plant homeodomain, 5.5% of all *EP300* mutations, Fig. 3C). In contrast, the highest frequency of *EP300* mutations, which also had an upregulated cytolytic activity in the tumor, were observed in the TAZ1 domain (37.5%, n = 3) and the interferon binding domain IBID (33.3%, n = 3, Fig. 3D). On the other hand, KAT domain mutations associated with increased cytolytic activity were only found 17% of cases (n = 4).

EP300 overexpression is associated with a glycolytic tumor metabolism. The association of EP300 expression with decreased anti-tumor immunity raises the question about a functional mechanism of

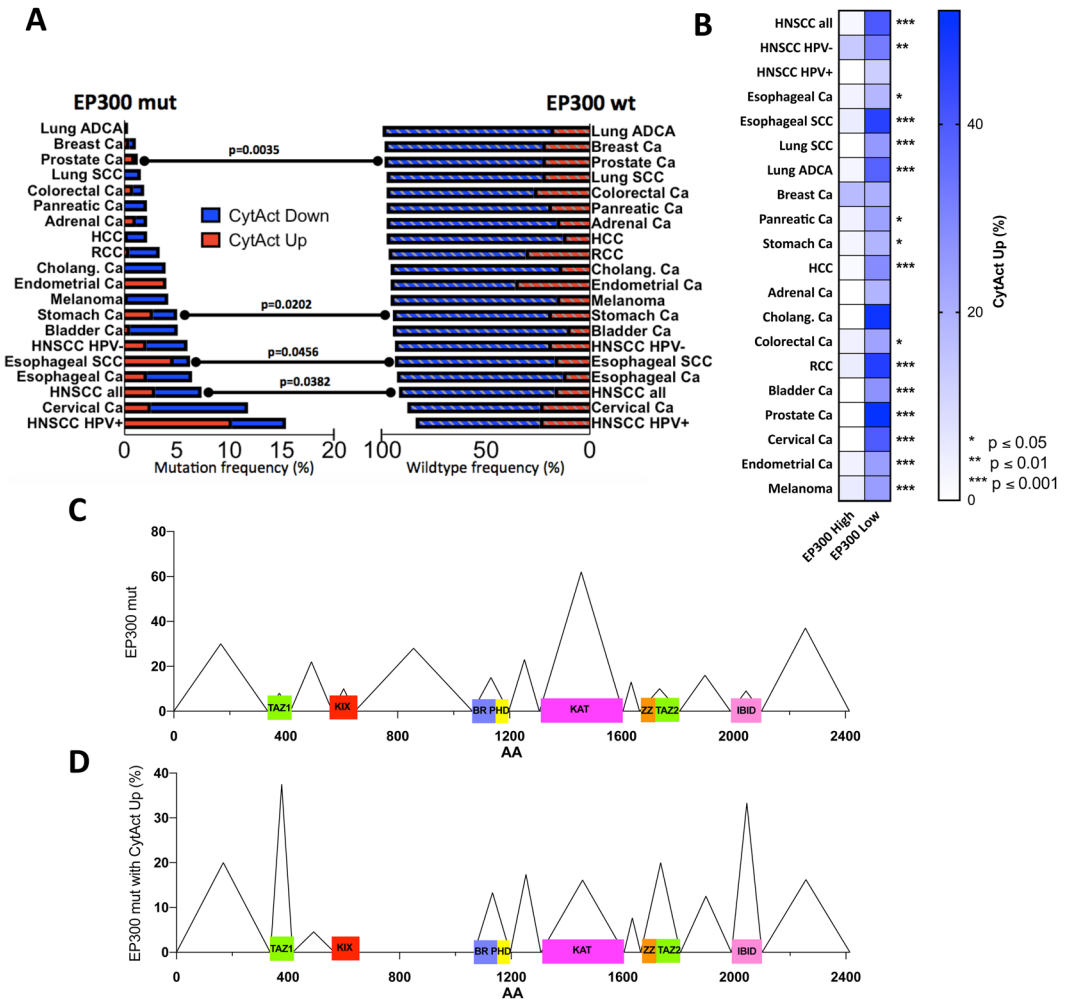

Figure 3. PanCancer correlation of EP300 mutation and expression status with anti-tumor immunity. (**A**) Display of *EP300* mutation frequency for 18 common solid malignancies (n = 7564) and association with cytolytic activity in comparison to *EP300* wt tumors. HNSCCs, esophageal SCC, stomach carcinomas and prostate carcinomas have a significantly higher cytolytic activity in *EP300* mut tumors. (**B**) PanCancer correlation of EP300 expression status with anti-tumor immunity for 18 solid malignancies showing a significantly higher cytolytic activity in in EP300 low tumors. (**C**) PanCancer distribution of *EP300* mutations with most mutations at the lysine acetyltransferase domaine KAT. (**D**) Percentage of *EP300* mutations with increased cytolytic activity relative to all mutations with spiking mutation counts at TAZ1 and IBID. Mut: mutated; wt: wildtype; CytAct: cytolytic activity; ADCA: adenocarcinoma; Ca: carcinoma; SCC: squamous cell carcinoma; HCC: hepatocellular carcinoma; RCC: renal clear cell carcioma; cholang: cholangiocellular; TAZ: Transcriptional adapter zinc finger; KIX: kinase inducible domain of CREB interacting domain; BR: Bromodomain; PHD: Plant homeodomain; IBID: Interferon binding domaine.

EP300 inhibiting the tumor immune response. We and others have previously shown that tumor metabolism is an important determinant of the tumor immune microenvironment[14,15,21]. Namely a glycolytic tumor metabolism with accumulation of lactate in the tumor microenvironment leads to an inhibition of cytotoxic T cells and to an unfavorable TIME. On the other hand, an oxidative phosphorylation- (OXPHOS-) dominant tumor metabolism supports a strong anti-tumor immune response. Just recently the metabolism-modulatory functions of EP300 have been described in more detail. Among others, these studies revealed EP300's role in promoting genes involved in glycolysis and demonstrated that EP300 inhibition leads to a disruption of glucose metabolism[22,23]. Consequently, we hypothesized that EP300 upregulation is associated with a glycolysis-dominant tumor metabolism, whereas EP300 downregulation correlates with an OXPHOS-dominant tumor metabolism.

First, we compiled lists of metabolic genes defining a glycolysis-dominant or OXPHOS-dominant metabolism. These genes were based on the publicly available collections of the glucose and OXPHOS metabolism RT[2] Profiler PCR Array, as provided by Qiagen (Hilden, Germany).

Next, we performed a panCancer metabolic characterization including all 18 solid malignancies mentioned in the study. Tumors were distinguished according to EP300 expression into EP300 high (n = 915) and EP300 low (n = 1181) tumors. Upregulation frequency (z-Score = 0) of all metabolic genes in both groups were calculated (Fig. 4A). 14 of 24 glycolysis-associated genes were significantly upregulated in EP300 low tumors, while 4 of

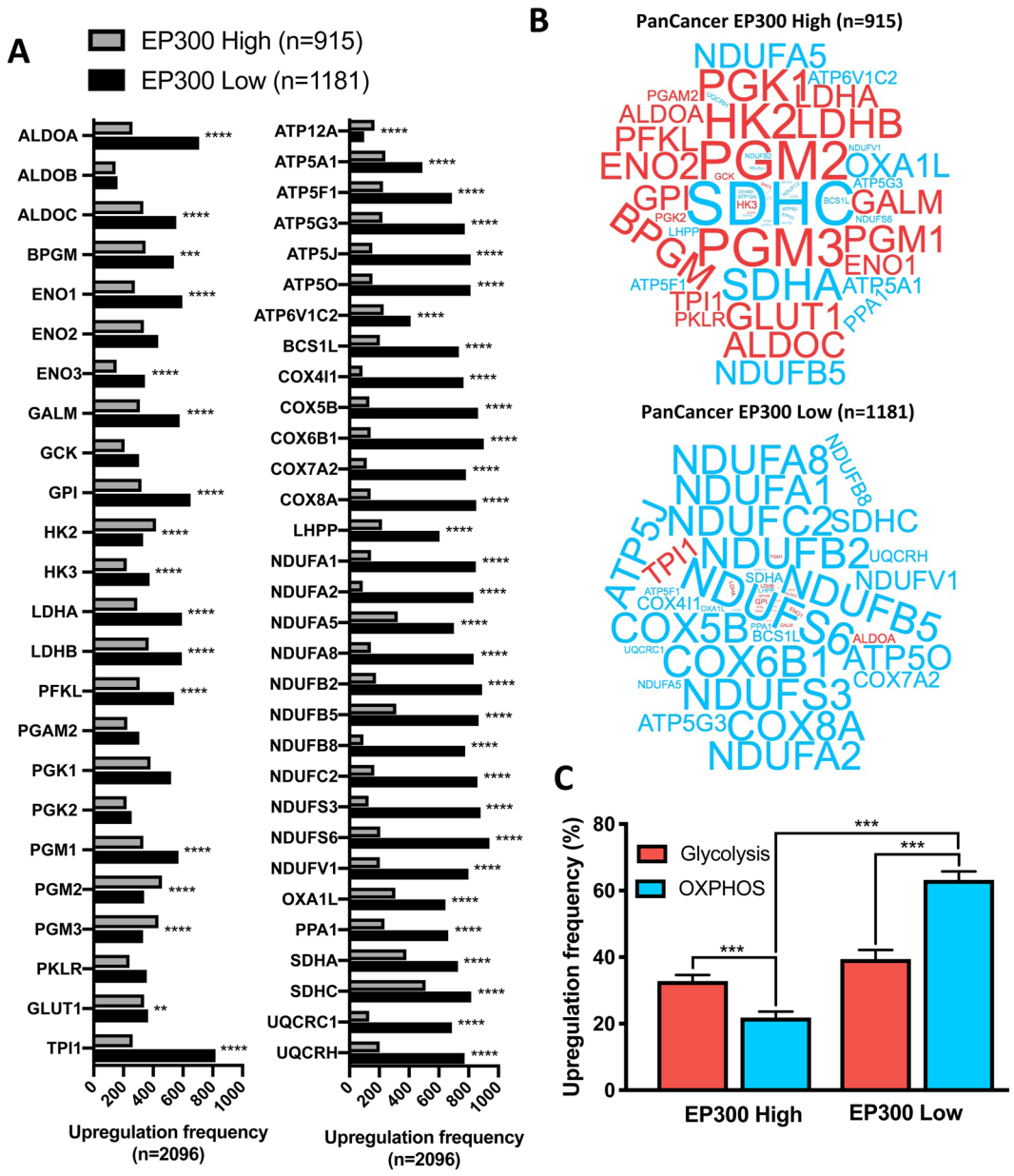

Figure 4. PanCancer analyses of metabolic phenotypes in relationship to EP300 expression: (**A**) Absolute upregulation frequency of 24 genes involved in glycolysis and 31 genes invovled in OXPHOS with significant upregulation of all OXPHOS genes, except for ATP12A in EP300 low tumors and significant downregulation of 14 glycolysis genes in EP300 low tumors. (**B**) PanCancer expression of metabolic genes (red: 24 genes involved in glycolysis; blue: 31 genes involved in OXPHOS) with predominance of glycolytic genes in EP300 high tumors and predominace of OXPHOS-associated genes in EP300 low tumors. Font size is relative to upregulation frequency. (**C**) Relative upregulation frequency of glycoyltic and OXPHOS-associated genes with a dominantly glycolysis-dependent metabolism in EP300 high tumors and an OXPHOS-dependent metabolism in EP300 low tumors. ** $p < 0.01$, ***$p < 0.0001$.

24 glycolysis-associated genes were downregulated. All OXPHOS-related genes were significantly upregulated in EP300 low tumors, except for ATP12A. Comparing the two tumor metabolism types, EP300 high tumors were dominated by an upregulation of glycolysis-associated genes, while in EP300 low tumors OXPHOS-related genes dominated (Fig. 4B). Assessing the mean upregulation frequency for all glycolysis-associated and OXPHOS-associated genes EP300 low and EP300 high tumors were significantly different with a predominantly OXPHOS-dependent metabolism for EP300 low tumors (Fig. 4C).

We also performed a panCancer comparison of the tumor metabolism in *EP300* wildtype (n = 4694) and *EP300* mutated (n = 233) tumors (Suppl. Fig. 2). Differences were only subtle, however glycolysis-related as well as OXPHOS-related genes were significantly more frequently upregulated in *EP300* mutated tumors.

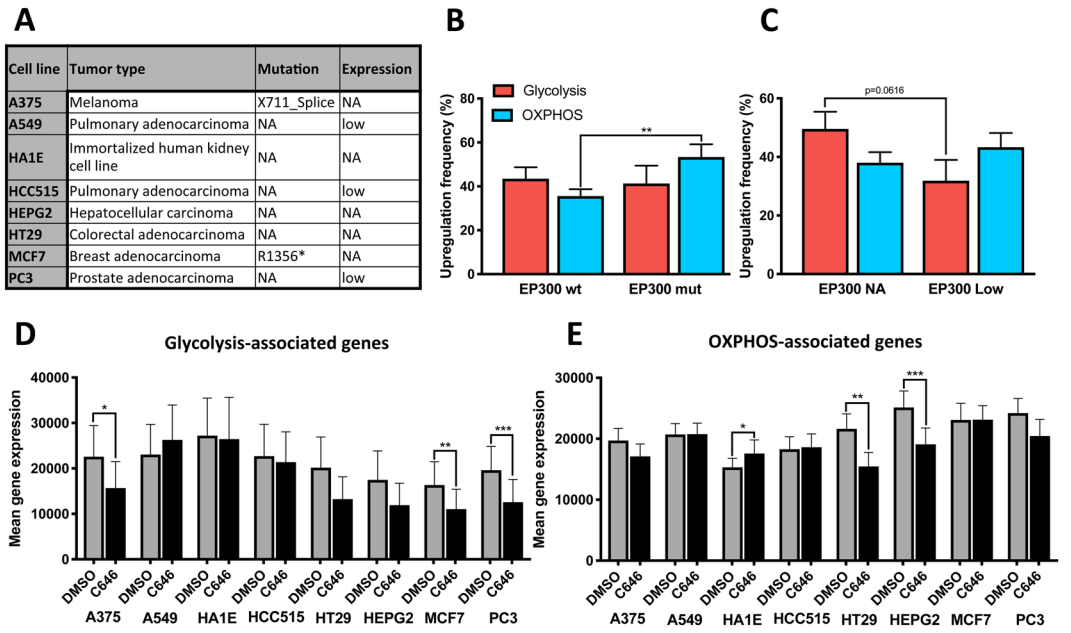

Cell line	Tumor type	Mutation	Expression
A375	Melanoma	X711_Splice	NA
A549	Pulmonary adenocarcinoma	NA	low
HA1E	Immortalized human kidney cell line	NA	NA
HCC515	Pulmonary adenocarcinoma	NA	low
HEPG2	Hepatocellular carcinoma	NA	NA
HT29	Colorectal adenocarcinoma	NA	NA
MCF7	Breast adenocarcinoma	R1356*	NA
PC3	Prostate adenocarcinoma	NA	low

Figure 5. Metabolic effects of EP300 inhibition on eight cell lines via *in silico* analysis. (**A**) List of cell lines with EP300 mutation and expression status (z Score = 1). (**B,C**) Baseline metabolic characterization with signifcant upregulation of genes involved in OXPHOS in cell lines with EP300 mutation (A375, MCF7) and trends towards a decrease of genes involved in glycolysis in cell lines with low EP300 expression (A549, HCC515, PC3). (**D–E**) Changes of mean gene expression levels after treatment with the EP300 inhibitor C646 with a significant downregulation of glycolysis-associated genes (mean expression level of 52 genes) in A375, MCF7 and PC3 as well as a significant downregulation of OXPHOS-associated genes (mean expression level of 112 genes) in HT29 and HEPG2. In HAE1E OXPHOS genes significantly increased after C646 treatment. NA: No alteration; wt: wildtype; mut: mutated. *$p < 0.05$, **$p < 0.01$, ***$p < 0.001$.

***In silico* modeling demonstrates decreased glycolytic metabolism in cell lines after EP300 inhibition.** Since our previous results suggested an association of EP300 expression with a glycolytic tumor metabolism, we wondered, if EP300 inhibition leads to changes in cell metabolism. The publicly available Connectivity Map (CMap) at the Broad Institute was used to investigate the effect of EP300 inhibition on gene expression profiles of different cell lines[16]. This database includes perturbations with the small molecule C646, a widely used and specific inhibitor of EP300[24].

First we assessed the EP300 mutation and expression status (z-Score = 1) of the eight cell lines, analyzed by CMap (Fig. 5A). These include the Melanoma cell line A375 and the breast adenocarcinoma cell line MCF7 with *EP300* mutations (X711_Splice and R1356*, respectively). Furthermore it includes two pulmonary adenocarcinoma cell lines A549 and HCC515 as well as one prostate carcinoma cell line (PC3) with relative downregulation of EP300 expression. Additionally, the hepatocellular carcinoma cell line (HEPG2), the colorectal adenocarcinoma cell line (HT29) and the immortalized human kidney cell line HA1E were included, which have no alterations in EP300. Upregulation of EP300 was not observed in any cell line. Metabolic characterization of the eight cell lines showed a significant upregulation of OXPHOS-associated genes for the two cell lines (A375 and MCF7) with *EP300* mutations (Fig. 5B). On the other hand, glycolysis-associated genes tended to be downregulated in the two cell lines (A549 and HCC515) with decreased EP300 expression (Fig. 5C). Next we investigated changes in cell metabolism after treatment with the EP300 inhibitor C646. 3 of 8 cell lines (A375, MCF7 and PC3) had a significantly downregulated glycolysis-associated metabolism after C646 treatment in comparison to DMSO incubation (Fig. 5D). Two additional cell lines, HT29 and HEPG2, tended to a decreased glycolytic metabolism after C646 treatment. Additionally, OXPHOS-related metabolism was significantly downregulated in HT29 and HEPG2, whereas it significantly increased in HA1E after C646 exposure.

Discussion

Over the last years the TIME of HNSCC and other solid malignancies has been extensively studied elaborating tumors with favorable, anti-tumor or unfavorable, pro-tumor immune microenvironments[4,15,25–28]. We are, however, far away from a detailed understanding of the TIME and how we can further exploit it for best therapeutic effects. In HNSCC, for example, overall response rate to immune checkpoint inhibition is only 20%[29]. Detection of PD-L1 expression in the tumor via immunohistochemistry is currently the most widely used biomarker to determine eligibility for treatment with the PD-1 inhibitor Pembrolizumab[30]. It is approved by the FDA for 15 different tumor types. In a recent meta-analysis, it was predictive in 28.9% of cases, whereas in 53.3% it was not predictive[30]. Analyses of microsatellite instability and the tumor mutational burden are other factors, which can be used to enrich for patients likely to respond to immunotherapy. Nevertheless, we only have a limited

understanding, which patient will benefit from immunotherapy and how we can expand the efficacy of checkpoint inhibition for patients with an immunotherapeutic ineligible TIME.

This study aimed to extend our knowledge on the association of the tumor genome and specific TIME types, in order to detect new biomarkers and therapeutic targets for immunotherapies. We started with HNSCC, as this is a tumor entity with a relatively high mutational burden. Additionally, the TIME of HNSCC is known to be associated with treatment response, but HNSCC often show a limited response to immunotherapeutic approaches[31,32]. In the first part of the study, we defined 3 different, clinically-relevant TIME subtypes in HNSCC based on immune-related gene expressions. In the next step we could connect about 8–11 altered genes (depending on the HPV status) to a specific TIME type. The association of TIME subtypes with mutated genes appeared to depend on the HPV status (HPV-positive or HPV-negative) of the tumor underlining the differences of these two distinct molecular entities. Furthermore, the diverging gene list between HPV-negative and HPV-positive HNSCC demonstrate that it is hardly possible to connect the HNSCC TIME subtypes to specific genetic alterations. It is rather a multifactorial combination of tumor genetic properties and host immune defense. Additionally, it is important to mention that we probably discovered only a limited number of genes with potential immune-oncological relevance. Our analysis approach included 155 of 530 patients of the HNSCC TCGA cohort, who fit into one of the immune subgroups. The strict definition of our immune subgroups prevented bigger cohorts for the screening approach. But this made it, on the other hand, more likely that genes with a significant association with one of the subgroups have a relevant connection to the TIME.

EP300 was besides *TP53*, the only mutated gene, which was associated with a specific TIME in HPV-negative as well as HPV-positive HNSCC. We therefore focused on EP300 for further analyses, as it has not drawn much attention to its role in tumor immune activity. EP300 is a lysine acetyltransferase similar to CREB-binding protein (CBP). It regulates the cell cycle as a transcriptional coactivator, e. g. of E2F, and via histone modification through acetylation. EP300 and CBP bind to more than 16000 genes in human cells leading to a wide range of functions in healthy and tumor tissue[33,34]. On the one hand, EP300 may have tumor suppressive functions by promoting other tumor suppressors as *TP53*, *RB1* or *BRCA1*[20]. On the other hand, EP300 overexpression has been described to be associated with poorer outcome and higher aggressiveness in several tumors including HNSCC and cutaneous squamous cell carcinomas, colorectal cancers and hepatocellular carcinoma[35–38]. It is, however, still unclear, how EP300 overexpression promotes aggressiveness of tumors. So far EP300 has rarely been associated with tumor immunity. Two studies elaborated the role of EP300 for regulatory T cell differentiation and function[39,40]. More importantly, Liu *et al.* showed that EP300 inhibition reduced tumor growth in wild type, but not immune-deficient mice and increased tumor infiltration as well as activity of cytotoxic T cells and decreased Tregs[40].

Our *in silico* analyses indicate a tumor promoting effect of EP300 via immunosuppression. Based on the pan-Cancer analyses of our study we were able to further dissect a potential functional background of EP300-related tumor immune suppression. We observed an immune-activated TIME in several *EP300* mutated as well as most EP300 downregulated tumors across many different solid malignancies. Evaluation of the location of *EP300* mutations associated with increased anti-tumor immunity demonstrated that there is no specific *EP300* mutation responsible for tumor immune-modulatory effects. Most *EP300* mutations are located in the histone modifying KAT domain. Focusing on *EP300* mutations with anti-tumor immunity association, we detected mutation spikes in the TAZ1 and IBID domain. While TAZ1 binds among others the transcriptional factor HIF1α, which is the key factor of tumor metabolism, IBID binds IRF-3, which is involved in innate immunity control[41]. This gives a first suggestion, that the TAZ1 and IBID domain might play functional roles in modulating the TIME.

Another exciting incidental finding of our study is the association of *EP300* mutations with HPV infection. Just recently an association of *EP300* mutations and intragenic *EP300* deletions were discovered for HPV-positive oropharyngeal squamous cell carcinomas in two independent studies[42,43]. The HPV proteins E2 and E7 have been described to bind to EP300[42,44–47]. Functional analyses suggest that EP300 is necessary to initiate E2 induced viral transcription and replication. Recruitment of EP300 together with retinoblastoma protein by E7 is suspected to be a key factor in retinoblastoma protein dependent disruption of the cell cycle control. At this point further assessments of the location of HPV-associated *EP300* mutations and functional *in vitro* studies would, however, be needed to explain the high *EP300* mutation frequency in HPV-related cancer.

Recent studies have shown that EP300 is a promoter of glycolysis and inhibition of EP300 leads to inhibition of glucose metabolism[22,23]. Tumor cell glucose metabolism, however, is known to exert inhibitory effects on T cell proliferation, tumor infiltration by T cells and T cell guided anti-tumor immune response[48]. In our panCancer metabolic studies we could demonstrate that tumors with high EP300 expression have a predominantly glycolysis-associated metabolism. Tumors with low EP300 expression, on the contrary, had an OXPHOS-dominated metabolism. *In silico* analyses of cell lines treated with the EP300 inhibitor C646 underlined this observation. We observed changes of metabolism-related genes in 6 of 8 cell lines after C646 treatment. Glycolysis-associated genes significantly decreased in 3 cell lines and tended to decrease in 3 additional cell lines. OXPHOS-associated genes decreased in 2 cell lines and increased in 1 cell line. Taken together, we see an inhibition of tumor cell metabolism in cell lines already after inhibition of EP300 for a short period of time (24 hours). Our cell line studies indicate that changes in the tumor metabolism could be the link between EP300 expression and tumor immune evasion.

We think that our results support testing the inclusion of EP300 inhibitors into immunotherapeutic approaches. By now there exist several EP300 and EP300/CBP specific inhibitors, which have shown promising tumor inhibiting effects *in vitro* and in preclinical studies[49–53]. The anti-tumor effects of the selective EP300 and CBP inhibitor CCSS1477 are currently investigated in a clinical trial of metastatic castration resistant prostate cancer and other advanced solid tumors (NCT03568656).

This *in silico* study allows the correlation of EP300 with different tumor characteristics over a large number of tumors and cancer entities. Thereby our results give exciting perspectives, how to expedite research focuses for

EP300 and how to integrate it into preclinical and clinical therapeutic approaches. Preclinical experiments investigating the effect of EP300 inhibition on the TIME, for example in syngeneic mouse models, would constitute a next step to assess EP300 as an immune-oncological target.

Received: 17 December 2019; Accepted: 18 May 2020;
Published online: 10 June 2020

References

1. Donnem, T. *et al*. Strategies for clinical implementation of TNM-Immunoscore in resected nonsmall-cell lung cancer. *Ann. Oncol. Off. J. Eur. Soc. Med. Oncol.* **27**, 225–232 (2016).
2. Turan, T. *et al*. Immune oncology, immune responsiveness and the theory of everything. *J. Immunother. Cancer* **6**, 50 (2018).
3. Bindea, G. *et al*. Spatiotemporal Dynamics of Intratumoral Immune Cells Reveal the Immune Landscape in Human Cancer. *Immunity* **39**, 782–795 (2013).
4. Rooney, M. S., Shukla, S. A., Wu, C. J., Getz, G. & Hacohen, N. Molecular and genetic properties of tumors associated with local immune cytolytic activity. *Cell* **160**, 48–61 (2015).
5. Chimal-Ramírez, G. K., Espinoza-Sánchez, N. A. & Fuentes-Pananá, E. M. Protumor Activities of the Immune Response: Insights in the Mechanisms of Immunological Shift, Oncotraining, and Oncopromotion. *J. Oncol.* **2013** (2013).
6. Blankenstein, T., Coulie, P. G., Gilboa, E. & Jaffee, E. M. The determinants of tumour immunogenicity. *Nat. Rev. Cancer* **12**, 307–313 (2012).
7. Goodman, A. M. *et al*. Tumor Mutational Burden as an Independent Predictor of Response to Immunotherapy in Diverse Cancers. *Mol. Cancer Ther.* **16**, 2598–2608 (2017).
8. Wang, S., He, Z., Wang, X., Li, H. & Liu, X.-S. Antigen presentation and tumor immunogenicity in cancer immunotherapy response prediction. *eLife* **8** (2019).
9. Lawrence, M. S. *et al*. Mutational heterogeneity in cancer and the search for new cancer genes. *Nature* **499**, 214–218 (2013).
10. Hanna, G. J. *et al*. Frameshift events predict anti-PD-1/L1 response in head and neck cancer. *JCI Insight* **3** (2018).
11. Zhao, F. *et al*. S100A9 a new marker for monocytic human myeloid-derived suppressor cells. *Immunology* **136**, 176–183 (2012).
12. Gutman, D. A. *et al*. The Digital Slide Archive: A Software Platform for Management, Integration, and Analysis of Histology for Cancer Research. *Cancer Res.* **77**, e75–e78 (2017).
13. Thorsson, V. *et al*. The Immune Landscape of Cancer. *Immunity* **51**, 411–412 (2019).
14. Krupar, R. *et al*. Immunologic and metabolic characteristics of HPV-negative and HPV-positive head and neck squamous cell carcinomas are strikingly different. *Virchows Arch. Int. J. Pathol.* **465**, 299–312 (2014).
15. Krupar, R. *et al*. Immunometabolic Determinants of Chemoradiotherapy Response and Survival in Head and Neck Squamous Cell Carcinoma. *Am. J. Pathol.* **188**, 72–83 (2018).
16. Subramanian, A. *et al*. A Next Generation Connectivity Map: L1000 Platform and the First 1,000,000 Profiles. *Cell* **171**, 1437–1452. e17 (2017).
17. Krupar, R. *et al*. Comparison of HPV prevalence in HNSCC patients with regard to regional and socioeconomic factors. *Eur. Arch. Otorhinolaryngol.* **271**, 1737–1745 (2013).
18. Cooks, T., Harris, C. C. & Oren, M. Caught in the cross fire: p53 in inflammation. *Carcinogenesis* **35**, 1680–1690 (2014).
19. Guo, G., Yu, M., Xiao, W., Celis, E. & Cui, Y. Local Activation of p53 in the Tumor Microenvironment Overcomes Immune Suppression and Enhances Antitumor Immunity. *Cancer Res.* **77**, 2292–2305 (2017).
20. Attar, N. & Kurdistani, S. K. Exploitation of EP300 and CREBBP Lysine Acetyltransferases by Cancer. *Cold Spring Harb. Perspect. Med.* **7** (2017).
21. Fischer, K. *et al*. Inhibitory effect of tumor cell-derived lactic acid on human T cells. *Blood* **109**, 3812–3819 (2007).
22. Huang, H. *et al*. EP300-Mediated Lysine 2-Hydroxyisobutyrylation Regulates Glycolysis. *Mol. Cell* **70**, 663–678.e6 (2018).
23. He, H. *et al*. Selective p300 inhibitor C646 inhibited HPV E6-E7 genes, altered glucose metabolism and induced apoptosis in cervical cancer cells. *Eur. J. Pharmacol.* **812**, 206–215 (2017).
24. Bowers, E. M. *et al*. Virtual ligand screening of the p300/CBP histone acetyltransferase: identification of a selective small molecule inhibitor. *Chem. Biol.* **17**, 471–482 (2010).
25. Chen, Y.-P. *et al*. Genomic Analysis of Tumor Microenvironment Immune Types across 14 Solid Cancer Types: Immunotherapeutic Implications. *Theranostics* **7**, 3585–3594 (2017).
26. Cao, B., Wang, Q., Zhang, H., Zhu, G. & Lang, J. Two immune-enhanced molecular subtypes differ in inflammation, checkpoint signaling and outcome of advanced head and neck squamous cell carcinoma. *Oncoimmunology* **7**, e1392427 (2018).
27. Lechner, A. *et al*. Characterization of tumor-associated T-lymphocyte subsets and immune checkpoint molecules in head and neck squamous cell carcinoma. *Oncotarget* **8**, 44418–44433 (2017).
28. Fang, J. *et al*. Prognostic significance of tumor infiltrating immune cells in oral squamous cell carcinoma. *BMC Cancer* **17**, 375 (2017).
29. Dogan, V., Rieckmann, T., Münscher, A. & Busch, C.-J. Current studies of immunotherapy in head and neck cancer. *Clin. Otolaryngol. Off. J. ENT-UK Off. J. Neth. Soc. Oto-Rhino-Laryngol. Cervico-Facial Surg.* **43**, 13–21 (2018).
30. Davis, A. A. & Patel, V. G. The role of PD-L1 expression as a predictive biomarker: an analysis of all US Food and Drug Administration (FDA) approvals of immune checkpoint inhibitors. *J. Immunother. Cancer* **7**, 278 (2019).
31. Cohen, E. E. W. *et al*. The Society for Immunotherapy of Cancer consensus statement on immunotherapy for the treatment of squamous cell carcinoma of the head and neck (HNSCC). *J. Immunother. Cancer* **7** (2019).
32. Zhang, X.-M. *et al*. Prognostic and predictive values of immune infiltrate in patients with head and neck squamous cell carcinoma. *Hum. Pathol.* **82**, 104–112 (2018).
33. Ramos, Y. F. M. *et al*. Genome-wide assessment of differential roles for p300 and CBP in transcription regulation. *Nucleic Acids Res.* **38**, 5396–5408 (2010).
34. Smith, J. L. *et al*. Kinetic profiles of p300 occupancy *in vivo* predict common features of promoter structure and coactivator recruitment. *Proc. Natl. Acad. Sci. USA* **101**, 11554–11559 (2004).
35. Chen, M.-K. *et al*. Overexpression of p300 correlates with poor prognosis in patients with cutaneous squamous cell carcinoma. *Br. J. Dermatol.* **172**, 111–119 (2015).
36. Cho, Y.-A. *et al*. The role of p300 in the tumor progression of oral squamous cell carcinoma. *J. Oral Pathol. Med.* **44**, 185–192 (2014).
37. Kowalczyk, A. E. *et al*. Expression of the EP300, TP53 and BAX genes in colorectal cancer: Correlations with clinicopathological parameters and survival. *Oncol. Rep.* **38**, 201–210 (2017).
38. Li, M. *et al*. High expression of transcriptional coactivator p300 correlates with aggressive features and poor prognosis of hepatocellular carcinoma. *J. Transl. Med.* **9**, 5 (2011).
39. Ghosh, S. *et al*. Regulatory T Cell Modulation by CBP/EP300 Bromodomain Inhibition. *J. Biol. Chem.* **291**, 13014–13027 (2016).
40. Liu, Y. *et al*. Inhibition of p300 impairs Foxp3^{+} T regulatory cell function and promotes antitumor immunity. *Nat. Med.* **19**, 1173–1177 (2013).
41. Wang, F., Marshall, C. B. & Ikura, M. Transcriptional/epigenetic regulator CBP/p300 in tumorigenesis: structural and functional versatility in target recognition. *Cell. Mol. Life Sci.* **70**, 3989–4008 (2013).

42. Haft, S. *et al*. Mutation of chromatin regulators and focal hotspot alterations characterize human papillomavirus-positive oropharyngeal squamous cell carcinoma. *Cancer* **125**, 2423–2434 (2019).
43. Dogan, S. *et al*. Identification of prognostic molecular biomarkers in 157 HPV-positive and HPV-negative squamous cell carcinomas of the oropharynx. *Int. J. Cancer*, https://doi.org/10.1002/ijc.32412 (2019).
44. Thomas, Y. & Androphy, E. J. Acetylation of E2 by P300 Mediates Topoisomerase Entry at the Papillomavirus Replicon. *J. Virol.* **93** (2019).
45. Jansma, A. L. *et al*. The high-risk HPV16 E7 oncoprotein mediates interaction between the transcriptional coactivator CBP and the retinoblastoma protein pRb. *J. Mol. Biol.* **426**, 4030–4048 (2014).
46. Fera, D. & Marmorstein, R. Different regions of the HPV-E7 and Ad-E1A viral oncoproteins bind competitively but through distinct mechanisms to the CH1 transactivation domain of p300. *Biochemistry* **51**, 9524–9534 (2012).
47. Bernat, A., Avvakumov, N., Mymryk, J. S. & Banks, L. Interaction between the HPV E7 oncoprotein and the transcriptional coactivator p300. *Oncogene* **22**, 7871–7881 (2003).
48. Singer, K., Cheng, W.-C., Kreutz, M., Ho, P.-C. & Siska, P. J. Immunometabolism in cancer at a glance. *Dis. Model. Mech.* **11** (2018).
49. Theodoulou, N. H., Tomkinson, N. C., Prinjha, R. K. & Humphreys, P. G. Clinical progress and pharmacology of small molecule bromodomain inhibitors. *Curr. Opin. Chem. Biol.* **33**, 58–66 (2016).
50. Lasko, L. M. *et al*. Discovery of a selective catalytic p300/CBP inhibitor that targets lineage-specific tumours. *Nature* **550**, 128–132 (2017).
51. Pegg, N. *et al*. Characterisation of CCS1477: A novel small molecule inhibitor of p300/CBP for the treatment of castration resistant prostate cancer. *J. Clin. Oncol.* **35**, 11590–11590 (2017).
52. Yan, Y. *et al*. Activity of NEO2734, a novel dual inhibitor of both BET and CBP-P300, in SPOP-mutated prostate cancer. *J. Clin. Oncol.* **37**, 62–62 (2019).
53. Wang, Y.-M. *et al*. Histone acetyltransferase p300/CBP inhibitor C646 blocks the survival and invasion pathways of gastric cancer cell lines. *Int. J. Oncol.* **51**, 1860–1868 (2017).

Author contributions

R. Krupar was involved in data analyses and figure construction and wrote the manuscript. C. Watermann was involved in data analyses and figure construction. C. Idel was involved in the design of the study and data analyses. J. Ribbat-Idel was involved in data analyses and figure construction. A. Offermann was involved in the design of the study and data analyses. H. Pasternack was involved in the design of the study and data analyses. J. Kirfel was involved in the design of the study and writing the manuscript. A. Sikora was involved in the design of the study and writing the manuscript. S. Perner was involved in the design of the study and writing the manuscript.

Competing interests

The authors declare no competing interests.

Additional information

Supplementary information is available for this paper at https://doi.org/10.1038/s41598-020-66329-7.

Correspondence and requests for materials should be addressed to R.K.

Reprints and permissions information is available at www.nature.com/reprints.

Publisher's note Springer Nature remains neutral with regard to jurisdictional claims in published maps and institutional affiliations.